TECHNICKÁ UNIVERZITA V LIBERCI
www.tul.cz

LIBEREC | ZITTAU/GÖRLITZ | JELENIA GÓRA

ACC JOURNAL
XIX
1/2013

Issue A

Natural Sciences and Technology

INTERNATIONALES HOCHSCHULINSTITUT ZITTAU

Uniwersytet Ekonomiczny we Wrocławiu

TECHNICKÁ UNIVERZITA V LIBERCI

HOCHSCHULE ZITTAU/GÖRLITZ

INTERNATIONALES HOCHSCHULINSTITUT ZITTAU

UNIWERSYTET EKONOMICZNY WE WROCŁAWIU
WYDZIAŁ EKONOMII, ZARZĄDZANIA I TURYSTYKI W JELENIEJ GÓRZE

ISSN 1803-9782

ACC JOURNAL je mezinárodní vědecký časopis, jehož vydavatelem je Technická univerzita v Liberci. Na jeho tvorbě se podílí čtyři vysoké školy sdružené v Akademickém koordinačním středisku v Euroregionu Nisa (ACC). Ročně vycházejí zpravidla tři čísla.

ACC JOURNAL je periodikum publikující původní recenzované vědecké práce, vědecké studie, příspěvky ke konferencím a výzkumným projektům. První číslo obsahuje příspěvky zaměřené na oblast přírodních věd a techniky, druhé číslo je zaměřeno na oblast ekonomie, třetí číslo pojednává o tématech ze společenských věd.

ACC JOURNAL má charakter recenzovaného časopisu. Jeho vydání navazuje na sborník „Vědecká pojednání“, který vycházel v letech 1995-2008. Od roku 2010 je ACC JOURNAL v databázi Rady pro vědu, výzkum, vývoj a inovace (Seznam recenzovaných neimpaktovaných časopisů vydávaných v České republice) hodnocených v RIVu.

ACC JOURNAL is an international scientific journal. It is published by the Technical University of Liberec. Four universities united in the Academic Coordination Centre in the Euroregion Nisa participate in its production. There are usually three issues of the journal annually.

ACC JOURNAL is a periodical publishing original reviewed scientific papers, scientific studies, papers presented at conferences, and findings of research projects. The first issue focuses on natural sciences and technology, the second issue deals with the science of economics, and the third issue contains findings from the area of social sciences.

ACC JOURNAL is a reviewed one. It is building upon the tradition of the "Scientific Treatises" published between 1995 and 2008. The ACC JOURNAL has been in the database of the Research and Development Council since 2010 (List of reviewed non-impact journals published in the Czech Republic) recorded and evaluated in the Information Register of R&D results.

Contents

INTRODUCTION OF NEURAL NETWORKS TO STUDENTS

Petr Doležel
*** Martin Mariška**

University of Pardubice
Faculty of Electrical Engineering and Informatics
Department of Process Control
Nam. Cs. Legii 565, 532 10 Pardubice, Czech Republic
petr.dolezel@upce.cz

* University of Pardubice
Faculty of Electrical Engineering and Informatics
Department of Process Control
Nam. Cs. Legii 565, 532 10 Pardubice, Czech Republic
mariska.martin@gmail.com

Abstract

The paper deals with the possibility of introducing artificial intelligence and especially artificial neural network methodology to students in an interesting way. To be more specific, the artificial neural network is described through the design of NPC's artificial intelligence in a simple computer game. In the first paragraphs, the methodology of artificial neural networks is described in rather exoteric way through its comparison to biological nervous systems and neural cells. Then, the methodology is used to design a computer game NPC which can observe and learn the behavior of human player. At the end of the paper, the NPC behavior is tested and analyzed, as well as there is mentioned a feedback from students of several education facilities.

Introduction

Artificial neural networks (ANN) are popular in many branches of science these days and they are even applied to solve various industrial and civil problems. However, education of ANN is limited to universities and, in addition, almost exclusively to optional subjects. The aim of the authors is to hand on information about ANN to a large number of students and, above all, to arouse interest in it. To achieve this objective, a set of popularizing lectures has been drawn up. The extract from these lectures is introduced below.

1 Main Idea

It is not simple to catch today's student's attention for more than five minutes. It is obvious that the lectures should deal with something close to students' interests. Thus, the sphere of computer games is chosen. Almost in every computer game, there is a so-called non-player character (NPC) which should be featured with some level of artificial intelligence. The authors' premise is that it can be remarkably interesting for students to show them the way to do it using ANNs.

Solely for educational purposes, the classical game of Pong is chosen – see Fig. 1. There are two players, each with a paddle and a ball that bounces back and forth between them. Each player tries to position his paddle (which can only move up and down) to bounce the ball back towards the other player. The goal is to make the other player to miss the ball. The aim for students is to design ANN to control the movement of one paddle.

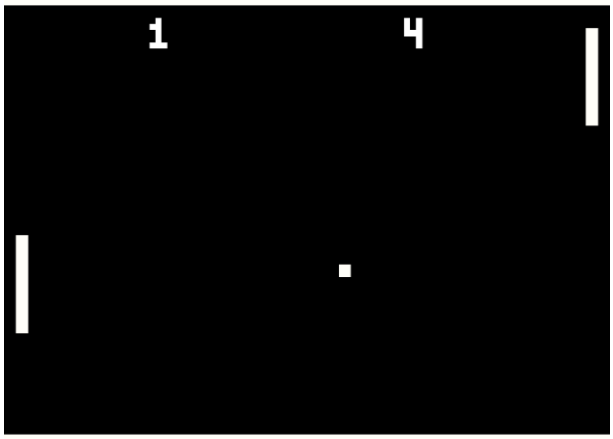

Source: Own

Fig. 1: *Pong game window*

On the other hand, ANNs have been used for NPC control in much more complicated computer games such as Black and White or Colin McRae Rally 2 [1].

2 The Basics of Feedforward ANN

2.1 Introduction

ANN is really huge methodology nowadays and it is impossible to describe it comprehensively in one paper. In following sections, only basics of ANN are introduced, in correspondence with the amount of information referred to students during popularizing lectures. More detailed description of ANN can be found in [1].

2.2 Analogy to Nervous System

The design of ANN is inspired by analogy with the brain, which is a living proof that fault-tolerant parallel processing is not only possible, but fast and effective, too. Human brain consists of neural cells (neurons). Function of neuron is surprisingly simple in comparison with the whole brain. Each biological neuron consists of a cell body, a collection of dendrites which bring information into the cell and an axon which transmits information out of the cell – see Fig. 2.

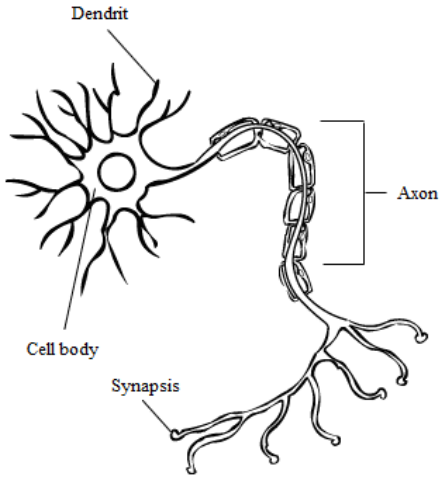

Source: Public Domain file from creationwiki.org

Fig. 2: *Neural Cell*

A neuron produces an output along its axon and the output is a response to collective effect of dendrites incoming to the cell body. The axon from one neuron can then influence the dendrites of other neurons through synapses (some synapses generate positive effect, the other negative one). The processes of learning and remembering are somehow associated to plasticity of the synapses, although this procedure has not been defined in a satisfactory manner yet.

Artificial intelligence (AI) methodology tries to model reasoning processes of human brain. Contrary to some other branches of AI (fuzzy logic, expert systems), ANNs try to model low level functionality of the brain, cell by cell. Thus, the first step is to design an artificial model of the neuron. ANN is then a network of interconnected artificial neurons.

2.3 Model of neuron

In a simplified way, biological neuron is a processor which generates a response to some set of weighted inputs. This process can be approximated by neuron model shown Fig. 3.

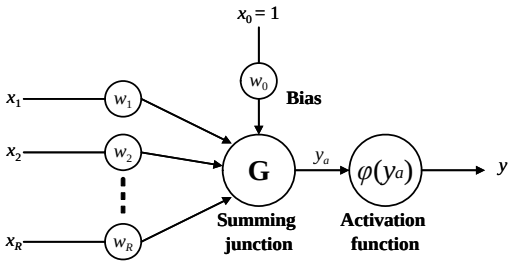

Source: Own

Fig. 3: *Artificial neuron*

Three basic elements can be identified here:

- A set of connecting links, each of which is characterized by a weight. Specifically, a signal x_i (which can be either input to the network or output from the previous neuron) connected to a neuron is multiplied by a weight w_i.
- An adder which transforms the set of weighted input signals to one scalar value called activation potential. The operations described in this paper constitute a linear combiner.
- An activation function which processes an activation potential and generates output of the neuron.

Artificial neuron in Fig. 3 also includes an externally applied bias denoted by $w_0 x_0$. The bias affects the input to the activation function.

Mathematically, the neuron depicted in Fig. 3 can be described by the following pair of equations.

$$y_a = \sum_{i=0}^{R} w_i x_i \tag{1}$$

$$y = \varphi(y_a) \tag{2}$$

Activation function, which is denoted by $\varphi(.)$, can be defined in many ways and its definition crucially affects the response of the whole ANN. In Fig. 4, there are graphs of the most common activations.

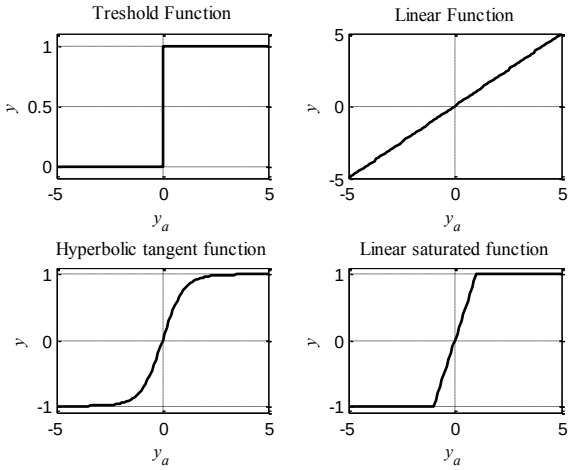

Source: Own

Fig. 4: *Set of activation functions*

The topology of the neuron (number of inputs, definition of adder and activation function) is mostly constant, but the other parameters (especially weights and biases) are tuned through learning.

However, one neuron can solve only simple tasks (most common example is the logic functions approximation). Thus, it is suggested to connect a set of neurons together to build the neural network.

2.4 ANN Topology

ANN consists of one or more neurons connected into one or more layers. Mostly, a layer is compounded of neurons that are not connected to other ones in any manner (there are some exceptions, of course). Examples of ANN possible topologies are shown in Fig. 5 and in Fig. 6 (each node represents one neuron). ANN topology is abbreviated formally by a set of integer numbers – e.g. [2-4-5-1] means ANN with two inputs, four neurons in the first hidden layer, five neurons in the second hidden layer and one neuron in the output layer.

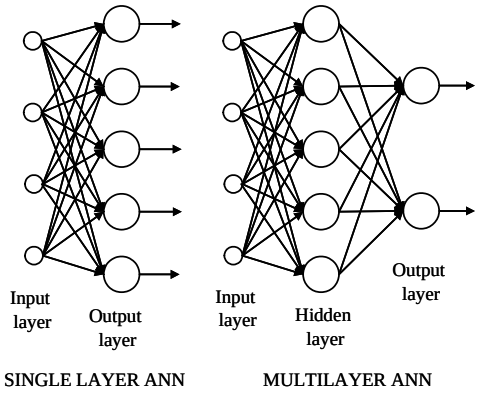

Source: Own

Fig. 5: *Feedforward ANNs*

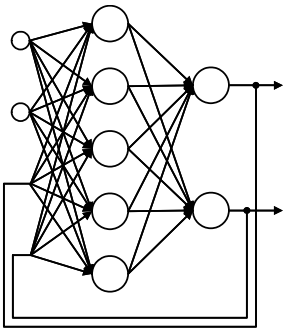

Source: Own

Fig. 6: *Example of recurrent topology of ANN*

The topology of the ANN depends on a task to be solved. Tasks like function approximation or pattern recognition can be solved using feedforward ANN with one or two hidden layers. On the other hand, recurrent networks are necessary to be used to time series prediction or dynamical processes modeling.

To work properly, weights and biases of each neuron in ANN should be tuned. This process is called learning.

2.5 ANN Learning

The possibility of learning is one of the most attractive features of ANN. Learning means using a set of observations to find optimal (in some sense) values of weights and biases. It is categorized as follows.

- Supervised learning
- Unsupervised learning

For adapting the weights and biases, supervised learning uses a training set of labeled examples, with each example consisting of an input signal and the corresponding response. Unsupervised learning rather implements a task-independent measure of quality of the set of inputs. It is not used as often as supervised learning and it is not discussed here anymore.

To use supervised learning, the first step is to obtain somehow a training set of labeled examples. In other words, a representative to be followed is needed. Then, the process of learning is shown in Fig. 7.

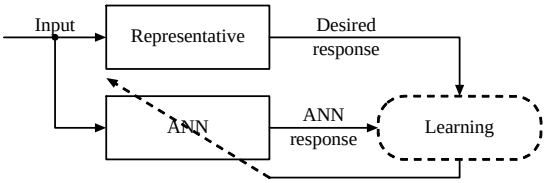

Source: Own

Fig. 7: *Basic diagram of ANN learning*

There have been introduced many learning algorithms. Some of them are gradient based (group of backpropagation algorithms [2]), others are not (Levenberg-Marquardt algorithm [3], [4], evolutionary-based algorithms [5]). However, the philosophy is mostly the same. In every iteration of the learning algorithm, the performance of ANN is measured using defined cost function. This information is used then to adapt weights and biases to lower the cost function.

Eventually, frameworks for ANN usage are included in many computing softwares (e.g. Matlab, Statistica) as well as there are several frameworks ready to use in JAVA, C#, C++ etc.

3 Pong Play Using ANN

3.1 Pong Dynamics

The aim of each player playing Pong is not to let the ball leave the game screen. In our particular version each player can press and hold one of the two buttons (one for accelerating upwards and the other for accelerating downwards). The paddle position and speed is affected by the value of acceleration and screen borders. Maximum speed is limited, too. Ball speed is constant. For better illustration, the position course of the paddle is shown in Fig. 8 (y axis of the first graph indicates up-button pressing if the value is 1 and down-button pressing if the value is -1).

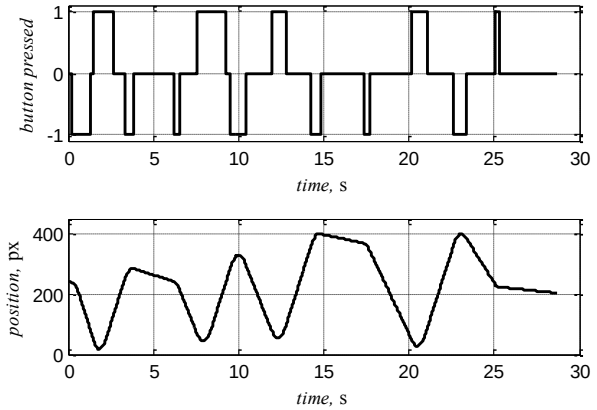

Source: Own

Fig. 8: *Dynamics of the paddle*

3.2 ANN for Paddle Control

To design a proper ANN to paddle control, the first thing to be done is to consider the data which are used by the player to control the paddle successfully.

First experiments are performed with ANN formally shown in Fig. 9.

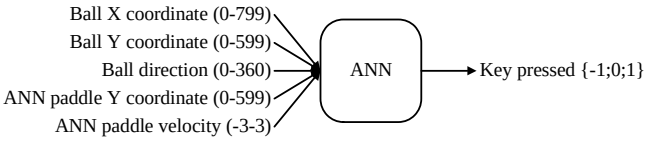

Source: Own

Fig. 9: *ANN for paddle control I*

Training set is simply acquired by a two players´ game. One of the players poses as an ANN teacher while data are collected during every single step of the game (10000 samples are used). Acquired data are standardized and used then for ANN learning using Neural Network Toolbox implemented in Matlab (Levenberg-Marquardt algorithm is used), whereas several topologies are tested. All tested ANNs consist of hyperbolic tangent activation functions in hidden layers and pure linear activation functions in the output layer which is recommended setting [1]. Output of the ANN is rounded to nearest integer from the set { 1; 0; 1} to obtain prospective output.

Testing of the proper behavior is performed in the following way: paddle controlled by ANN is expected to rebound series of balls (100 samples) with random direction (see Fig. 10). Hit ratio is considered then as a performance index.

Source: Own
Fig. 10: *ANN testing*

The test results are shown in Fig. 11. It is obvious that the percentage of successful rebounding is too low even for very complex topologies. Thus, another approach should be used.

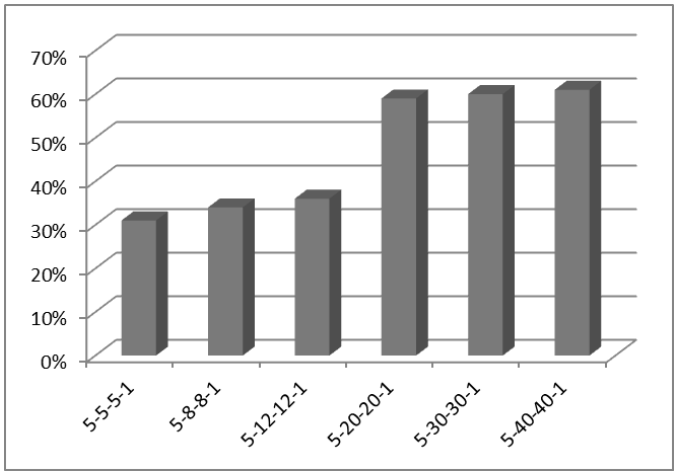

Source: Own
Fig. 11: *Test results I*

After several trials, following composition proved itself as the most suitable – see Fig. 12. This concept probably corresponds more with human player stream of thought – firstly, a player estimates the desired position of the paddle according to the ball dynamics and then he tries to push the paddle into the right position. ANN can also be used as a contoller but in this case discrete version of classical PID controller is used instead because paddle position control is quite a simple linear problem. Learning and testing is performed in the same way as in the previous case and the results are shown in Fig. 13.

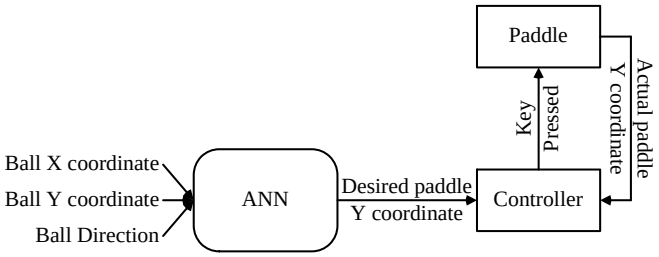

Source: Own

Fig. 12: *ANN for paddle control II*

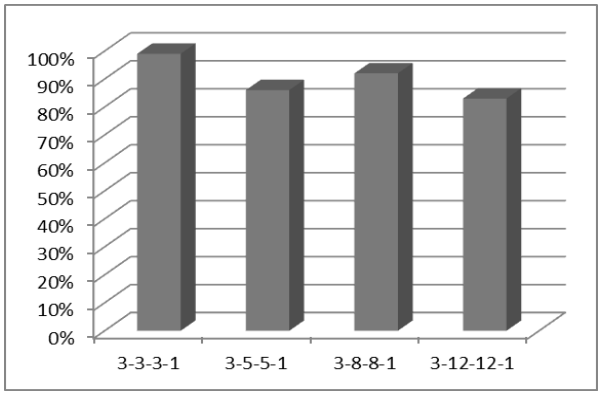

Source: Own

Fig. 13: *Test results II*

4 Popularizing Course Summary

The course is divided into two parts. The lecture introduces the basics of ANN (as it is described in the section 2) and it is followed by the seminar where the students are suggested to design their own ANN for Pong paddle control using specialized software. The summary of the course is resumed in Fig. 14.

4.1 Software for the Seminar

Special software (based on Matlab language) has been prepared for the seminar – see Fig. 15. In one mode, the software can simulate the Pong game for two players while all relevant data are measured. One player is considered here as a supervisor for NPC. In another mode, ANN is designed and trained so that it can approximate its supervisor behavior. In the last mode, NPC's behavior can be tested in the game against human opponent.

Using this software, the students are familiarized with basics of ANNs, they can test how ANN topology affects training results and, last but not least, they enjoy some fun.

The percentage of successful rebounding is almost 100% and the interesting thing is that simple topologies provide higher hit rate. Paddle controlled in this way is a peer opponent to the human player.

Conclusion

The aim of the paper is to suggest the way of introducing ANN to a large number of students in an entertaining way – it means to significantly reduce the theory and to perform some catchy demonstrations. The problem introduced here – Pong paddle control – is decent example for students to start dealing with ANNs. The tasks associated with ANN (data acquisition for training set, topology optimization, …) are well imaginable and the results are well recognizable. The methodology described above has been used with students of two Czech high schools and one university so far and the feedback has been positive.

Literature

[1] HAYKIN, S. *Neural Networks: A Comprehensive Foundation.* New Jersey : Prentice Hall, 1999. 842 s. ISBN 0-13-273350-1.

[2] RUMELHART, D.E.; HINTON, G.E.; WILLIAMS, R.J. Learning representations by back-propagating errors. *Nature*, 1986, No. 323, pp. 533-536. ISSN 0028-0836.

[3] LEVENBERG, K. A method for the solution of certain problems in least squares. *The Quarterly of Applied Mathematics*, 1944, Vol. 2, pp. 164-168. ISSN 0033-569X.

[4] MARQUARDT, D.W. An algorithm for least-squares estimation of nonlinear parameters. *Journal of the Society for Industrial and Applied Mathematics*, 1963, Vol. 11, pp. 431-441. ISSN 0887-459X.

[5] BLANCO, A; DELGADO, M.; PEGALAJAR, M.C. A Real-Coded genetic algorithm for training recurrent neural networks. *Neural Networks*, 2001, Vol. 14, pp. 93-105. ISSN 0893-6080.

PŘEDSTAVENÍ MOŽNOSTÍ NEURONOVÝCH SÍTÍ STUDENTŮM

Článek představuje možnost, jak zajímavou cestou seznámit studenty s problematikou umělé inteligence a především umělých neuronových sítí. Konkrétně, možnosti umělých neuronových sítí jsou uvedeny na příkladu budování umělé inteligence v jednoduché počítačové hře. V první části textu je metodika umělých neuronových sítí obecně popsána a srovnána s biologickými nervovými soustavami a nervovými buňkami. Následně jsou popsané přístupy použity pro návrh inteligentního chování oponenta v počítačové hře tak, aby byl oponent schopen učit se z chování lidského hráče. V závěru je navržená umělá inteligence oponenta testována a vyhodnocena, přičemž jsou také zmíněny ohlasy studentů, kterým byly umělé neuronové sítě tímto způsobem představeny.

VORSTELLUNG DER MÖGLICHKEITEN NEURONALER NETZE FÜR STUDENTEN

Der Artikel stellt eine Möglichkeit vor, wie man auf interessantem Wege die Studenten mit der Problematik der künstlichen Intelligenz, vor allem den künstlichen neuronalen Netzen, bekannt macht. Konkret gezeigt wird die Möglichkeit der künstlichen neuronalen Netze an einem Beispiel, wo man künstliche Intelligenz in einem einfachen PC-Spiel errichtet. Im ersten Teil des Artikels wird die Methodik der künstlichen neuronalen Netze allgemein beschrieben und mit dem biologischen Nervensystem und den Nervenzellen verglichen. Im Folgenden werden Zugriffe beschrieben, die man für einen Entwurf intelligenten Verhaltens des Opponenten im PC-Spiel benutzt hat, und zwar so, dass der Opponent in der Lage ist, aus dem Verhalten des menschlichen Spielers zu lernen. Am Schluss wird der Entwurf der künstlichen Intelligenz des Opponenten getestet und ausgewertet, wobei auch die Reaktionen der Studenten, denen diese künstliche neuronale Netze vorgestellt worden sind, erwähnt werden.

PREZENTACJA MOŻLIWOŚCI SIECI NEURONOWYCH DLA STUDENTÓW

Artykuł przedstawia ciekawy sposób zapoznania studentów z zagadnieniami sztucznej inteligencji, a zwłaszcza sieci neuronowych. Możliwości sztucznych sieci neuronowych są pokazane na przykładzie budowy sztucznej inteligencji w prostej grze komputerowej. W pierwszej części opisano metodologię sztucznych sieci neuronowych, porównując ją z biologicznymi układami nerwowymi i komórkami nerwowymi. Następnie opisano podejście zastosowane do zaprojektowania inteligentnego zachowania przeciwnika w grze komputerowej w taki sposób, aby mógł on się uczyć na podstawie zachowania graczaczłowieka. W zakończeniu zaprojektowana sztuczna inteligencja przeciwnika poddana jest testowaniu i ocenie, przy czym uwzględniono tu również spostrzeżenia studentów, którym w ten sposób zaprezentowano sztuczne sieci neuronowe.

AN AUTOMATED FABRIC FAULT DETECTION AND CLASSIFICATION SYSTEM BASED ON COMPUTER VISION AND SOFT COMPUTING

Hadir Eldeeb
Mahmoud Mohy
Tamer Elbagoury
Khaled Aboseda
Ebraheem Shady
*** Mohamed Eldessouki**

Mansoura University
Faculty of Engineering
Department of Textile Engineering
Mansoura, Egypt
* mohamed.eldessouki@gmail.com

Abstract

Fabric inspection is one of the essential quality control processes in weaving mills. The automation of this process using computer vision systems is expected to increase the efficiency of the process and increase the total profit revenues on the long run. This work introduces a computer vision system that has the capability to detect and classify a relatively large number of fabric defects. Image enhancement techniques were used in processing the fabric acquired images. Spatial and spectral features were extracted from the processed images and used as inputs to soft-computing classifiers. Two approaches were used in the classification with the aim of reducing the calculation time required during the image analysis. The successful classification rate was 97.3% using the direct approach that has a slightly longer processing time. The performance of the classifiers in the series approach ranges between 91 to 100% depending on the classification level and the used image features. Results of this work with high classification rate and short processing time are promising to apply the introduced technique in real time fabric inspection systems.

Introduction

The conventional inspection process in the weaving mills usually depends on human visual inspection which only detects 60 to 70% out of the total fabric defects. The other defects pass without detection and cause several problems in the following processes of manufacturing. In addition, fixing defects is a complicated process and the defective parts are usually discarded as wastes that might be recycled or sold at low prices (usually 45 to 65% from the free defect price). Several researchers have tried to solve this problem using image processing techniques and implemented different spatial and spectral methods for image analysis and feature extraction. Kuo and Su [1] applied the co-occurrence matrix and gray relational analysis. The gray relational analysis was also used to investigate correlations of the analyzed factors among the selected features in a randomized factor sequence through image processing. The system classified different defects such as broken warps, broken wefts, holes, and oil stains with 94% recognition accuracy of the system.

Shady et al. [2] used image analysis and neural networks for six different knitted fabric defects detection and classification. Statistical approaches and Fourier Transforms were used for feature extraction and artificial neural networks were used to classify the defects. The results of using the Fourier transform features were slightly more successful than the statistical approach in detecting the defect-free samples and classifying most of the defects.

Mallik and Datta [3] presented a theoretical based technique for real-time fabric defect detection using a joint transform correlator that is extension of Fourier transform analysis. The joint power spectrum showed better classification results compared to the Fourier and experimental results. The technique introduced reasonable results for identifying and classifying some defects such as the existence of thick yarns, knots, and missing yarns.

Hu and Tsai [4] used wavelet packet transform and an artificial neural network (ANN) to inspect four kinds of fabric defects. The approach was reliable and effective in classifying fabric defects with a total classification rate of 100% for a wavelet function with a maximum vanishing moment of four and three resolution levels. Wen et al. [5] also used wavelet transform and co-occurrence matrix to extract features of textured images. The system was able to detect whether the fabric is defective or not at 92% rate of success. Also, the system was able to locate the defect position at 84% rate of success.

It can be seen from the survived literature that most of the applied detection systems were able to classify a few number of defects which may not efficient in practical production environments. Therefore, this work introduces an automated fabric fault detection and classification (FFDC) system to detect and classify a larger number of woven fabric defects.

1 Methods

The overview of the FFDC computer vision system is shown in Figure 1. The system utilizes a digital camera to acquire and transmit fabric images to a computer which enhances and extracts some features for each image. The features are then processed using an Artificial Intelligence (AI) technique to detect and classify the fabric defects. Also, the FFDC system predicts the sources of the defects to be fixed. These defects are recorded in a database providing a report of the frequent defects for fixing their sources and consequently increasing the quality of the manufactured fabrics. Therefore, applying such automatic system in weaving mills is expected to increase the profit and the product quality.

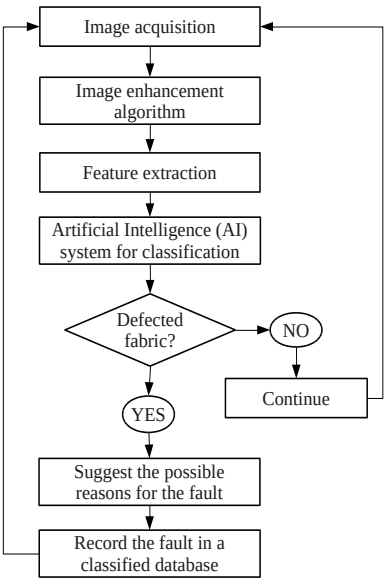

Source: Own

Fig. 1: *Flow chart of the FFDC algorithm*

1.1 Image enhancement

The size of the acquired images is 3088 x 2056 pixels which represents a fabric sample with dimension of 30 x 20 mm. To make defects more detectable in the acquired images, each

image was divided into nine sub-images. Image enhancement was applied to remove the noise and hairiness from the woven fabric images and adjust their gray levels, shown in Figure 2. The enhanced images should facilitate the allocation of the fabric defects.

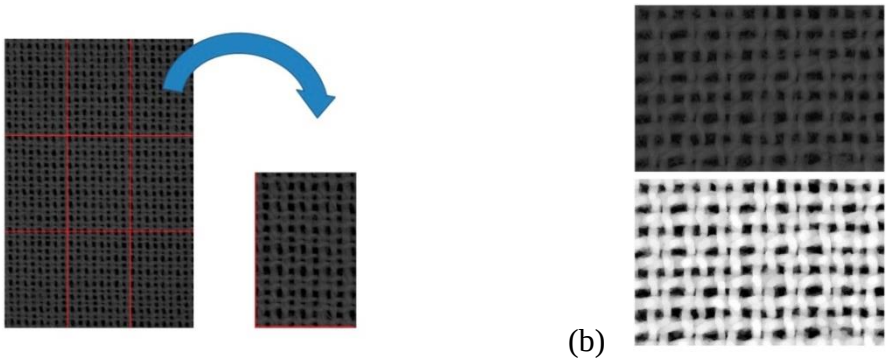

(a) (b)

Source: Own

Fig. 2: *(a) A fabric image that was divided into nine sub-images; (b) A true-color image (top) and enhanced image (bottom) after noise removal and gray level adjustment*

1.2 Feature extraction

The feature pool consists of three statistical and six spectral features. The statistical features (the mean, the summation, and the standard of deviation) were chosen for their simplicity and faster calculation. The determination of the statistical features was performed according to the following relations:

The mean

$$\bar{x} = \frac{1}{n}\sum_{i=1}^{n} x_i \tag{1}$$

The summation of columns or rows:

$$R = \sum_{i=1}^{n} x_i \tag{2}$$

The standard deviation:

$$s = \sqrt{\frac{1}{n-1}\sum_{i=1}^{n}(x_i - \overline{x})^2} \tag{3}$$

The spectral features were based on the Fourier transform technique that transforms pictures from their spatial domain to the spectral domain. If the image is considered as a function *f(m,n)* with two discrete spatial variables *m* and *n*, then the two-dimensional Fourier transform *F(m,n)* is defined by the relationship:

$$F(w_1, w_2) = \sum_{m=-\infty}^{\infty}\sum_{n=-\infty}^{\infty} f(m,n)\ e^{-j\omega_1 m}\ e^{-j\omega_2 n} \tag{4}$$

After transforming the image to the spectral domain, the power spectrum of the image can be calculated and some dominant peaks can be used as image features. An example of some of these features is illustrated in Figure 3.

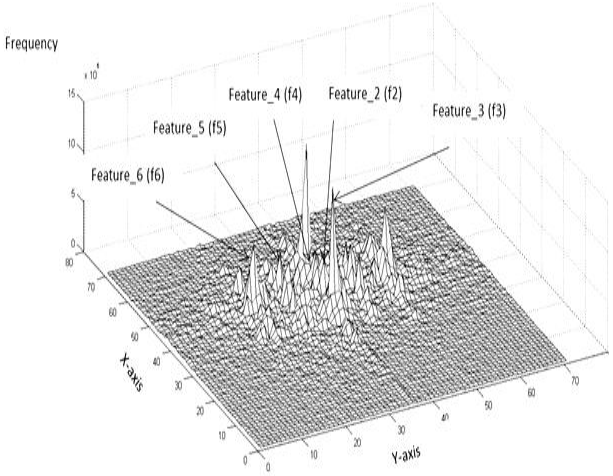

Source: Own

Fig. 3: *Some spectral features of the Fourier transformed image*

1.3 Artificial neural network

Artificial neural networks (ANN) were used as soft computing techniques for classifying defected and non-defected samples. Different network architectures were used and the optimized network structure includes a multi-layer network with two hidden layers (25 neurons per layer). The input and output layers were adjusted according to the used features and the required fault categories. Three groups of features were used: solely statistical features, solely spectral features, and combination of statistical and spectral features. The classification went through two approaches by either identifying the defect type directly from the input features (the direct approach) or by identifying the defect at different levels (series approach). In the series approach the classification three steps have been taken; the first step classifies if the fabric sample is defected or defect-free. The second step classifies the defect category (warp, weft, or areal) and the third step identifies the defect type.

2 Experimental setup

The fabric samples used in this study were manufactured at "Samanoud Company for Woven & Pile Fabrics" on a Sulzer-Ruti weaving machine. The fabric structure is plain weave 1/1 with a yarn count of 20/1 Ne for warp and 14/1 Ne for weft. The densities of warp and weft yarns are 20 and 18 per cm, respectively. The chosen defects were intentionally introduced on the machine based on the knowledge of defects sources. The used defects, shown in Figure 4, were categorized into three main categories; defects in warp direction (double end and float warp), defects in weft direction (double pick, heavy peat, light peat, and missing picks), and areal defects (hole, knots, and stains).

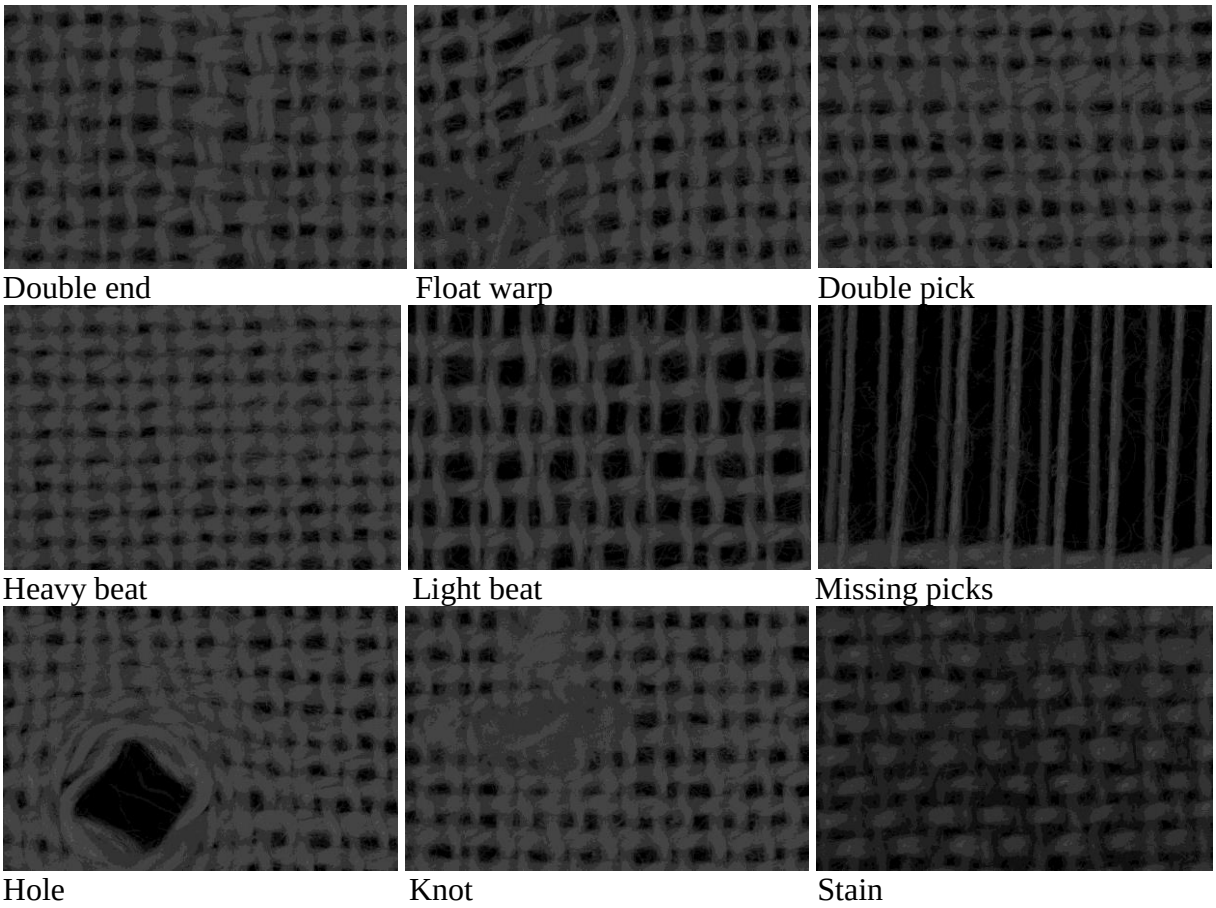

Source: Own

Fig. 4: *Images for some fabric faults*

3 Results and Discussions

The set of image features was divided into three groups for the artificial neural network (ANN) training, validating, and testing. The results of the testing sets are summarized in Table 1 for the direct and the series approaches. The results of the direct approach show that the classification using only Fourier features gets better results than using solely statistical features and the application of both features (statistical and spectral) gets the best results among the three inputs.

Tab. 1: *The overall performance of the ANN classification system*

		Statistical features	**Spectral features**	**Statistical and spectral features**
	Direct approach	84.5	92.7	97.3
Series approach	Defect or defect-free	91	89	87
	Warp, weft, or areal	89.3	95.3	94.7
	Warp defects	100	95	100
	Weft defects	100	100	100
	Areal defects	90	93.3	100

Source: Own

The series approach was suggested in this study to minimize the calculation time allowing a real time processing of the fabric samples. According to this approach, no further processing for the defect-free samples is required in the case of their classification at the first stage. Defected samples go for further classification in the next classifiers by categorizing the defect (warp, weft, or areal) in the second ANN. The category is considered as an input of the next classifier to determine the exact fault type.

The results of the series approach differ according to the level of classification as shown in Table 1 and the testing of the classifiers using different features show that:

- *First classifier*: The purpose of this classifier is to determine if the fabric is defected or not. The classification using only Fourier features gets better results than using both types of features (statistical and spectral) while using the statistical features only gets the best results. This result may be counter intuitive; however, the consideration of many features as inputs for the classifier may "confuse" the system and decrease its classification performance. Therefore, optimizing the input features should be considered to reduce the number of inputs for the system. The principle component analysis technique might be useful for input reduction and optimization.
- *Second classifier*: The purpose of this classifier is to categorize the fabric fault (warp, weft or areal). The best classification results were obtained using the Fourier spectral features while the combination of the spectral and spatial features performs better than the application of statistical features only.
- *Third classifier*: The purpose of this classifier is to identify the fault and produce its exact type. The performance of this classifier depends on the fault category as shown in Table 1 where the combination of statistical and spectral features gives the best classification results with 100% rate of successful classification. It is noticeable that the classifier has the ability to differentiate the weft defects using any set of features (statistical only, spectral only, or their combination) although having the highest number of faults in this category. The 100% successful classification for the warp and weft categories using solely statistical features may be useful in the real-time classification because of the short time calculation of these spatial features.

Conclusion

This work utilizes a digital camera to acquire and transmit fabric images to a computer which enhances and extracts the features for individual images. The features are then processed using an artificial intelligence technique to classify the fabric faults. Two approaches were implemented in this study with direct classification approach and series approach. The results of the direct approach show that the use of a combination of statistical and spectral features gives a 97.3% successful classification. The series approach aimed to reduce the processing time and its testing shows the dependence of the classifiers performance on the given set of features. The application of a whole set of statistical and spectral features performs best in most classification categories while solely statistical features only were sufficient (with their short calculation time) in determining whether the fabric was defected or not and in determining the faults within the warp and weft categories. The results of this study are promising and may allow the application of the introduced technique in real time fabric inspection systems because of the high successful classification rate and the relatively short processing time.

Literature

[1] KUO, C.-F. J.; SU, T.-L.: Gray Relational Analysis for Recognizing Fabric Defects. *Textile Research Journal*, vol. 73, pp. 461-465, 2003.

[2] SHADY, E.; GOWAYED, Y.; ABOUIIANA, M.; YOUSSEF, S.; PASTORE, C.: Detection and Classification of Defects in Knitted Fabric Structures. *Textile Research Journal*, vol. 76, pp. 295-300, 2006.

[3] MALLIK, B.; DATTA, A. K.: Defect Detection in Fabrics with a Joint Transform Correlation Technique: Theoretical Basis and Simulation. *Textile Research Journal*, vol. 69, pp. 829-835, 1999.

[4] HU, M. C.; TSAI, I. S.: Fabric Inspection Based on Best Wavelet Packet Bases. *Textile Research Journal*, vol. 70, pp. 662-670, 2000.

[5] WEN, C.-Y.; CHIU, S.-H.; HSU, W.-S.; HSU, G.-H.: Defect Segmentation of Texture Images with Wavelet Transform and a Co-occurrence Matrix. *Textile Research Journal*, vol. 71, pp. 743-749, 2001.

AUTOMATIZACE KONTROLY TKANIN POMOCÍ POČÍTAČOVÝCH KAMEROVÝCH SYSTÉMŮ

Kontrola tkanin je jedním ze základních procesů řízení kvality v tkalcovnách. Od automatizace tohoto procesu pomocí počítačových kamerových systémů se očekává zvýšení efektivnosti procesu a z dlouhodobého hlediska celkové zvýšení zisků. Tato práce představuje počítačový kamerový systém, který má schopnost rozpoznat a klasifikovat relativně velké množství textilních vad. Při zpracovávání obrazu tkaniny byly použity techniky na jeho vylepšení. Ze zpracovaných obrazů byly extrahovány prostorové a spektrální vlastnosti a použity jako vstupy do výpočtových klasifikátorů. V klasifikaci byly použity dva přístupy s cílem snížit dobu výpočtu potřebnou při analýze obrazu. Úspěšná klasifikace činila 97,3 % pomocí přímého přístupu, který má o něco delší dobu zpracování. Výkonnost klasifikátorů série se pohybuje v rozmezí 91 až 100 % v závislosti na klasifikačním stupni a použitých obrazových funkcích. Výsledky této práce s vysokou mírou úspěšnosti klasifikace a krátkou dobou zpracování slibují možnost zavést tuto techniku do kontrolních systémů tkanin v reálném čase.

EINE AUTOMATISIERTE TEXTILFEHLERAUFDECKUNG UND EINE AUF COMPUTERVISION UND ELASTISCHE BERECHNUNGEN BASIERTE KLASSIFIZIERUNG

Die Kontrolle von Geweben ist eine der wichtigsten Vorgänge bei der Gestaltung von Qualität in Webereibetrieben. Von einer Automatisierung dieses Prozesses mit Hilfe von computergesteuerten Kamerasystemen werden eine Steigerung der Effektivität des Prozesses und insgesamt eine langfristige Gewinnsteigerung erwartet. Die vorliegende Arbeit stellt ein computergesteuertes Kamerasystem vor, welches die Fähigkeit besitzt, eine relativ große Menge an Textilfehlern zu erkennen und zu klassifizieren. Bei der Verarbeitung des Gewebebildes wurden Techniken zu dessen Verbesserung verwendet. Aus den verarbeiteten Bildern wurden räumliche und spektrale Eigenschaften extrahiert und als Eingang in Berechnungsklassifikatoren genutzt. Bei der Klassifizierung wurden von zwei Ansätzen ausgegangen mit dem Ziel, die Zeitdauer der zur Bildanalyse notwendigen Zeitdauer zu senken. Die erfolgreiche Klassifizierung betrug mit Hilfe des direkten Ansatzes 97,3%. Dieser Ansatz benötigt eine etwas längere Bearbeitungszeit. Die Leistungsfähigkeit der Klassifikatoren bewegt sich zwischen 91 und 100%, in Abhängigkeit vom Klassifikationsgrad und den verwendeten Bildfunktionen. Die Ergebnisse der vorliegenden Arbeit, die auf einem hohen Klassifikationsmaß und einer geringen Bearbeitungszeitberuhen, versprechen die Möglichkeit, diese Technik in einer realen Zeit in die Kontrollsysteme der Gewebe einzuführen.

AUTOMATYZACJA KONTROLI TKANIN PRZY POMOCY KOMPUTEROWYCH SYSTEMÓW WIZYJNYCH

Kontrola tkanin należy do podstawowych procesów zarządzania jakością w tkalniach. Od automatyzacji tego procesu przy pomocy komputerowych systemów wizyjnych oczekuje się zwiększenia efektywności procesu a długofalowo ogólnego zwiększenia zysków. Niniejsze opracowanie przedstawia komputerowy system kamer, który potrafi rozpoznać i klasyfikować stosunkowo dużą ilość wad tekstyliów. Przy przetwarzaniu obrazu tkaniny wykorzystano techniki mające na celu jego ulepszenie. Z przetworzonych obrazów ekstrahowano właściwości przestrzenne i spektralne, które wykorzystano jako dane wejściowe do klasyfikatorów obliczeniowych. W klasyfikacji zastosowano dwa podejścia w celu skrócenia

czasu wyliczeń niezbędnego do analizy obrazu. Udana klasyfikacja wynosiła 97,3% przy podejściu bezpośrednim, które ma o nieco dłuższy czas wykonania. Wydajność klasyfikatorów serii mieści się w granicach 91 do 100% w zależności od stopnia klasyfikacyjnego i zastosowanych funkcji obrazu. Wyniki tej pracy z wysokim stopniem klasyfikacji i krótkim czasem opracowania są obiecującą możliwością wprowadzenia tej techniki do systemów kontroli tkanin w czasie rzeczywistym.

RESPONSE OF THERMOPHYSIOLOGICAL COMFORT PROPERTIES OF POLYESTER – MODAL BLENDED FABRIC TO CHEMICAL FINISHING

R. P. Jamdagni
*** Suman Bhattacharya**

The Technological Institute of Textile and Sciences
Bhiwani, Haryana, India
rjamdagni@hotmail.com
* bhattacharya@hotmail.com

Abstract

The present study has been undertaken to identify and analyze the response of air and moisture transmission properties of fabric woven with air-jet spun polyester – modal blended yarn (as weft) to chemical finishing. In this study, the fabrics of three different blends are treated with different concentration of anti-crease resin (DMDHEU) and softening agent (modified silicon). The concentration of anti-crease finishing agent and softener used for chemical treatment are decided based on Box and Behnken design of experiment. Mathematical models (in the form of regression equations) have been developed to predict the thermophysiological comfort parameters using SYSTAT 13 statistical package. It was observed that under all experimental conditions, the moisture transmission, absorbency and air permeability of grey fabric reduces after finishing at all blend levels. Moisture transmission properties and air permeability of finished fabric is negatively influenced by the concentration of silicon softener. The concentration of resin does not influence the air permeability of the fabric, but it improves the moisture vapour permeability marginally, though it is not statistically significant. The wicking power is increased with increase in polyester component and resin concentration; however the latter does not have, unlike softener, any significant influence of total absorbency of fabric.

Introduction

Moisture transmission through textile, which is carried out through perspiration both in vapour and liquid form, has a great influence on the thermophysiological comfort of the human body .The clothing to be worn should allow this perspiration to be transferred to the atmosphere otherwise it will result in discomfort to the wearer. If moisture transfer rate through clothing is slow during sweating, relative and absolute humidity level of the clothing microclimate will increase, suppressing the evaporation of sweat. Further, it is also important to reduce degradation of thermal insulation caused by the moisture built up. Thus both in hot and cold weather and during normal and high activity levels, moisture transmission through fabrics both in sensible (liquid) and insensible (vapour) form play a major role in ensuring thermophysiological comfort of the wearer. Besides moisture transmission properties, air permeability also affects the comfort properties of clothing. Too high air permeability per unit area of a fabric gives lowers the protection against winds especially for outer wear garments, while too low air permeability affects body perspiration. Apart from transmission properties of air and moisture, absorbency of fabric is also significant. The ability of liquid water absorbency of the material determines how much liquid water can be absorbed by the clothing material from the skin. The perception of dampness will be higher when the moisture is held as free liquid, rather than an internally absorbed [1]. Hence, a low absorbent fabric will feel damper than the higher one at same percentage of excess moisture. Therefore, for a particular end-use it is necessary to select fabrics with appropriate air and moisture transmission and water absorbency characteristics. In the course of time, considerable efforts have been made

in identifying the key factors and their effects on thermophysiological comfort of fabric. It is obvious that the composition of textile materials in combination with several other factors like yarn structure or fabric constructional parameters greatly influence thermophysiological comfort of the fabric. The subject is further complicated by the type of the finish applied. The application of the finish, both mechanical and chemical, is quite common for imparting desirable characteristics, including look, feel and tailorability to the fabric. The finish applied to the fabric modifies the surface as well as morphological structure of the textile and hence is expected to affect the transmission properties of the fabric. Though a number of studies have been carried out to investigate the effect of fibre profile, yarn structure and fabric constructional parameters on the transmission properties of fabric, very few systematic studies have been carried out on the effect of chemical finish usually applied to the fabric. Furthermore, whatever studies carried out in this direction mostly focus on polyester, cotton, viscose and their blends. The availability of literature on blends of high wet modulus regenerated cellulose fibre is limited. Hence, the present study has been undertaken to identify and analyze the response of air and moisture transmission properties of fabric woven with polyester – modal blended yarn in varying proportions to chemical finishing.

1 Material and Method

1.1 Materials

Murata Jet Spun (MJS) yarn and ring yarn spun from blends of polyester and modal fibres. The specification of polyester and modal fibres used in the study is given in Table 1.

Tab. 1: *Specifications polyester and modal fibre*

Fibre Characteristics	Polyester	Modal
Staple Length (mm)	44	44
Fineness (Denier)	1.4	1.2

Source: Own

1.2 Preparation of samples

1.2.1 Preparation of yarn sample

A predetermined quantity (depending on the required blend percentage mentioned in Table 2 of hand opened polyester and modal fibre were mixed (stack blending) and opened again in the blender. The opened material is hand fed to carding. Two draw frame passage including one with auto leveler as finisher (RSB-851 drawframe) is given to prepare drawn sliver which is used for spinning two ply warp yarn (ring spun) and the same sliver is given additional passage to adjust the hank for Murata Jet Spun (MJS) yarn which is used as weft.

Tab. 2: *Experimental plan for preparation of fabric sample to study the effect of finishing on polyester modal fabric of different blend percentage*

Sample code	**Details of fabric sample preparation**		
Sample Ref no	**Polyester content (%)**	**Concentration of resin (gpl)**	**Concentration of softener (gpl)**
F1	35	60	20
F2	35	100	20
F3	65	60	20
F4	65	100	20
F5	35	80	10
F6	35	80	30
F7	65	80	10
F8	65	80	30
F9	50	60	10
F10	50	60	30
F11	50	100	10
F12	50	100	30
F13	50	80	20
F14	50	80	20
F15	50	80	20

Source: Own

1.3 Fabric sample preparation

The fabric samples for this project are woven in a non-automatic sample loom. The warp and weft used in all the fabric samples are 2/40s Ne. and 30sNe respectively. For all the fabric samples the blend composition of warp and weft are kept identical. The other constructional parameters e.g. weave, ends and picks per cm) are given below.

Ends /cm: 32 Picks/cm: 28 Construction: 3/1 twill

1.3.1 Finishing of fabric

In order to study the effect of finishing on moisture transport properties, the fabrics of three different blends are treated with different concentration of anti-crease finishing agents and softener. The concentration of anti-crease finishing agent and softener used for chemical treatment for different blends are decided based on Box and Behnken design of experiments. The actual values of three variable (e.g. blends and concentration of softener and anti-crease resin used in the study corresponding to the coded levels are given in the Table I. The process flowchart for chemical finishing is shown below.

1.3.1.1. Process sequence of finishing

Grey fabric → washing with non ionic detergent → drying → heat setting in stenter (at 2000c) → finishing with softener and anti-crease finishing agent (varying concentration of anti-crease resin and softener) in stenter, following pad – dry – cure method as suggested by the supplier of the chemicals.

1.3.1.2. Application of finish to the fabrics

The fabric is padded with required amount as mentioned in the experimental plan (given in Table 2) of Cresotex – ULFC (low formaldehyde content DMDHEU resin) along with Ceraperm K M (modified silicone softener) at pH of 4 at 65% wet pick up. The treated fabric is dried and subsequently cured at 1600 C in a stenter at a speed of 20m/min.

1.4 Test methods

Fabric properties

1.4.1 Air permeability

Air permeability of fabric was measured in SDL Air Permeability Tester in accordance with IS 11056-1984 standard. Ten specimens with area 508 mm^2 (25.4 mm diameter) were tested for each sample to determine the mean value.

1.4.2 Moisture Vapour Permeability

Moisture vapour transmission rate of fabric was measured in SDL Moisture vapour permeability tester in accordance with ASTM: E-96-05 standard. Ten specimens were tested for each sample to determine the mean value in gm/m2/24 hrs.

1.4.3 Vertical Wicking

Vertical wicking test is carried out in accordance with the standard BS 3424 method 21 (1973). In this test a strip of fabric (25 cm x 2 cm) was suspended vertically with its lower edge in a reservoir of distilled water. The rate of rise of the leading edge of the water was then measured. To detect the position of the water head blue ink was added to the water. The measured height of rise in 30 minutes is taken as a direct indication of the wickability of the test fabrics. Ten specimens from each sample were taken to determine the mean wicking height. The same procedure was repeated also for weft direction.

1.4.4 Total absorbency

Total absorbency of water was measured by a static immersion test as mentioned in BS 3449. In this method four specimens, each 80 mm x 80 mm, were conditioned, weighed and then they were immersed in distilled water for 20 minutes to a depth of 10cm using a wire stick. The samples were taken out and the excess water was removed. Then they were transferred directly to pre-weighed airtight containers and weighed again. The absorbency of fabric was calculated and the weight of water absorbed expressed as a percentage of the dry weight of the fabric.

$$\text{Water absorbency in \%} = (B - A) / A \times 100 \quad (1)$$

Where, A = specimen weight before immersion (g) and B = specimen weight after immersion (g)

1.5 Analysis of the test results

Response of moisture transport properties of polyester- modal blended fabrics at different blend levels to finishing treatment (combination of anti-crease resin and softener at varying levels) is analyzed by employing Design of Experiment as proposed by Box-Behnken. Mathematical models (in form of regression equations) have been developed to predict the value of dependent variables using SYSTAT 13 statistical package. The corresponding significant tests of model equations were carried out on the basis of correlation coefficient (R), coefficient of determination (R2), standard error. For visualization of the interaction effect, response surface graph were plotted taking two independent variables at a time (keeping the third variable at centre level). For Response surface Plot statistical software package SIGMAPLOT version 12 was employed.

2 Results and discussions

Results of the experiments and their statistical analysis for test significance to assess the effect of various independent variables (e.g. polyester content in the blend, concentration of resin and softener) in isolation and their interactions on the response variable are presented in Table 3, 4, and Table 5 respectively. Response surface equations for the dependent variables are given in the Table 6.

Tab. 3: *Thermophysiological comfort properties of polyester modal blended fabrics after chemical finishing*

Code No.	Air Permeability ($cc/sec/cm^2$)	Moisture Vapor Permeability ($gm/m^2/day$)	Wicking height (mm)		Total Absorbency (%)
			Warp Way	Weft Way	
F1	24.85 (33.67)*	1,535.00 (1610)	49 (99)	46 (71)	168.6 (247.2)
F2	25.56	1,556.00	62	57	166.87
F3	27.87 (36.76)	1,410.00 (1496)	54 (107)	51 (87)	147.6 (214.8)
F4	26.78	1,435.00	65	60	142.7
F5	32.45	1,562.00	66	62	189.5
F6	23.21	1,512.00	42	37	136.8
F7	33.76	1,410.00	64	58	157.5
F8	23.55	1,395.00	44	40	133.7
F9	31.22 (34.23)	1,485.00 (1554)	59 (104)	53 (79)	167.4 (233.1)
F10	24.61	1,457.00	44	41	138.6
F11	32.89	1,479.00	67	59	185.6
F12	22.65	1,430.00	58	56	137.8
F13	26.54	1,443.00	62	57	146.0
F14	25.97	1,446.00	64	62	147.5
F15	26.15	1,449.00	61	58	149.5

**Values within the parenthesis indicate the value of that particular parameter of the corresponding heat set blended fabric before application of the chemical finish.*
Source: Own

Tab. 4: *Thermophysiological comfort properties of polyester modal blended fabrics after chemical finishing*

Code No.	Thermal Conductivity (W/m/K)	Thermal Resistance (m^2K/W)	Thermal Absorptivity ($Ws^{1/2}m^2K^{-1}$)
F1	40.3 (43.2)	28.4 (25.8)	0.127 (0.148)
F2	40.6	28.3	0.129
F3	41.7 (43.4)	27.6 (26.7)	0.138 (0.146)
F4	40.2	28.7	0.128
F5	41.4	27.5	0.136
F6	41.3	27.1	0.140
F7	41.3	27.9	0.139
F8	40.7	27.7	0.126
F9	39.8 (43.7)	29,3 (25.9)	0.125 (0.148)
F10	40.9	28.2	0.127
F11	42.2	26.8	0.143
F12	41.8	27.0	0.139
F13	40.8	28.8	0.128
F14	39.4	28.9	0.126
F15	39.8	28.6	0.128

** Values within the parenthesis indicate the value of that particular parameter of the corresponding heat set blended fabric before application of the chemical finish.*
Source: Own

Tab. 5: *ANOVA test results for significance testing*

Factor / **Properties**	**Air permeability**	**Moisture vapour Permeability**	**Wicking height (warp)**	**Wicking height (weft)**	**Total absorbency**
Polyester% (A)	s	s	s	S	s
Conc. of Resin (B)	ns	s	s	s	ns
Conc. of softener (C)	s	s	s	s	s
A*A	ns	ns	ns	ns	ns
B*B	ns	ns	s	s	ns
C*C	s	ns	s	s	s
A*B	S	ns	s	s	ns
B*C	ns	ns	ns	ns	ns
A*C	ns	ns	ns	ns	ns

s – Significant at 95% confidence level; ns – Not significant at 95% confidence level
Source: Own

Tab. 6: *Response surface equation for thermophysiological comfort properties of polyester-modal fabric to blend composition, R and S concentration*

Properties	**Response surface equation**	**R**	**R^2**	**R^2_{adj}**	**S.E.**
Air permeability ($cc/sec/cm^{2)}$	25.131 – 0.103 P – 0.233 R – 730S + 0.001 P * P + 0.001 R * R + 0.018 S * S – 0.001 P * R – 0.005 R * SOFTENER – 0.002 P * S	0.995	0.990	0.972	55.672
Moisture vapour permeability ($gm/m^2/day$)	2222.250 – 15.725 P – 5.760 R – 3.092 S + 0.100 P * P + 0.039 R * R + 0.012 S * S – 0.003 P * R – 0.026 R * S + 0.058 P*S	0.989	0.978	0.938	13.283
Vertical wicking height (mm) (warp way)	–10.852 + 1.807 P – 0.587 R – 0.017 S-0.017 P * P – 0.002 R*R – 0.044 S * S – 0.002 P *R + 0.007 R * S + 0.007 P * S	0.969	0.940	0.831	3.554
Vertical wicking height (mm) (weft way)	–16.139 + 1.847 P + 0.615 R – 0.008 S – 0.019 P * P – 0.003 R * R – 0.055 S * S – 0.002 P * R + 0.011 R * S + 0.012 P * S	0.934	0.873	0.643	4.945
Total absorbency (%)	355.068 – 2.710 P + 0.015 R – 0.038 S + 0.013 P * P – 0.015 R * R – 0.038 S * S – 0.003 P * R – 0.024 R * S + 0.048 P * S	0.989	0.979	0.941	4.267
Thermal Conductivity	No correlation could be observed among the dependent and independent variables				
Thermal Resistance					
Thermal Absorptivity					

Source: Own

2.1 Air permeability

The response of air permeability of finished fabric to the polyester content, resin and softener concentration is shown in the Figure 1 to Figure 4. High value of $R^2_{adjusted}$ shows that the regression model for air permeability correlates well with the variable. ANOVA results for the regression model (Table 5) shows that the significant factors that affect the air permeability are concentration of the softener and polyester content. It can be seen from the response surface plot that air permeability is negatively influenced by softener concentration. This may be because of the fact that the softener molecules develop a smooth micro film over the (macro emulsion) yarn surface [2] which reduces the permeability of the fabric. Further, it can be seen that for given concentration of softener air permeability increases with increase in polyester content .This might be because of the fact that polyester fibres due to circular cross section and low intrinsic flexural rigidity can pack closely in the yarn leading to reduction in diameter [3]. Thus inter-yarn space increases which causes more air to pass. However, this effect is offset at higher concentration of softener due to more deposition of micro layer over the fabric.

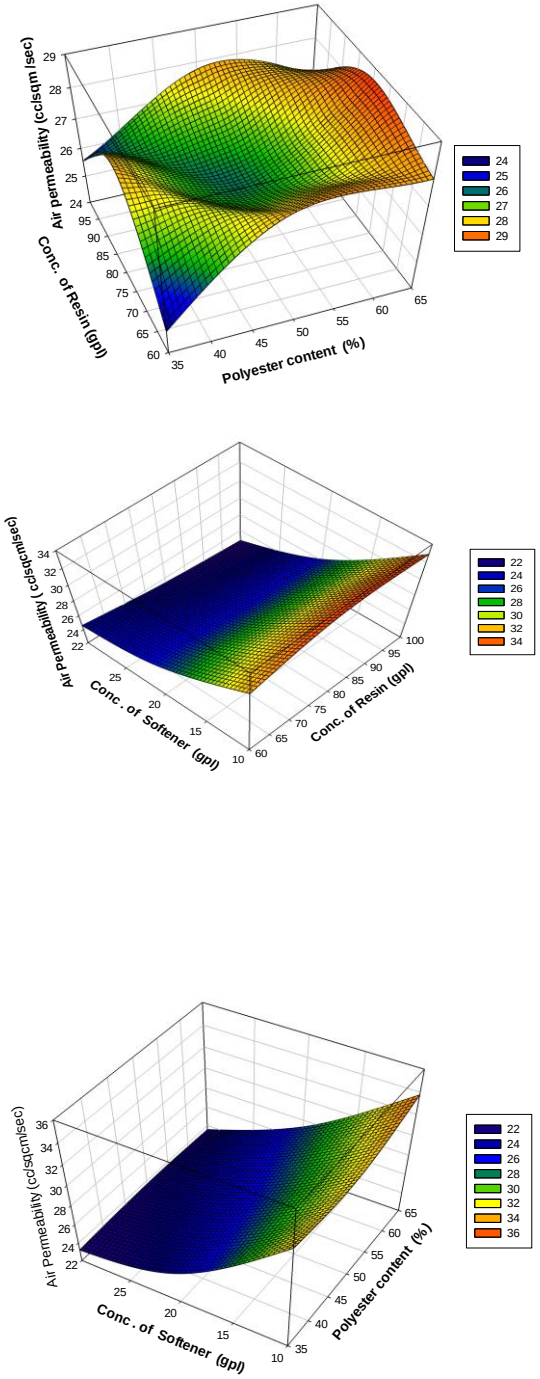

Source: Own

Fig. 1: *Effect of Polyester content, concentration of softener and resin on air permeability of finished polyester- modal blended fabric*

2.2 Moisture vapour permeability

The response moisture vapour permeability (MVP) of finished fabric to the polyester content, resin and softener concentration is shown in the figure. High value of R^2 and $R^2_{adjusted}$ and the negligible difference between them confirms that the good correlation between the dependent and independent variables and the proposed regression model is significant at 95% confidence level. It is evident that moisture vapour permeability of finished fabric reduces with the increase in polyester content and concentration of softener. This behavior can be explained by

the moisture vapour transmission mechanism which takes place by diffusion and sorption-desorption [4]. Water vapour diffuses through a textile structure in two ways, simple diffusion through the air spaces between the fibers and yarns and along the fiber itself [4]. For a given construction of fabric the diffusion rate along the textile material depends on the water vapour diffusivity of the fiber, which increases with the increase in moisture regain [5]. So as the modal fibre proportion in the blended fabric increases (i.e. polyester portion reduces), moisture regain of the material increases causing higher diffusivity. With the increase in the modal component in the fabrics, more amount of moisture is absorbed in the fibrous structure and then distributed for evaporation over a wider area rather than liquefying locally in one region [6]. In the same way moisture transfer through sorption-desorption process will increase with the hygroscopicity of the material. A hygroscopic fabric has a better ability to absorb water vapour from the humid microclimate and release it in dry air. This enhances the flow of water vapour from the microclimate to the environment in comparison with a fabric which absorbs less water vapour and reduces the moisture built up in the microclimate.

It can be seen from the response surface plot that presences of softener significantly reduce the moisture vapour permeability in all cases irrespective of level of other variables. The methyl groups of the OSi(CH3)2- structure shield the oxygen atoms from outside contact. Therefore, the surface of fibres finished with polydimethylsiloxane is mostly non-polar and hydrophobic [2]. In the case of cellulosic fibres, there are strong hydrogen bonds between the hydroxyl group present in the fibres and modified di-methyl silicone. These bonds act as an anchor for the silicone, which forms an evenly distributed film on the fibre surface and hence results in hydrophobic surface [2]. This prevents building up of moisture concentration and reduces moisture vapour permeability. Moisture vapour permeability is lowest at high polyester content and softener concentration which is quite evident from the above discussions. The response surface plot reveals that there is marginal though significant increase in moisture vapour permeability with increase in concentration of resin. This may be attributed to the fact that the application of resin (durable press finishes) increases the pore volume in the fibrous strand [7] leading to more diffusion of water vapour through the interfibre spaces within the yarn. However, in all the cases the moisture vapour permeability of the fabric is lower as against the grey stage irrespective of concentration of softener and resin used in the study. This is attributed to surface deposition of softener on the yarn surface suppress the effect of other variables.

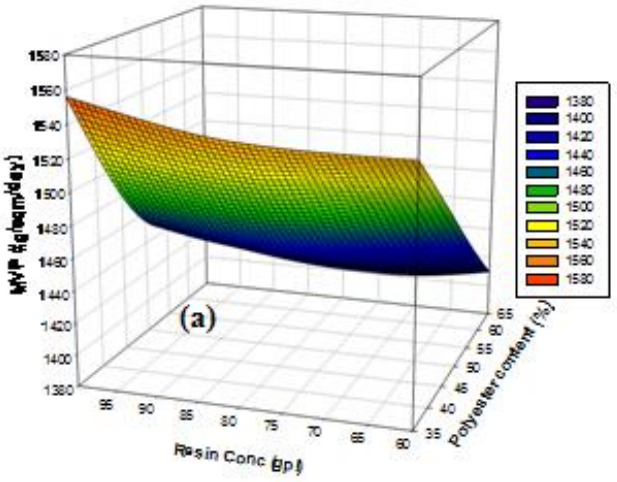

(a)

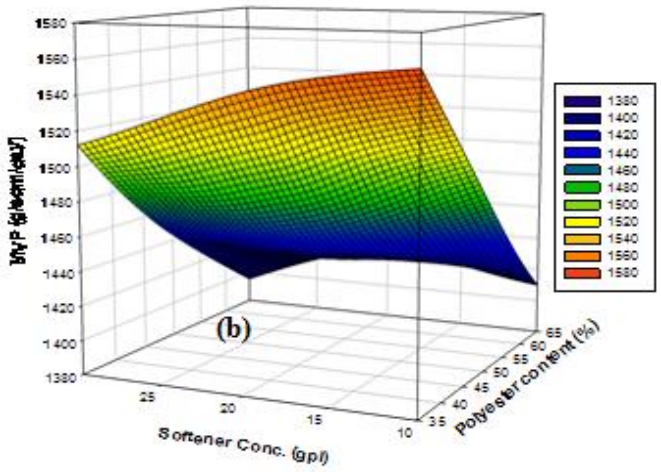

(b)

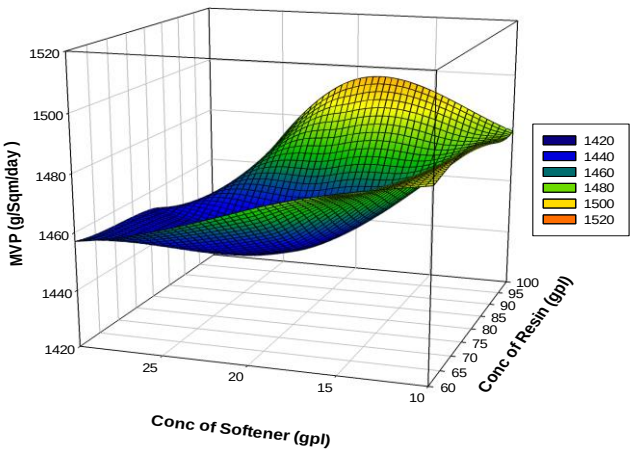

(c)

Source: Own

Fig. 2: *Effect of Polyester content, conc. of softener and resin on moisture vapour permeability of finished polyester – modal blended fabrics*

2.3 Wicking height

The response of warp and weft way wicking height of finished fabric to the polyester content, resin and softener concentration is shown in the figure. The wicking of the fabric in warp and weft behaves in the similar way except the fact that wicking height of the former is always higher. This is undoubtedly because of two ply and coarse yarn used in warp which favours wicking. High value of R^2 and $R^2_{adjusted}$ and the negligible difference between them confirms that the good correlation between the dependent and independent variables and the proposed regression model is significant at 95% confidence level. It can be seen that wicking height reduces with increase in softener concentration. This is expected as the softener form a hydrophobic layer on to the surface of yarn which increases the time of wetting and causes delayed wicking .The increase in concentration of resin results in the increase in pore volume. Further, the hydroxyls groups of cellulose present in modal component reacts with the resin and are thus unavailable to interact with water when water moves up along the capillary. This might be the reason for increased wicking height at higher concentration. Presence of increased amount of hydrophobic fibre component favours wicking as it does not form bonds with water molecules [8], though the effect is much less pronounced after finishing .This might be because of the fact that after finishing the hydroxyl groups in modal fibres already form cross link with resin molecules. The water molecule after wetting the fabric dragged very smoothly and enhances the wicking phenomena.

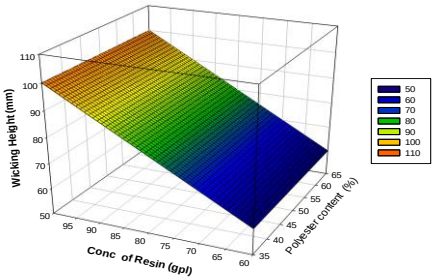

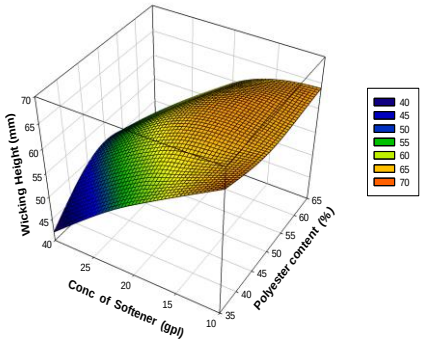

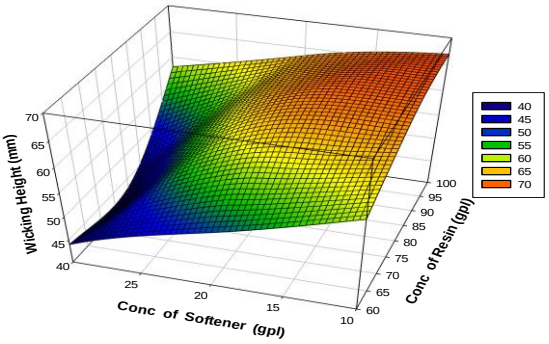

Source: Own

Fig. 3: *Effect of polyester content , conc. of resin and softener on wicking height (warp way) of polyester – modal blended fabric*

2.4 Total absorbency

Regression analysis shows that the variables that influence the total absorbency of the fabric are polyester content in the fabric and softener concentration. Both of them negatively influence the total absorbency of the fabric. Absorbency as determined by the static method

indicates the water retaining capacity of the fabric which is in turns governed by the construction of fabric and the presence of hydrophilic group in the material. As the fabric constructional parameter remains the same in all cases, the increase in hydrophobic polyester content steadily decreases the absorbency of the fabric absorbency of the fabric. Further, it can be seen that absorbency reduces with an increase in softener concentration. This is expected as the softener forms a hydrophobic layer on to the surface of yarn which increases the resistance of water takes up.

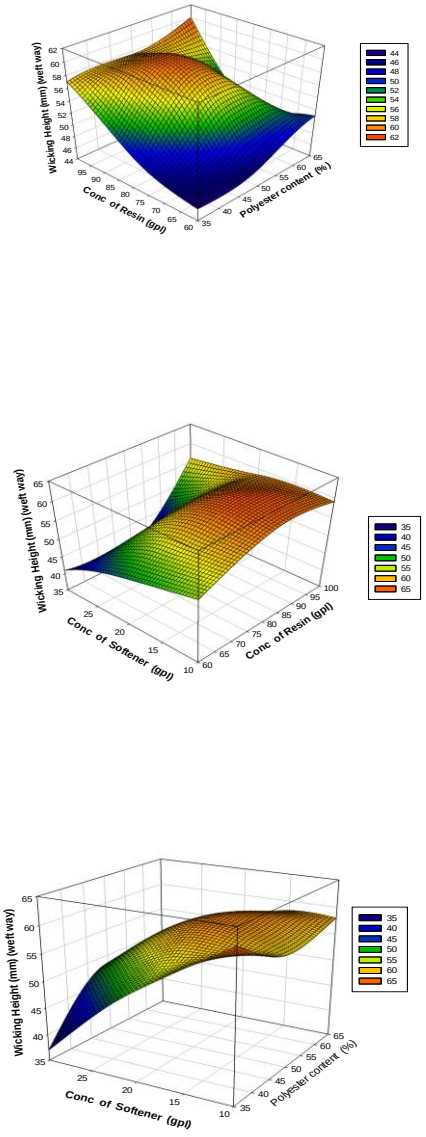

Source: Own

Fig. 4: *Effect of polyester content, conc of resin and softener on wicking height (weft way) of finished polyester – modal blended fabric*

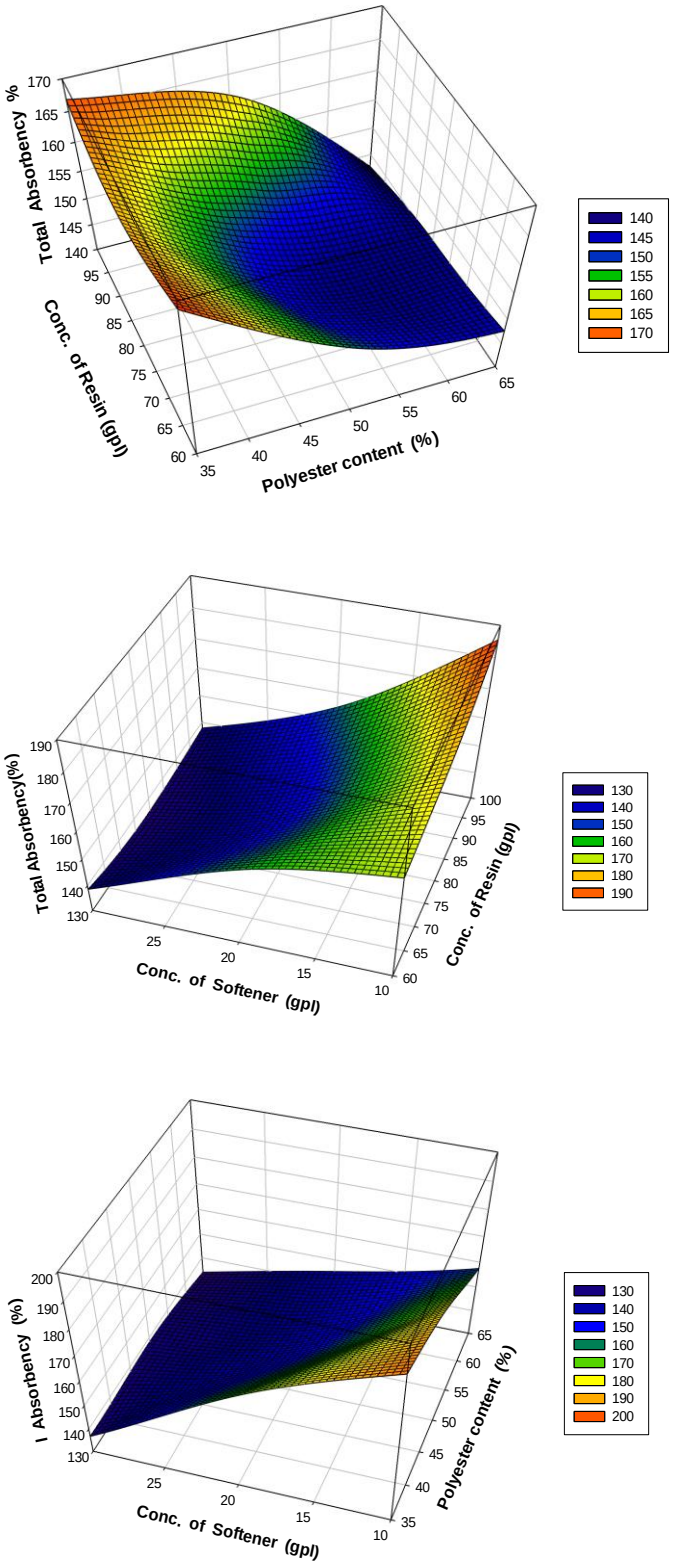

Source: Own

Fig. 5: *Effect of polyester content, concentration of resin and softener on absorbency of finished polyester modal blended fabric*

2.5 Thermal properties of the finished fabrics

It can be seen that irrespective of blend and concentration of finishing ingredients (e.g. resin and softener) there is an increase in thermal conductivity and absorbency and increase in thermal resistance. However, no definite trend could be observed with respect to the concentration of resin and silicon softener. This may attributed to the fact that variation of the concentration of finishing agent does not bring about any major change in construction of the fabric. Decrease in thermal conductivity of the fabric after finishing may be explained considering the fact that there is resistance to transfer heat from the body to the surrounding air as the sum of three parameters, these being (i) the thermal resistance or conductivity to transfer of heat from the surface of the material (ii) the thermal resistance or conductivity of the clothing material and (iii) the thermal resistance of the air in the inner layer. After finishing, thermal conductivity of clothing material is found to be reduced as it becomes less permeable to air. Further, thermal resistance value as measured by Alambeta increases after finishing as the thickness measured by Alameta increases marginally.

Another parameter measured in the same instrument, is thermal absorptivity, a determinant of the 'warm-cool feeling" of textiles which measures the contact temperature of two bodies, found to decrease after finishing. Thermal absorptivity is a surface property and it is a measure of the heat flow q (W/m2) which passes between the human skin and the contacting textile fabric. It is directly proportional to conductivity; the lower the value of conductivity, the lower the value of thermal absorptivity. Thus the fabrics after chemical finishing become warmer to touch.

Conclusion

All the moisture transmission properties (both in form of liquid water and vapour) and air permeability of finished fabric are negatively influenced by the concentration of silicon softener. Air permeability is reduced because of the formation of a film over the surface of the fibre and yarn which cause obstruction to the passage of air where moisture transmission and absorption properties are affected because of the hydrophobic character of softener and development film over the surface which reduces the rate of diffusion through the pores.

The concentration of resin does not influence the air permeability of the fabric, but it improves the moisture vapour permeability, the improvement, though marginal, is significant irrespective of blend percentages.

The water absorbing capacity of fabric is invariably reduced with the increase in both polyester and softener concentration. But the same remains unchanged with the increase in resin concentration.

The wicking power is increased with the increase in polyester component and resin concentration. The resin forms bond with the hydroxyl groups of modal fibre and prevents them from interfering at the time of the rise of water column through the capillary.

Under all experimental conditions the moisture transmission (both wicking and moisture vapour permeability), absorbency and air permeability of grey fabric reduces after finishing at all blends levels. Irrespective of blend and concentration of finishing ingredients (e.g. resin and softener) there is an increase in thermal conductivity and absorbptivity and an increase in thermal resistance. However, no definite trend could be observed.

Unlike softener, resin does not have any significant influence on total absorbency of fabric.

Literature

[1] PLANTE, A. M.; HOLCOMBE, B. V.; STEPHENS, L. G.: Fiber hygroscopicity and perceptions of dampness, Part I: Subjective of dampness, Part I: Subjective Trial, *Text. Res. J.*, Vol 65, No 5, 1995, pp. 293-298.

[2] BERRECK .A, WEBER B. *Melliand Textilberichete*. 2000, 81, 11/12,992-997.

[3] CHENG, K. P. S.; CHEUNG, Y. K.: Feb 48-50, Textile Asia, 1994.

[4] BROJESWARI, Das; A. Das; KOTHARI, V. K.; FANGUEIRO, R.; ARAÚJO, M: Moisture Transmission Through Textiles, Part I: Processes Involved In Moisture Transmission And The Factors At Play, *Autex Res. J.*, Vol 7, No 2, June 2007, pp. 100-110.

[5] MORTON, W. E.; HEARLE, J. W. S.: Physical Properties of Textile Fibers. *The Textile Institute*. Manchester, U.K., 1962, pp. 170.

[6] SLATER, K.: Testing and Quality Management. *The Textile Institute*. Manchester, U.K., Chapter Thermal Comfort Properties of Fabrics, pp. 383.

[7] RHEE, H.; YOUNG, R. A.; SARMADI, A. M.: The Effect of functional finishes and laundering on Textile Materials Part II, Characterization of Liquid Flow, *J Text ,Inst'* 1993, 84, No 3406-418.

[8] BROJESWARI, Das; APURBA, Das; KOTHARI, V.; FANGUIERO, R.; ARAÚJO, M. D.: Moisture Flow through Blended Fabrics – Effect of Hydrophilicity Journal of Engineered Fibers and Fabrics, Volume 4, Issue 4 – 2009 *Fiber and Textile Research in India*, pp 20-27.

[9] FRYDRYCH, I.; DZIWORSKA, G.; BILSKA, J.: Comparative Analysis of the Thermal Insulation Properties of Fabrics Made of Natural and Man-Made Cellulose Fibres. *FIBRES & TEXTILES in Eastern Europe*. October/December 2002, pp 40-44.

ODEZVA VZDUCHU A PAROPROPUSTNOST TKANINY UTKANÉ ZE VZDUCHEM PŘEDENÉHO POLYESTERU

Přenos vlhkosti přes textil, který probíhá prostřednictvím potu, a to jak párou, tak v tekuté formě, má velký vliv na termofyziologický komfort lidského těla. Kromě samotných vlastností paropropustnosti také ovlivňuje komfort oděvů. Aplikace povrchové úpravy, a to jak mechanickou, tak chemickou cestou, běžně dodává textilnímu materiálu žádoucí vlastnosti, včetně jejího vzhledu, omaku a možnosti dalšího zpracování. Povrchová úprava aplikovaná na textilní materiál upravuje její povrch, stejně jako morfologickou strukturu textilie, a proto se očekává, že bude mít vliv na přenosové vlastnosti látky. Záměrem této studie bylo identifikovat a analyzovat odezvu vzduchu a paropropustnost tkaniny utkané ze vzduchem předeného polyesteru – modálních směsových přízí (v útku) s chemickými dokončovacími pracemi. V této studii je popsáno, jak jsou látky ze tří různých směsí ošetřovány různou koncentrací nemačkavé pryskyřice (DMDHEU) a změkčovadla (upravený křemík). Koncentrace prostředku proti mačkání a aviváže používaných pro účely chemického ošetření je určována na základě experimentálního designu Box a Behnken. Matematické modely (ve formě regresních rovnic) byly vyvinuty s cílem předvídat termofyziologický komfort pomocí parametrů statistického balíčku Systat 13. Bylo zjištěno, že za všech experimentálních podmínek přenosu vlhkosti se savost a prodyšnost šedé tkaniny snižuje po ukončení na všech úrovních prolnutí. Přenos vlhkosti a prodyšnost hotové textilie jsou negativně ovlivněny koncentrací křemičitého změkčovače. Koncentrace pryskyřice nemá vliv na prodyšnost tkaniny, ale částečně zlepšuje paropropostnost, i když statisticky nevýznamně. Odvod energie se zvyšuje s nárůstem polyesterové složky a koncentrace pryskyřice, ten však nemá na rozdíl od změkčovače žádný významný vliv na celkovou nasákavost tkaniny.

DIE REAKTION DER LUFT UND DIE VERDUNSTUNGSDURCHLÄSSIGKEIT VON GEWEBEN AUS MIT LUFT GESPONNENEM POLYESTER

Die Übertragung von Feuchtigkeit über Textilien, die sowohl als Ausdunstung als auch in flüssiger Form über den Schweiz verläuft, hat einen großen Einfluss den thermophysiologischen Komfort des menschlichen Körpers. Außer den eigentlichen Eigenschaften der Verdunstungsdurchlässigkeit beeinflusst er ebenso den Komfort der Kleidung. Die Anwendung der Oberflächenbearbeitung, und zwar sowohl der mechanischen als auch der chemischen, verleiht dem Textilmaterial in der Regel die erforderlichen Eigenschaften, inklusive des Aussehens, des Tastgefühls und der Möglichkeit weiterer Verarbeitung. Das Ziel dieser Studie bestand darin, die Reaktion der Luft und die Verdunstungsdurchlässigkeit des aus mit Luft gesponnenem Polyester gewobenen Stoffes zu identifizieren und zu analysieren. In dieser Studie wird beschrieben, wie Stoffe aus drei verschiedenen Mischungen mit einer unterschiedlichen Konzentration aus knitterfestem Harz (DMDHEU) und einem Weichmacher behandelt werden. Die Konzentration des Mittels gegen Knittern und die Avivage, die für Zwecke der chemischen Behandlung Verwendung finden, wird auf Grundlage des experimentellen Designs Box und Behnken bestimmt. Die mathematischen Modelle (in Form von Regressionsgleichungen) wurden mit dem Ziel entwickelt, den thermophysiologischen Komfort mit Hilfe der Parameter des statistischen Pakets Systat 13 vorherzubestimmen. Dabei wurde festgestellt, dass unter sämtlichen experimentellen Bedingungen der Feuchtigkeitsübertragung die Saugfähigkeit und die Luftdurchlässigkeit des grauen Gewebes auf allen Durchdringungsebenen gesenkt werden. Die Feuchtigkeitsübertragung und die Luftdurchlässigkeit fertiger Textilien werden durch die Konzentration eines quarzigen Enthärters in negativer Weise beeinflusst. Die

Harzkonzentration hat keinerlei Auswirkung auf die Luftdurchlässigkeit des Gewebes, verbessert aber teilweise die Verdunstungsdurchlässigkeit, wenn auch statistisch in unbedeutendem Maße. Die Ableitung von Energie erhöht sich mit dem Anstieg der Polyesteranteile und der Harzkonzentration. Dieser Anstieg hat jedoch im Unterschied zum Enthärter keinen bedeutenden Einfluss auf die Wasseraufnahmefähigkeit des Gewebes.

RUCH POWIETRZA A PAROPRZEPUSZCZALNOŚĆ TKANINY WYKONANEJ Z PRZĘDZY POLIESTROWEJ TEKSTUROWANEJ POWIETRZEM

Przepuszczanie wilgoci przez tkaninę, które zachodzi poprzez pot, zarówno w formie pary, jak i w postaci ciekłej, ma duży wpływ na termofizjologiczny komfort ciała człowieka. Pomijając właściwości jako takie, paroprzepuszczalność wpływa także na komfort ubrań. Zastosowanie odpowiedniego wykończenia, zarówno mechanicznego, jak i chemicznego, nadaje tkaninie pożądane właściwości, w tym wygląd, cechy odczuwane w dotyku oraz możliwości dalszego przetworzenia. Wykończenie warstwy wierzchniej tkaniny zmienia jej powierzchnię oraz strukturę morfologiczną i dlatego zakłada się, że będzie miało wpływ na przepuszczalne właściwości tkaniny. Celem przeprowadzonych badań było zidentyfikowanie oraz przeanalizowanie ruchu powietrza oraz paroprzepuszczalności tkaniny z przędzy poliestrowej teksturowanej powietrzem – modalnej przędy mieszankowej (w wątku) z chemicznym wykończeniem. W opracowaniu opisano, w jaki sposób tkaniny z trzech różnych mieszanek pielęgnowane są różnymi stężeniami niemnącej żywicy (DMDHEU) oraz zmiękczacza (wzbogacony krzem). Stężenie środka zapobiegającego gnieceniu i płynu do płukania tkanin stosowanych do celów chemicznej pielęgnacji określane jest na podstawie eksperymentalnejgo planu Boxa-Behnkena. Modele matematyczne (w formie równań regresji) opracowano w celu prognozowania termofizjologicznego komfortu przy pomocy parametrów pakietu statystycznego Systat 13. Stwierdzono, że we wszystkich warunkach eksperymentalnych przenoszenia wilgoci chłonność i przewiewność szarej tkaniny zmniejsza się po zakończeniu na wszystkich poziomach przenikania. Na przenoszenie wilgoci i przewiewność gotowej tkaniny negatywnie wpływa stężenie krzemowego zmiękczacza. Stężenie żywicy nie ma wpływu na przewiewność tkaniny, ale częściowo poprawia paroprzepuszczalność, chociaż pod względem statystycznym w sposób nieistotny. Odprowadzanie energii zwiększa się wraz ze wzrostem składnika poliestrowego oraz stężenia żywicy, nie ma o jednak w odróżnieniu od zmiękczacza żadnego istotnego wpływu na ogólną wsiąkliwość tkaniny.

GLOBAL HEAT AND MASS TRANSPORT IN SYSTEM: NEWBORN BABY SKIN – TEXTILE COMPOSITE – SURROUNDING

Ryszard Korycki
*** Izabella Krucinska**

Lodz University of Technology
Faculty of Material Technologies and Textile Design
Department of Technical Mechanics and Computer Science
Lodz, Poland
ryszard.korycki@p.lodz.pl

* Lodz University of Technology
Faculty of Material Technologies and Textile Design
Department of Material and Commodity Sciences and Textile Metrology
Lodz, Poland

Abstract

Global model of heat and mass transport is defined by heat balance with term introducing mass exchange during sweat evaporation. Heat is supplied by metabolic heat production and lost by means of different phenomena. Necessary parameters of neonate body help to solve global correlation for different parameters of bonnet and external clothing. Different cases are discussed to prevent hyperthermia and hypothermia.

Introduction

Heat and mass transport can be described by different physical and mathematical methods although bounding basic rule is always balance formulation. There are two main approaches.

- Physiology of newborn baby, i.e. we introduce metabolic heat production and different heat losses of an organism. Determinant is now the children's body whereas the influence of clothing and surrounding are modelled by means of empirical correlations. Advantages of this approach are: (i) global formulation of transport mechanisms in macro-scale; (ii) description of heat loss by different phenomena; (iii) description of coupled heat and mass transport during evaporation. Disadvantages are now: (i) moisture cannot be determined because the model does not introduce mass distribution; (ii) temperatures are determined globally and there is impossible to describe locally pcm-materials, composite structure of clothing etc.; (iii) correlations are empirical, i.e. description can be not universal.
- Clothing structure, i.e. we determine heat and mass transport within textile composite. Dominant is the textile structure, whereas the children's body and surroundings are modelled by the set of boundary and initial conditions without clear physiological references. The coupled heat and mass transport is described by means of the second-order differential equations. Advantages and disadvantages are described in reverse manner as above.

Let us introduce the first approach, i.e. the global model of heat and mass transport from neonate skin through textile composite to surrounding. Main aspects are the following:

- There is the multiparametric model, i.e. heat is transported by various phenomena, whereas mass by sweat evaporation. Basic heat balance is the global correlation [1, 2],

particular parameters of newborn babies are discussed in [1]. All terms are expressed in $kJ\ h^{-1}kg^{-1}$.

- Multimodal balance is discussed for the whole body, whereas the influence of clothing, covering by the bonnet and surroundings is introduced by appropriate parameters. Balance is formulated for neonate body within an incubator. Heat is supplied by metabolic heat production $\dot{M}$; lost and accumulated by conduction K, radiation on external surfaces R, convection on external surfaces C as well as skin evaporation E. Global segmental heat losses are convection C_{resp} and evaporation E_{resp} from the mucosa of respiratory tract.

1 Model description

The only heat source of neonate is metabolism which can be determined empirically as the function of postnatal age A expressed in days by following correlation.

$$\dot{M} = \left(0{,}00165A^3 - 0{,}138A^2 + 3{,}56A + 35{,}4\right)4{,}185/24 \tag{1}$$

Heat is lost in 6 parts of newborn baby: head, trunk, two arms and two legs. Global heat balance can be also defined in the general form.

$$\dot{M} - \left[\sum_{\text{i, all bodyparts}} \left(R_i + C_i + K_i + E_i\right) + C_{resp} + E_{resp}\right] = S \tag{2}$$

where S is body heat storage rate. According to balance of metabolic heat production $\dot{M}$ and heat losses, we can determine the following cases:

- $S = 0$, i.e. metabolic heat production is balanced by heat lost; thermal equilibrium determines the constant temperature distribution on skin.
- $S > 0$, i.e. metabolic heat production is greater than heat lost to surroundings; heat storage rate is accumulated within the body; the temperature increases, which causes hyperthermia.
- $S < 0$, i.e. metabolic heat production is less than heat lost; there is the heat deficit, and the temperature decreases, which can cause hypothermia.

Next, let us determine all the required terms of thermal balance. All terms are described by exact correlations and different experimental coefficients. Necessary parameters and coefficients are formulated for different heat transport conditions as well as clothing materials.

Heat is lost by conduction for the specified part of children's body K_i through skin contacting the mattress. We can describe this phenomenon by means of the following formula:

$$K_i = h_k \left(T_i - T_m\right) A_{ki} W_t^{-1} \tag{3}$$

where h_k=0.84 $kJ\ h^{-1}m^{-2}$ is conductive heat transfer coefficient; T_i–T_m denotes temperature difference between the skin surface of particular body segment and mattress in $°C$; A_{ki} is local skin contact area described in m^2; W_t is neonate body mass described in kg.

Heat loss by radiation at skin surface R_i can be described typically as difference of fourth power of temperatures. Thus, this term can be described in following manner.

$$R_i = \sigma\, \varepsilon_{sk}\, A_{ri} \left[\left(T_i + 273\right)^4 - \left(T_r + 273\right)^4\right] F_{cl} W_t^{-1} \tag{4}$$

where $\sigma=5.666667\cdot10^{-8}$ *kJ* $h^{-1}m^{-2}K^{-1}$ is the Stefan-Boltzmann constant; $\varepsilon_{sk}=0.97$ is skin emissivity; A_{ri} is effective surface area of skin segment subjected to radiation in m^2; T_r is mean temperature of radiation measured by infrared thermometer in °*C* according to [3]; T_i is mean temperature of skin segment measured similarly in °*C*; F_{cl} is dimensionless reduction factor of thermal radiation and convection by clothing, $F_{cl}=0.86$ for combined medical clothing made of PVC foil and fabric, $F_{cl}=0.98$ for special clothing made of PVC foil, the range is from $F_{cl}=1$ for impermeable textiles to $F_{cl}=0$ for completely permeable clothing.

Heat loss by convection at skin surface C_i depends on the heat flow described by a temperature difference. It can be described mathematically as follows:

$$C_i = h_{ci}\left(T_i - T_a\right)A_{ci}F_{cl}W_t^{-1} \tag{5}$$

where h_{ci} determined in *kJ* $h^{-1}m^{-2}°C^{-1}$ describe convection coefficient of the specified part of neonate body; $T_i–T_a$ denotes temperature difference between the skin surface of body segment and surrounding air in °*C*; A_{ci} defines effective surface area of skin segment subjected to convection in m^2.

Heat flow by evaporation at skin surface is the only possibility to transport the mass (i.e. sweat) from skin to surrounding. It depends on the difference of water vapor partial pressure between skin and surrounding. Maximal evaporative heat flow is caused by sweat evaporation from the whole skin surface. Now, we can denote mathematically [1, 2]:

$$E_i = \left(P_{s,H_2O} - P_{a,H_2O}\right)R_{dyn}^{-1} = h_{ei}w\left(P_{s,H_2O} - P_{a,H_2O}\right)A_{ei}F_{pcl}W_t^{-1} \tag{6}$$

where $P_{s,H20}–P_{a,H20}$ is difference of water vapor partial pressure between skin $P_{s,H20}$ and surrounding $P_{a,H20}$, atmospheric pressure is $P_{a,H2O}=1\cdot10^5$ *hPa*; R_{dyn} is dynamic total evaporative resistance of clothing and boundary layer of air in m^2 *kPa* W^{-1}; $h_{ei}=1.67\ h_{ci}$ denotes evaporative heat transfer coefficient of specified body segment in *kJ* $h^{-1}mb^{-1}m^{-2}$ and as it can be determined from Levis equation, w is relative humidity of skin segment, $w=0.06$ for moderate temperature and dry skin, this parameter describe influence of clothing; $A_{ei}=A_{ci}$ is an effective surface area of skin segment subjected to evaporation in m^2; F_{pcl} is dimensionless reduction factor of mass transport by clothing, the range is from $F_{pcl}=1$ for completely permeable clothing to $F_{pcl}=0$ for impermeable textiles.

Irrespective of heat losses defined for the specified body segments, there are two components determined in respiratory tract i.e. segmental heat losses by convection C_{resp} and evaporation E_{resp}. Both can be described as follows.

$$C_{resp} = \dot{V}_E C_P\left(T_E - T_l\right)W_t^{-1}\ ;\ E_{resp} = \dot{V}_E\delta\left(M_E - M_l\right)W_t^{-1} \tag{7}$$

where $\dot{V}_E$ is pulmonary ventilation rate in *kg* h^{-1}; $C_p=1{,}044$ *kJ kg* $^{-1}°C^{-1}$ denotes heat capacity of air in normal conditions; T_E defines temperature of exhaled air according to Hanson in °*C*

$$T_E = \frac{32{,}6 + 0{,}066T_a + 32P_{a,H_2O}}{462\left(T_a + 273\right)} \tag{8}$$

$T_l=T_a$ is temperature of inhaled air equal to surrounding temperature °*C*; $\delta=243$ *kJ/g* H_20 denotes latent heat of vaporization, M_E is absolute humidity of exhaled air in *kg* H_20*/kg of dry air* [3]; M_l is absolute humidity of inhaled air in *kg* H_20*/kg of dry air* [3]; P_E is partial pressure of water vapor in exhaled air in *kPa* described as follows

$$M_E = 0{,}622\frac{P_E}{\left(100 - P_E\right)}\ ;\ P_E = 0{,}611\,\mathrm{e}^{\frac{17{,}27T_E}{T_E+273}} \tag{9}$$

2 Model solution

Let us introduce necessary parameters to solve the above model [1]. Surrounding conditions are typical for a nursery. Additionally, front part as well as upper section of incubator are open to the surroundings. The temperature of surrounding air within an incubator changes from initial $T_{a0}=33.2°C$ to final $T_{ak}=31.8°C$ in time $t=30\ min$; speed of change is negative – $0.04°C/min$. The temperature of the surrounding air within a nursery is $T_a=(23.2±0,2)°C$, mean radiation temperature is $T_r=(19.9±0,2)°C$; moisture of the surrounding air is $w=(44±1,9)\%$. Conditions within an incubator are the following: the temperature for mixed air between interior and surroundings $T_a= (23.2±0.2)°C;$ speed of air $v=0.06ms^{-1};$ relative air humidity $w=(35±4)\%$.

Body mass of a neonate is $W_t=(1,060±0,026)kg$; postnatal age is $(4.5±0.4)days$; body surface $(0.100±0.010)m^2$; mean radiation temperature $T_r=30.6°C$.

Surface temperature of mattress is equal to $T_m=(31.4±0.1)°C$.

The same source [1] helps to determine mean temperatures of body segments and convection coefficients as well as areas of the particular parts of a body, cf. Table 1, Table 2. It is immediately obvious that the only part of a body takes an active part in individual form of heat transfer, c.f. from 50% for radiation and convection to 10% for conduction. Neonate clothing is typical medical garment for newborn children transparent for infrared radiation (*98%* of transparence).

Tab. 1: *Temperatures and convection coefficients for particular parts of neonate body*

Particular part of neonate body	Covered		Uncovered	
	T_i °C	$h_{ci}\ kJ\cdot h^{-1}\cdot m^{-2}\cdot °C^{-1}$	T_i °C	$h_{ci}\ kJ\cdot h^{-1}\cdot m^{-2}\cdot °C^{-1}$
Head	35.53±0.72	3.63±0.11	32.82±1.84	3.60±0.17
Trunk	34.93±0.79	2.84±0.09	32.33±1.30	2.82±0.10
Arm (one)	32.10±0.65	4.02±0.03	29.50±1.85	3.97±0.05
Leg (one)	34.36±0.79	3.84±0.04	31.57±1.50	3.82±0.05
Whole body	34.37±0.68	3.63±0.07	31.71±1.76	3.60±0.08

Source: [1]

Tab. 2: *Table 2. Areas of particular parts of neonate body*

Particular part of neonate body	Area · 10^{-3} m^2		
	A_{ri}	A_{ci}	A_{ki}
Head	21.43±0.08	22.63±0.05	1.44±0.04
Trunk	7.10±0.08	1.97±0.07	3.75±0.05
Arm (one)	4.42±0.05	5.40±0.05	0.40±0.05
Leg (one)	10.06±0.04	11.99±0.05	0.90±0.04
Whole body	55.04±0.07	56.76±0.06	7.74±0.05

Source: [1]

Our next goal is to determine the heat loss for particular parts of a neonate body. To simulate the reduction of the heat loss, let us first assume a head is covered by the bonnet. Thus,

thermal insulation of a bonnet I_{cl} can be described in $m^2 \cdot °C \cdot W^{-1}$ by the following empirical correlation.

$$I_{cl} = 0{,}067 \cdot 10^{-2} A_{co} + 0{,}217\, Th\, A_{co} \tag{10}$$

where A_{co} is dimensionless proportional area of head covered by bonnet; *Th* describe material thickness in *m*.

Bonnet can reduce both heat and mass transport to surrounding. Heat reduction factor for radiation and convection can be described according to Nishi and Gagge [4] by means of experimental correlation as follows:

$$F_{cl-head} = \left[\left(h_{c-head} + h_{r-head} \right) I_{cl} + \left(1 + 1{,}971 I_{cl} \right)^{-1} \right]^{-1} \tag{11}$$

where $h_{c\text{-}head} = h_{r\text{-}head}$.

Heat reduction factor for evaporation according to [4] is described experimentally.

$$F_{p\,cl-head} = \left\{ \left(1 + 2{,}22 h_{c-head} \right) \left[I_{cl} - \left[1 - \left(1{,}971 I_{cl} \right)^{-1} \left(h_{c-head} + h_{r-head} \right)^{-1} \right] \right] \right\}^{-1} \tag{12}$$

The main parameter is the time to reach the safety limit (*38˚C*) time of hyperthermia (*40˚C, 43˚C*) and rate of body cooling for hypothermia.

Let us first determine thermal insulation by a bonnet and general heat balance for constant metabolic heat production (Tables 3, 4, 5). We have to discuss the thermal insulation effect of a covering bonnet on hyperthermia (overheating) and hypothermia (overcooling) of an organism.

The heat loss of head by radiation is calculated for different parameters of the bonnet, Table 3. According to mathematical correlations Eq. (10) and Eq. (11), heat resistance depends on two parameters. Material composition does not influence heat insulation. Let us also assume three different material thicknesses (*1mm=0,001m*; *3mm=0,003m*; *5mm=0,005m*) as well as three relative areas of a covering bonnet (*20%*, *60%* and *100%*). A fully covered head is the maximal value and determines maximal heat insulation of a bonnet.

Tab. 3: *Heat loss by radiation for head*

Material thickness [m]	Relative area of covering bonnet		
	20%	60%	100%
0.001	1.726537723	1.463927064	1.26446982
0.003	1.655039492	1.312611774	1.078808162
0.005	1.588556011	1.187095692	0.937262784

Source: Own

Heat loss by radiation can change significantly; maximal difference is about *100%*. It is evident that the most critical part of a neonate with respect to radiation is its head.

Heat loss by convection is determined for the same parameters, Table 4. Convection is a significant phenomenon and it can change considerably. Thus, radiation and convection of a head can change the global heat balance of a neonate organism and prevent hypo- and hyperthermia.

Tab. 4: *Heat loss by convection for head*

Material thickness [m]	Relative area of covering bonnet		
	20%	60%	100%
0.001	0.872631811	0.739902354	0.639092083
0.003	0.836494963	0.663424132	0.545254417
0.005	0.802892685	0.599985422	0.473714133

Source: Own

Heat loss by evaporation is shown in Table 5. Evaporative heat transport is lesser than by radiation and convection. However, it is still a significant value.

Tab. 5: *Heat loss by evaporation for head*

Material thickness [m]	Relative area of covering bonnet		
	20%	60%	100%
0.001	1.662947478	1.410009052	1.217898034
0.003	1.594082603	1.264266867	1.039074495
0.005	1.530047781	1.143373679	0.902742385

Source: Own

Heat can be transported by convection during an immediate contact between a body and a mattress. Convectional heat loss is shown in Table 6 for minimal thickness of the covering bonnet. The obtained values are considerably lower than others, cf. Tables 3, 4, and 5. Consequently, thermal insulation of a bonnet does not influence significantly heat loss by convection.

Tab. 6: *Heat loss by convection for head*

Particular part of neonate body	Heat loss by convection
Head	0.004712875
Trunk	0.010490094
Arm (one)	0.000221887
Leg (one)	0.002111094
Whole body	0.018216747

Source: Own

Heat is also radiated by other parts of a body. Radiation is reduced by special clothing which can be combined medical clothing for neonate made of PVC foil of a reduction factor of infrared radiation $F_{cl}=0,98$. Alternative is newborn baby clothing made of PVC foil and fabric of reduction factor $F_{cl}=0,86$. Calculations are demonstrated in Table 7.

Tab. 7: *Heat loss by radiation for other body parts*

Particular part of neonate body	Heat loss by radiation	
	F_{cl}=0.98	F_{cl}=0.86
Trunk	0.588482716	0.516423608
Arm (one)	0.293127285	0.257234148
Leg (one)	0.799882707	0.701937885
Whole body	4.379545427	3.843274558

Source: Own

The values shown in Table 7 are different for both structures and the same body part. We can regulate effectively heat balance by means of clothing material. In view of heat reduction, PVC-foil is not optimal enough to secure the organism against hyperthermia. It is necessary to apply the additional textile layer to optimize heat transfer from the body to the surroundings and improve the negative feel of a foil.

Heat loss by convection for other body parts is given in Table 8 for the same conditions.

Tab. 8: *Heat loss by convection for other body parts*

Particular part of neonate body	Heat loss by convection	
	F_{cl}=0.98	F_{cl}=0.86
Trunk	0.060674023	0.05324455
Arm (one)	0.178619977	0.156748143
Leg (one)	0.475045067	0.416876283
Whole body	2.1277588	1.867216906

Source: Own

Differences of obtained results are significantly lower than for radiation, cf. Table 7.

Comparison of evaporative heat loss for other body segments is shown in Table 9.

Tab. 9: *Heat loss by evaporation for other body parts*

Particular part of a neonate body	Heat loss by evaporation
Trunk	0.009141994
Arm (one)	0.035471224
Leg (one)	0.075232721
Whole body	0.336670742

Source: Own

General components are additionally determined in respiratory tract i.e. segmental heat losses by convection C_{resp} and evaporation E_{resp}, see Table 10.

Tab. 10: *Heat loss in respiratory tract*

Heat loss by	
convection C_{resp}	evaporation E_{resp}
0.082403062	0.045849057

Source: Own

It is evident that the most critical body part is the head. The most significant heat transport is radiation and convection for the whole body as well as evaporative heat loss for the head. Hence, we compare heat losses for the head and other parts separately, cf. Table 11 and Figure 1. Moreover, we assume the most adverse physiological case for a newborn baby:

- special medical clothing made of PVC foil which reduces thermal radiation and convection by means of clothing insignificantly $F_{cl}=0,98$;
- minimal material thickness of the bonnet *1mm = 0,001m*, minimal relative area of covering by bonnet *20%*.

Tab. 11: *Heat loss in respiratory tract*

Heat loss	Body part	
	Head	Trunk + arms + legs
Dry heat loss (radiation + convection)	2.5991	4.1417
Heat and mass transport (evaporation)	1.6629	0.2305
Conduction	0.0047	0.0197
Heat losses in respiratory tract (convection + evaporation)	C_{resp}=0.0824	E_{resp}=0.0458
Sum	8.7868 kJ · h^{-1} · kg^{-1}	

Source: Own

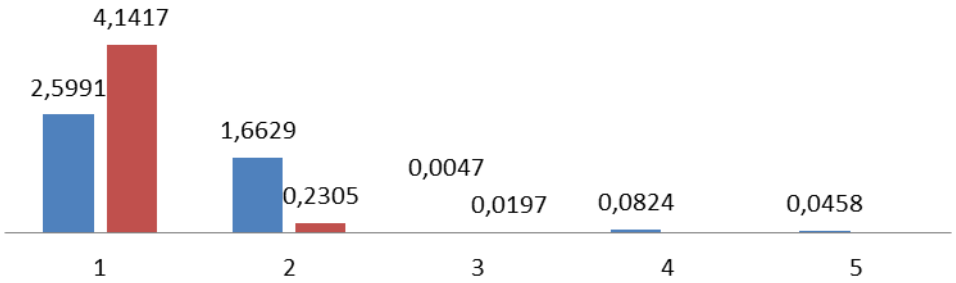

blue – head; red – other body parts; 1 – radiation + convection ; 2 – evaporation ; 3 – conduction ; 4 – convection in respiratory tract; 5 – evaporation in respiratory tract
Source: Own

Fig. 1: *Visualization of heat losses for head and other body parts*

According to Eq. (1), metabolism is determined as the function of postnatal age A expressed in days. Introducing now $A=4.5$ *days* we obtain $\dot{M} = 8.505289934\ kJ\ h^{-1}kg^{-1}$. We can calculate after some simple transformations the following heat storage rate.

$$S = \dot{M} - \left[\sum_{\text{i, all bodyparts}} \left(R_i + C_i + K_i + E_i \right) + C_{resp} + E_{resp} \right] = 8{,}5052 - 8{,}7868 = -0{,}2816 \tag{13}$$

It is immediately obvious that this rate is negative. It means that metabolic heat production is lower than the heat lost by the body. The temperature decreases, which can cause hypothermia.

Thus, heat transfer can be regulated by three basic parameters: surface area of a head covered by a bonnet, material thickness of a bonnet, clothing material. Thin plastic clothing can cause hypothermia for small thickness and minimal covering area. In other cases, metabolic heat production is greater than heat loss, which can cause hyperthermia but characteristic times $t_{38^\circ C}$; $t_{40^\circ C}$; $t_{43^\circ C}$ are sufficiently long.

Conclusions

The model applied is global because it introduces one heat source (i.e. metabolism) and a few different phenomena of heat transport (i.e. different heat loss mechanisms). There is coupled heat and mass transport because evaporation introduces a part of heat transported with mass (i.e. sweat). Heat transport is determined within each body part and systemically for respiratory tract. The global approach can determine skin temperature but moisture distribution is not analysed. Moisture can be determined by approximate correlations.

It is also necessary to introduce the local description which allows determining above phenomena in local scale. We can determine the local distribution of state fields i.e. temperature and moisture within a textile structure.

The obtained and discussed results are approximate. Detailed reasons are the following:

- Each newborn baby has an individual heat transport system;
- Input parameters are wide tolerated, its range of reference is extended;
- Some correlations are empirical, defined for numerically limited sample of neonates;
- Some additional assumptions are introduced to simplify the model solution.

The crucial idea is to determine the heat losses for particular body parts. The most critical part is neonate's head characterized by the maximal heat loss. We can influence the heat transfer conditions and global heat balance by means of structure, material thickness and area of covering by a bonnet. The heat transport can be mainly limited by covering level of the bonnet; material thickness is of less significance. Heat loss can also be reduced by application of different clothing materials. All these parameters help to control the hyperthermia as well as hypothermia of newborn baby. These parameters can be determined by means of special times i.e. times to reach the specified temperatures *38˚C*; *40˚C*; *43˚C*.

Acknowledgements

This research work was conducted within the frame of project Contract number UMO–2011/03/B/ST8/06275 granted by the National Science Centre.

Literature

[1] AGOURRAM, B.; BACH, V.; TOURNEUX, P.; KRIM, G.; DELNAUD, S.; LIBERT, J.-P.: Why wrapping premature neonates to prevent hypothermia can predispose to overheating, *Journal of Applied Physiology*, 108, 1674 – 1681, 2010.

[2] Anonymous: EN ISO 7933, Ergonomics of thermal environment – Analytical determination and interpretation of heat stress using calculation of the predicted heat strain, European Committee for Standardization, Brussels, 2004.

[3] Anonymous: ISO 7726:2002, Ergonomics of the thermal environment – Instruments for measuring physical quantities, 2002.

[4] NISHI, Y.; GAGGE, A. P.: Moisture penetration for clothing a factor governing thermal equilibrium and comfort, *ASHRAE Trans* 75, 137 – 145, 1970.

GLOBÁLNÍ TRANSPORT TEPLA A HMOTY V SYSTÉMU: POKOŽKA NOVOROZENCE – TEXTILNÍ KOMPOZITA – OKOLÍ

Globální model transportu tepla a hmoty je definován tepelnou rovnováhou při změně hmoty během odpařování potu z těla. Teplo je vytvářeno metabolickou produkcí tepla a ztrácí se vlivem různých jevů. Podmínky pro zajištění nezbytných parametrů těla novorozence jsou řešeny globálně pro různé parametry dětské čepičky a vrchního oblečení. Studie se zabývá různými možnostmi, jak zabránit hypertermii a hypotermii.

GLOBALER WÄRME- UND MASSETRANSPORT IM SYSTEM: DIE HAUT NEUGEBORENER – TEXTILKOMPONENTEN – UMGEBUNG

Das globale Modell des Transportes von Wärme und Masse wird durch das Wärmegleichgewicht beim Stoffwechsel während der Verdunstung des Schweißes aus dem Körper definiert. Wärme wird durch die metabolische Produktion von Wärme gebildet und verliert sich unter dem Einfluss verschiedener Vorgänge. Die Bedingungen für die Sicherstellung der unabdingbaren Parameter der Körper von Neugeborenen werden global für verschiedene Parameter von Kindermützen und Oberbekleidung geklärt. Diese Studie befasst sich mit verschiedenen Möglichkeiten der Vorbeugung von Hyperthermie und Hypothermie.

GLOBALNY TRANSPORT CIEPŁA I MASY W SYSTEMIE: SKÓRA NOWORODKA – SKŁADNIKI TEKSTYLNE – OTOCZENIE

Globalny model transportu ciepła i masy zdefiniowany jest jako równowaga cieplna przy zmianie masy w trakcie odparowywania potu z ciała. Ciepło produkowane jest w wyniku metabolicznej produkcji ciepła a do jego utraty dochodzi pod wpływem różnych zjawisk. Warunki mające na celu zapewnienie niezbędnych parametrów ciała noworodka są rozpatrywane w sposób globalny dla różnych parametrów dziecięcej czapeczki i ubrania wierzchniego. Opracowanie poświęcone jest różnym możliwościom zapobiegającym hipertermii i hipotermii.

AN EXPERIMENTAL INVESTIGATION INTO THE MECHANICAL BEHAVIOR OF 3D WOVEN HYBRID COMPOSITES

*** Rajesh Mishra**
B. P. Dash
B. K. Behera

Indian Institute of Technology Delhi
Department of Textile Technology
India
* rajesh.mishra@gmail.com

Abstract

In general, the purpose of hybridization is to achieve a composite architecture which synergizes the properties of both materials and/or lowers the cost since one of the fibers could be too expensive. In this study, 3D woven glass/aramid/epoxy hybrid composites were fabricated by using Kevlar and zylon in Z direction and glass in both X and Y direction. There mechanical behavior such as tensile, compression, 3 point bending, impact resistance, stab resistance and DMA has been investigated. 3D hybrid composites clearly shows better impact resistance, stab resistance and DMA properties as compared to neat composite of comparable FVF.

Introduction

It has been revealed that 3D woven composites have distinct mechanical and physical properties compared with their 2D laminated counterparts [1, 2]. They cost reasonably due to their relatively simple resin impregnation process [3] and better performance because of their resistance to delamination [4, 5]. In addition, 3D composites have good ballistic impact damage resistance and significantly high low velocity impact tolerance [6–8]. Low velocity impact properties of 3D woven composites are important for their various applications. This type of loading can occur when tools are dropped on the surface of a composite or when the material is impacted by debris, fragments, or projectiles. Hybrid composites contain two or more different types of reinforcement fibers which have different mechanical and/or other properties, allowing researchers to design a composite with tailored properties in specific applications [9–11]. In general, the purpose of hybridization is to achieve a composite architecture which synergizes the properties of both materials and/or lowers the cost since one of the fibers could be too expensive. Structures of hybrid composites may be classified as interply hybrids, intraply hybrids, intimately mixed (intermingled) hybrids, selective placement and super hybrid composites [12]. Brittle inorganic fibers and ductile organic fibers are often combined to make hybrid composites such as palm/glass, glass/mineral fiber, aramid/glass, etc. [13–15]. The so-called hybrid effect often occurs in the form of a positive deviation of a certain property from the ‘rule of mixtures’ [16].

Mechanical properties including low velocity impact properties of a hybrid composite have not been studied extensively. Among limited publications in this subject area, Pegoretti and co-workers [12] studied low velocity impact behavior of E-glass/PVA hybrid laminated woven composites in two structures, namely interply and intraply hybrids. In that research, the intraply composites were composed of fabric layers, in which the warp yarns and the weft yarns were different types. It was found that the intraply hybrid composites had better tensile and impact performance than their interplay counterparts. Impact properties of 3D woven composites have been studied [3, 17–20]. However, little has been reported regarding the

mechanical behavior of hybrid 3D woven composites, in particular varying through the thickness direction fiber. As an inorganic fiber, glass fibers are widely used in textile composites due to relatively low cost and good performance. They have a very good tensile strength. Especially if they are made thinner, the strength per unit cross section becomes greater. Glass fiber is stronger than the steel wire of the same thickness. It has break elongation is 3.5-4 percent.

Aramid fibers, on the other hand, have good tensile strength and modulus as well as superior impact resistance, though they are much more expensive than glass fibers. Therefore a 3D woven hybrid composite of these two fibers will be reasonably priced with reasonable tensile, compression and impact properties. However, it is not clear how the impact properties of the hybrid composites will be changed when the construction of the 3D woven changes. In this study, 3D woven glass/aramid/epoxy hybrid composites were fabricated by using Kevlar and zylon in Z direction and glass in both X and Y direction.

1 Development of 3D woven hybrid fabrics in 2D weaving system using various

1.1 Fabric construction parameters

The neat fabric was prepared from multifilament 600 Tex E-glass tow in rigid rapier weaving machine. Kevlar and Zylon tows of 666 tex and 650 tex were used as binder for hybrid fabrics. The stuffer and filler tows remained 600 tex E-glass. Modifications were made for mounting an extra beam to supply binder warp in existing 2D weaving system. Constructional details of each fabric are laid down below in Table 1.

Tab. 1: *Construction parameters of different fabric*

	3D Orthogonal Glass	3D Orthogonal Glass-Kevlar	3D Angle Orthogonal Glass-Zylon
Reed count	24	24	24
Stuffer or warp ends / mt	158	158	158
Binder ends /mt	315	315	315
Fabric width in mt	0.41	0.41	0.41
Picks / mt	315	315	315

Source: Own

1.1.1 Weave design of fabrics

Weave design and peg plan and images of 3D neat glass and hybrid fabric samples are given in Fig. 1.

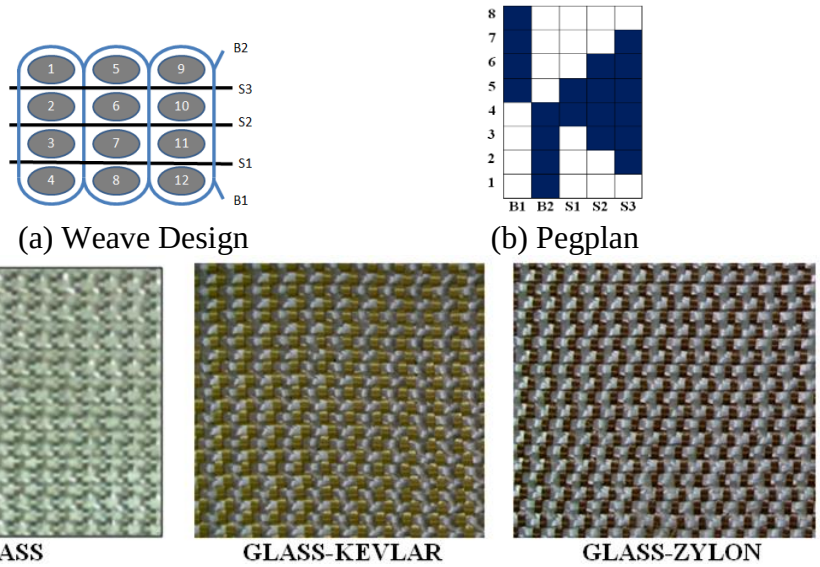

Source: Own

Fig. 1: *Weave design, Pegplan and Images of 3D neat glass and hybrid fabrics*

1.2 Fabric dimensional parameters

Measured values of fabric dimensional parameters are given in Table 2.

Tab. 2: *Measured parameters of fabric samples*

Fabric type	3D Orthogonal Glass	3D Orthogonal Glass-Kevlar	3D Angle Orthogonal Glass-Zylon
Thickness (mm)	1.4	1.65	1.62
Areal Density (Kg/m2)	1.248	1.278	1.272
FVF of fabric	0.35	0.35	0.34

Source: Own

2 Experimental Design for optimization of process parameters for composite manufacture

When multiple variables are involved, it becomes difficult to study the system using the common approach of varying only one factor at a time, while holding the others constant. A more efficient way to investigate these systems is to develop a mathematical model describing the relationship between the response and independent variables, in which the significance of individual factors and multifactor interactions can be determined [21-24]. A Box-Behnken Design (BBD) is a versatile method to statistically model and optimizes response variables that are affected by multiple independent factors. Statistical analysis, modeling, and numerical optimization were performed using Design Expert software, Design-Expert 8.0.7.1. The BBD matrix generated by Design Expert software displays factor levels in the experimental design in two ways: (i) the actual factor levels, which are the values from the experiment, and (ii) the coded factor levels, +1, -1, and 0, for high levels, low levels, and center point, respectively. The BBD experimental design matrix is shown in terms of both actual and coded factor levels in Table 3. Twelve replicates were run for each experiment along with one center point.

Tab. 3: *Box-Behnken design matrix in terms of both actual and coded factor levels generated by design expert software*

Run	Factor 1 Add on %	Factor 2 Hardner %	Factor3 Pressure (Bar)	Response 1 Total Energy (Joule)	Response 2 Peak Force (Newton)
1	-1(45)	0(12)	1(12)	12.6	2597
2	0(50)	-1(10)	1(12)	12.7	2824
3	0(50)	0(12)	0(10)	11.5	2553
4	1(55)	1(14)	0(10)	8.5	1887
5	0(50)	1(14)	-1(8)	9.7	2353
6	1(55)	0(12)	-1(8)	9.0	1998
7	0(50)	1(14)	1(12)	10.5	2331
8	1(55)	0(12)	1(12)	9.4	2098
9	-1(45)	1(14)	0(10)	11.5	2553
10	-1(45)	0(12)	-1(8)	10.4	2309
11	-1(45)	-1(10)	0(10)	11.0	2442
12	1(55)	-1(10)	0(10)	11.2	2514
13	0(50)	-1(10)	-1(8)	10.9	2420

Source: Own

2.1 Statistical Analysis of the Model

For both total energy and peak force, regression analysis of the experimental data showed that in terms of coded factors, these were described as:

$$Total\ energy = 11.5-0.94*add\ on-0.68*hardner+0.65*pressure-0.75*add\ on*hardner-0.44*add\ on-0.24*hardner*pressure-0.8*add\ on^2-0.19*hardner^2\ 0.34*pressure^2 \quad (1)$$

and

$$Peak\ force = 2553-175.5*add\ on-134.5*hardner+96.1*curing\ pressure-184.5*add\ on*hardner-47*add\ on*curing\ pressure-106.5*hardner*pressure-217*add\ on^2+13.9*hardner^2 - 84.7*pressure^2 \quad (2)$$

For total energy all three parameters along with interaction between add on and hardner were found to be significant since their corresponding F values are less than 0.05. Similarly for peak force, along with the previously stated factors interaction between hardner % and pressure and square of add on were found to be significant.

Tab. 4: *ANOVA for Response Surface Quadratic Model (Total Energy)*

Analysis of variance table [Partial sum of squares - Type III]						
	Sum of		Mean	F	p-value	
Source	Squares	df	Square	Value	Prob > F	
Model	19.0731	9	2.119233	11.10284	0.0363	significant
A-Add on	7.125313	1	7.125313	37.33012	0.0088	significant
B-Hardner	3.745585	1	3.745585	19.62344	0.0214	significant
C-Pressure	3.411272	1	3.411272	17.87195	0.0242	significant
AB	2.25	1	2.25	11.78794	0.0414	significant
AC	0.765625	1	0.765625	4.011175	0.1389	
BC	0.237169	1	0.237169	1.242549	0.3462	
A^2	1.473849	1	1.473849	7.721622	0.0491	significant
B^2	0.088706	1	0.088706	0.46474	0.5443	
C^2	0.255749	1	0.255749	1.339892	0.3308	
Residual	0.572619	3	0.190873			
Cor. Total	19.64572	12				

Source: Own

Tab. 5: *ANOVA for Response Surface Quadratic Model (Peak Force)*

Analysis of variance table [Partial sum of squares - Type III]						
	Sum of		Mean	F	p-value	
Source	Squares	df	Square	Value	Prob > F	
Model	797951.9	9	88661.32	43.89245	0.0050	significant
A-Add on	246254.6	1	246254.6	121.9102	0.0016	significant
B-Hardner	144802.7	1	144802.7	71.68567	0.0035	significant
C-Pressure	73935.51	1	73935.51	36.60233	0.0091	significant
AB	136161	1	136161	67.40752	0.0038	significant
AC	8834.12	1	8834.12	4.373397	0.1276	
BC	45390.3	1	45390.3	22.47081	0.0178	significant
A^2	108591.4	1	108591.4	53.75899	0.0052	significant
B^2	445.7628	1	445.7628	0.220678	0.6706	
C^2	16394.05	1	16394.05	8.115997	0.0652	
Residual	6059.902	3	2019.967			
Cor. Total	804011.8	12				

Source: Own

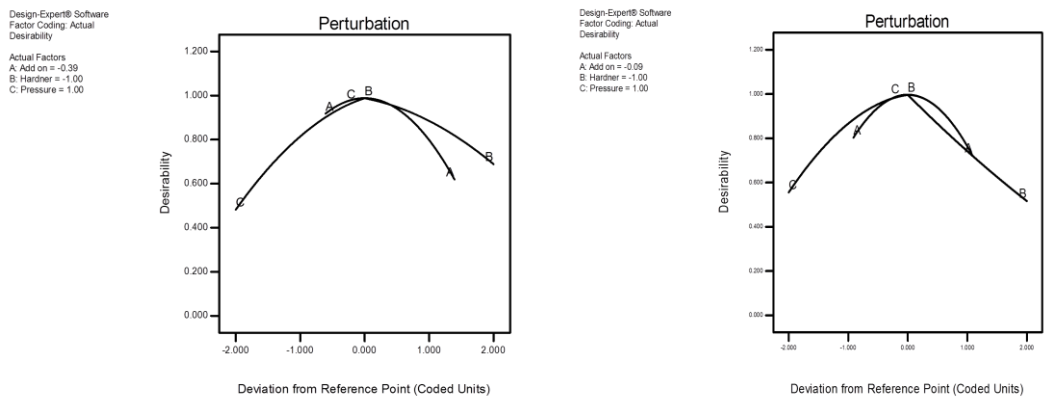

Source: Own

Fig. 2: *Perturbation plots for total energy and peak force*

The perturbation plots of the total energy and peak force against Add on, Hardner and curing pressure shown in Fig. 2 depicts the contribution of each factor. The perturbation plot illustrates the changes in total energy and peak force as each factor moves from the chosen reference with all other factors held constant at the middle level of the design space.

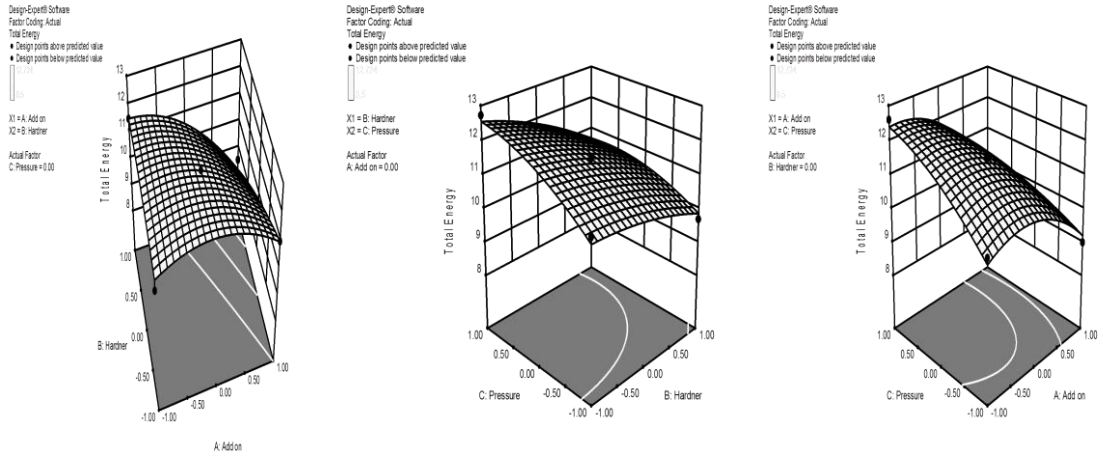

Source: Own

Fig. 3: *3D Surface plot showing effect of add on and hardner, hardner and curing pressure and add on and curing pressure on total energy*

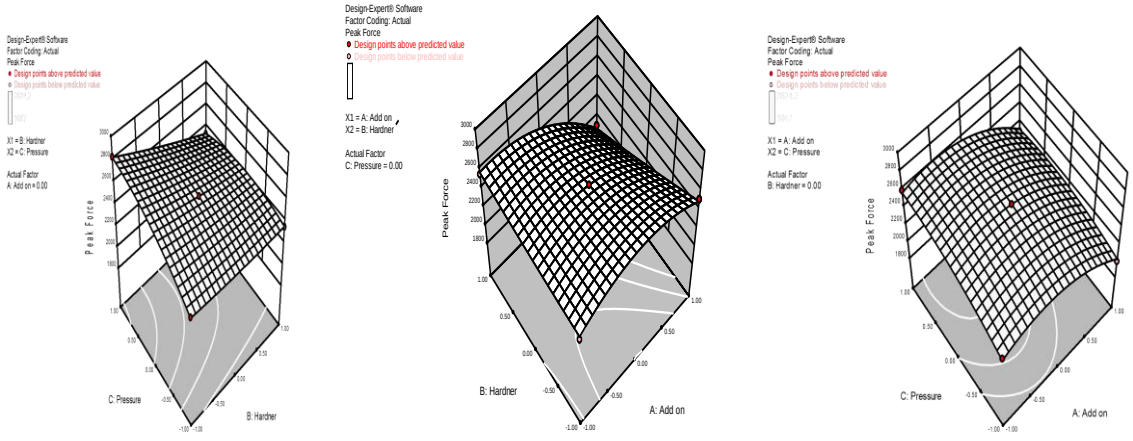

Source: Own

Fig. 4: *3D Surface plot showing effect of hardner and curing pressure, add on and hardner and add on and curing pressure on peak force*

After observing both the perturbation plots and the 3D surface plots Fig.2, Fig.3 and Fig.4 it was concluded that 3D woven composite could be made with 48% add on, 10% hardner and 12 bar curing pressure to get highest total energy. Similarly for getting the highest peak force 49.55% add on, 10%hardner and 12 bar pressure should be maintained. Hence it was decided to manufacture 3D woven composites with 50%add on, 10% hardner and 12 bar curing pressure. All composites are prepared by compression moulding technique. LY556 Epoxy resin was used as a matrix component and it was applied by hand lay-up technique. The principal advantage of compression molding is its ability to produce parts of complex geometry in short periods of time. SANTECH compression moulding available in the workshop is used to prepare composites. The parameters set on the machine while preparing composites are mentioned below.

Machine parameters maintained for composite manufacturing

- Machine used : SANTECH compression moulding machine
- Curing time: 900 sec.
- Breathing pressure: 6 bar
- Curing pressure: 12 bar
- Curing temperature: 120 0c
- Hardener /Epoxy ratio: 1:10

Tab. 6: *FVF of different composites.*

Type of reinforcement	FVF
3D Orthogonal Glass	39.6
3D Orthogonal Glass-Kevlar	43.27
3D Orthogonal Glass-Zylon	42.21

Source: Own

3 Test methods for composite

3.1 Tensile Testing

Tensile testing was performed with Instron 5582 using 50 KN load- cell according to ASTM 3039.The sample size was 250mm X 25mm, gauge length 150mm, cross head speed 2 mm/min. Ten readings were taken for each sample.

3.2 Compression Testing

Compression testing was performed with MTS 793 using 25 KN load- cell according to ASTM D3410.The sample size was 127mm X 25mm, gauge length 12.7 mm, cross head speed 1.5 mm / min. Ten readings were taken for each sample. This test method determines the in-plane compressive properties of polymer matrix composite materials reinforced by high-modulus fibers. In this test the compressive force into the specimen through shear at wedge grip interfaces. This type of force transfer differs from the procedure in test method D695 where compressive force is transmitted into the specimen by end-loading. The shear force was applied via wedge grips in a specially-designed fixture.

3.3 Flexural Testing

Compression testing was performed with Zwick Z 010 using 1 KN load-cell according to ASTM D 790. The sample size was 120 mm X 12.7 mm, support span 50 mm, cross head speed 3 mm/min. Five readings were taken for each sample. All samples were tested in a control limit of 5% extension to measure the force required to bend the samples so that the modulus can be calculated. The span-to-depth ratio higher than 16:1 was chosen such that failure occurs in the outer fibers of the specimens and is due only to the bending moment eliminating shear effects.

3.4 Low velocity impact testing

Impact test of all the composite structures was carried out to estimate the amount of impact energy absorbed by each composite. The tests were performed as per the ASTM D 7136. This test method determines the damage resistance of multidirectional polymer matrix composite laminated plates subjected to a drop-weight impact event. A flat, rectangular composite plate is subjected to an out-of-plane, concentrated impact using a drop-weight device with a hemispherical impactor. Sample size was 12 cm×12 cm, impactor speed – 5 m/min, and five reading were taken for each sample.

3.5 Knife penetration Test

To carry out this test, the testomeric tester M350-10CT was used. Each composite sample was placed on the plate of the machine. The machine head was dropped onto the sample thus holding the sample in place. The knife was then allowed to penetrate the fabric sample at a velocity of 1000 mm/min. A recording monitor was connected to this machine and it recorded the maximum force exerted on penetrating the sample. Five readings were taken for each composite sample.

3.6 DMA Test

Dynamic Mechanical Analysis, otherwise known as DMA, is a technique where a small deformation is applied to a sample in a cyclic manner. This allows the materials response to stress, temperature, frequency and other values to be studied. Dynamic Mechanical Analysis (DMA) measures the mechanical properties of materials as function of temperature, frequency and time. It is a thermal analytical method by which the mechanical response of a sample subjected to a specific temperature program is investigated under periodic stress. Dynamic mechanical analyzer is a thermal analytical instrument used to test the mechanical properties of many different materials.

The storage modulus is measure of elasticity of material. It is also called “the ability of the material to store energy”. It is equivalent to the ability of a sample to store energy, i.e. its elasticity. Energy storage occurs as molecules are distorted from their equilibrium position by application of a stress. Removal of the stress results in a return to equilibrium position of the molecular segments.

Loss modulus represents the capability of a material to dissipate energy (mechanical, acoustic) as heat, owing to viscous motions inside the material itself. It is limited to the molecular motion within the sample that dissipates energy as heat.

Tan Delta (3) is measure of material damping, such as vibration or sound damping. Damping refers to damping the loss of mechanical energy as the amplitude of motion gradually decreases. It also means the ability of a material to dissipate mechanical energy by converting it into heat. Tan Delta is a useful index of material viscoelasticity since it is a ratio of viscous

and elastic moduli. Tanδ is an important indication of viscoelasticity of materials, it is independent from the shape and dimension of samples and it is dimensionless.

$$Tan\ \delta = Loss\ Modulus\ /\ Storage\ Modulus \quad (3)$$

Dynamic mechanical analysis was performed with DMA DX04T RMI instrument according to ASTM D 7028. The test was performed in three point bending mode with gauge length and sample width of 30 mm and 10 mm respectively. The samples were subjected to an oscillating frequency of 1 Hz and 100% oscillating amplitude in the temperature range 30 °C to 300 °C at the heating rate of 5 °C min^{-1}. Five readings were taken for each sample. Storage Modulus and Tandelta were generated as output.

4 Results and Discussion

4.1 Tensile test

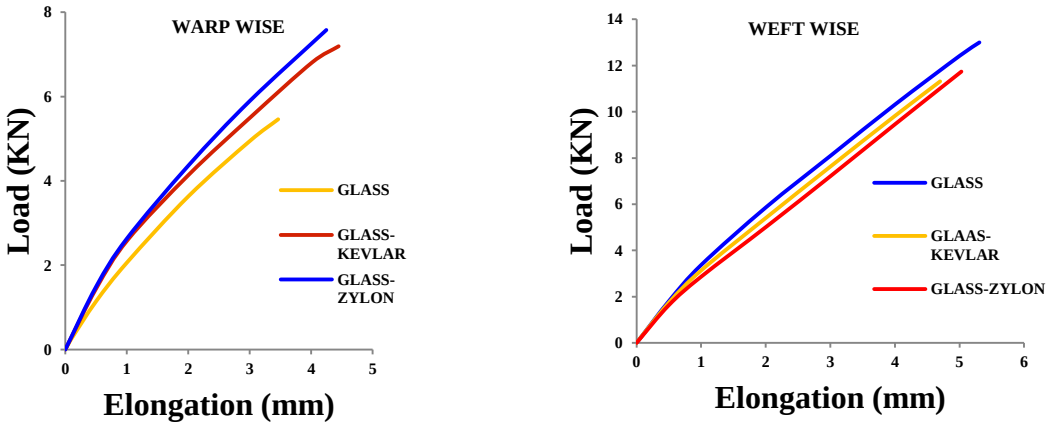

Source: Own

Fig. 5: *Load elongation curve of different structures*

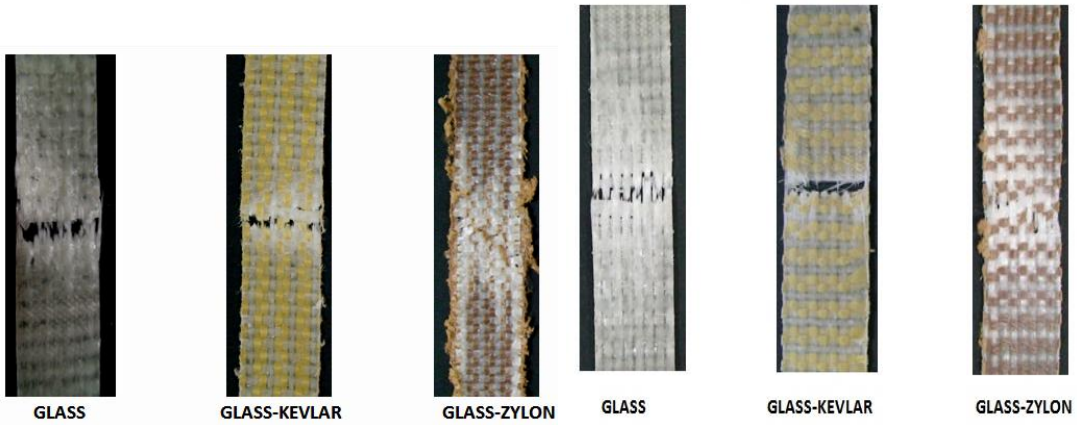

Source: Own

Fig. 6: *Images of hybrid composites after tensile testing*

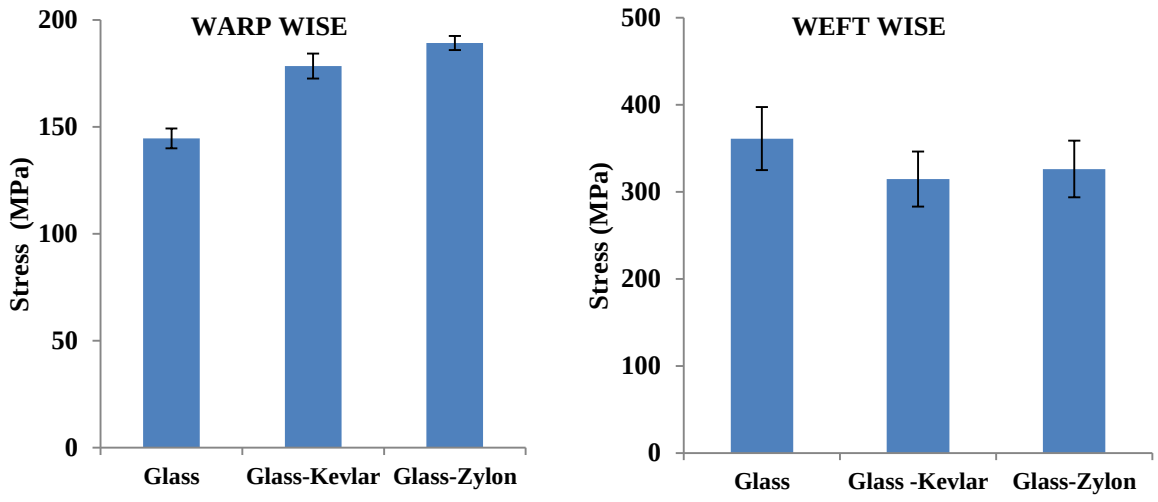

Source: Own

Fig. 7: *Bar diagram for tensile stress of hybrid composites in both warp way and weft way*

The typical load elongation curve generated from tensile test, the tested samples and the bar diagram depicting values of stress of different composites have been shown in Fig. 5, Fig. 6 and Fig. 7 respectively. Close observation into the tensile test results reveal that the ultimate load and stress increased 23% and 31% for glass-kevlar and glass-zylon hybridization. This improvement might have been due to the increase in fabric assistance values, due to the bulkier yarn structure of Kevlar and zylon. Moreover, during weaving the inter yarn friction between glass Kevlar and glass zylon was less resulting in less breakage of filaments. However, in weftwise direction the hybrid composites were found to have less strength than the neat glass composite, but this deviatiation is not significant. Moreover, from the images of tested samples it is observed that the damage area is less for the hybrid composites. This is evident by watching the opaque region surrounding the break.

4.2 Compression Test

The typical load displacement curve generated from compressive test, the tested samples and the bar diagram depicting values of stress of different composites have been shown in Fig. 8, Fig. 9 and Fig. 10 respectively. Compressive properties of thin composite laminates are difficult to measure owing to sidewise buckling of specimens. A number of test methods and specimen designs have been developed to overcome the buckling problem. ASTM D 3410 method uses flat wedge grips instead of conical wedge grips. Flat wedge surfaces provide a better contact between the wedge and the tapered sleeve and improve the axial alignment to avoid the problem of buckling. Flat wedge grips can also accommodate variation in specimen thickness. Investigation into the compressive breaking stress of the composites reveals that the hybrid composites do exhibit poor strength when compared to the neat ones, in both warp way and weft way. But it was found that the warp way reduction was not significant while in weft way it is significant. This may be due to poor compressive properties of the Kevlar and zylon fiber accompanied by low interfacial bondage between these fibers and epoxy resin.

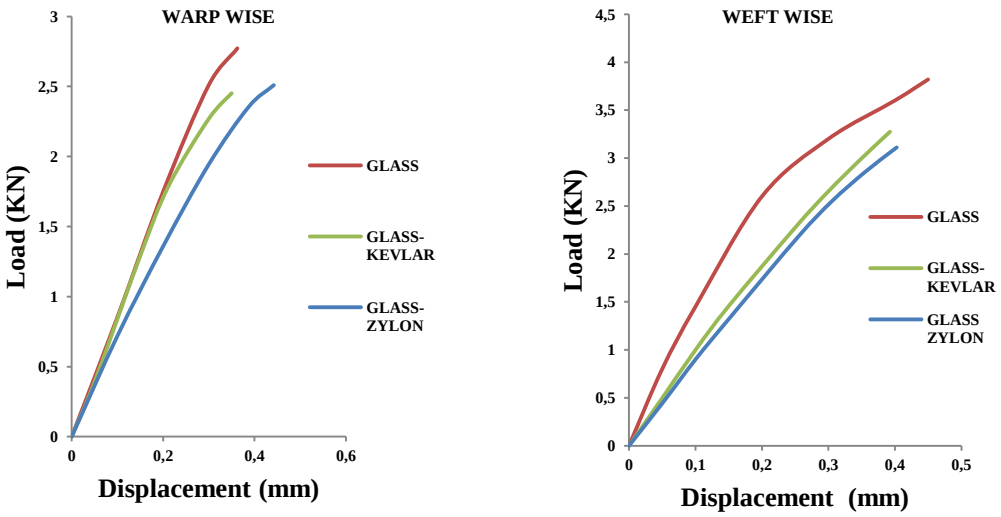

Source: Own

Fig. 8: *Load elongation curve for compression test of hybrid composites in warp wise and weft wise direction*

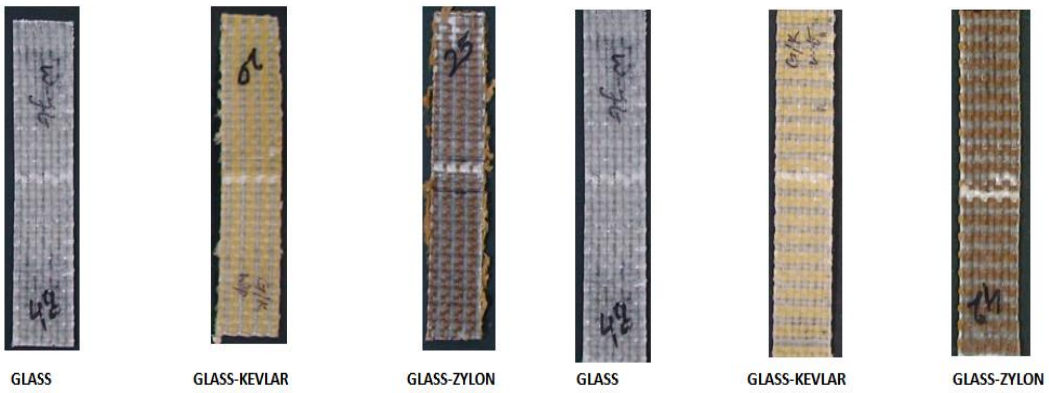

Source: Own

Fig. 9: *Images of hybrid composites after compression test*

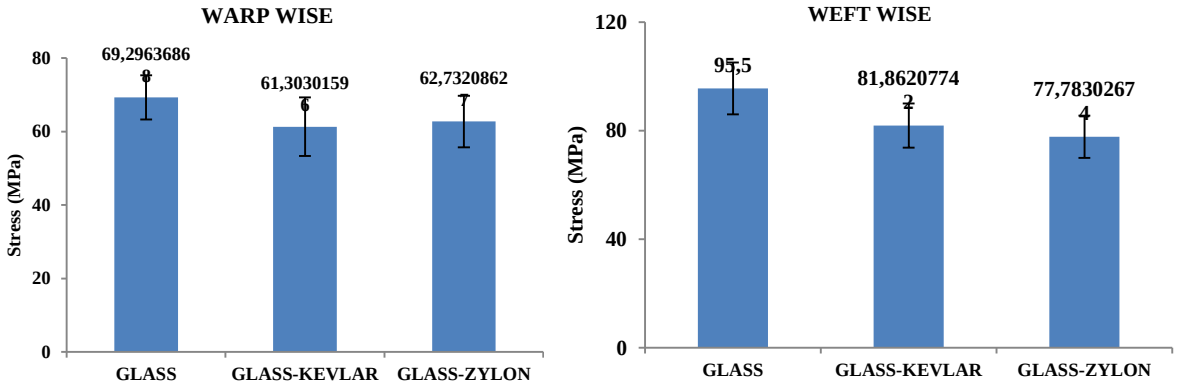

Source: Own

Fig. 10: *Bar diagram for compressive stress of hybrid composites warp way and weft way*

4.3 Three point bending test

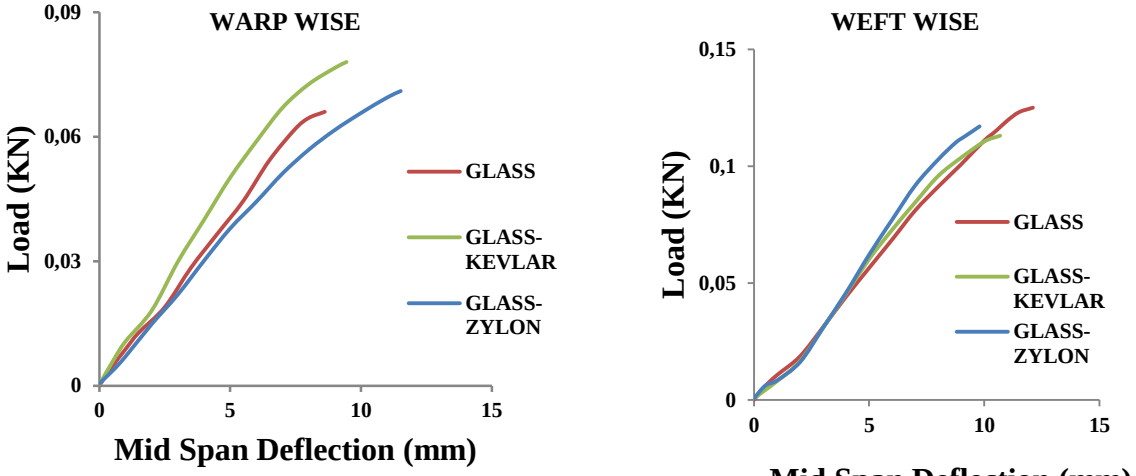

Source: Own

Fig. 11: *Load deflection curve for 3 point bending of composites*

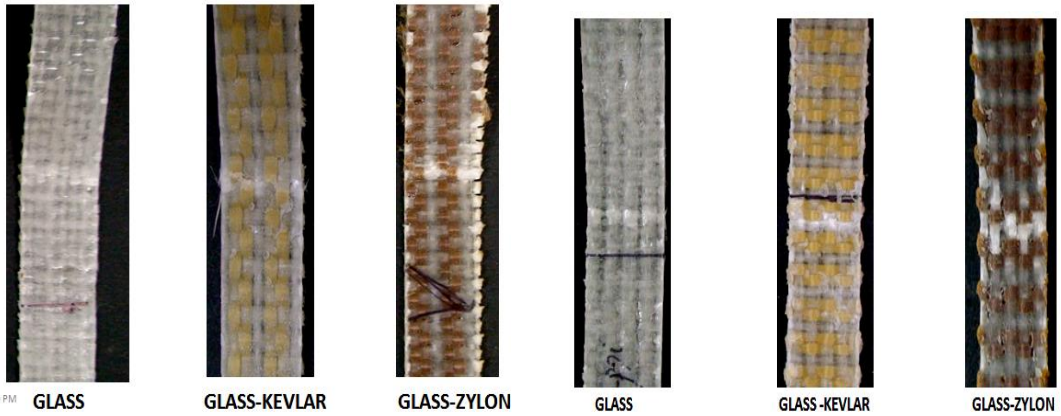

Source: Own

Fig. 12: *Images of composites after 3 point bending*

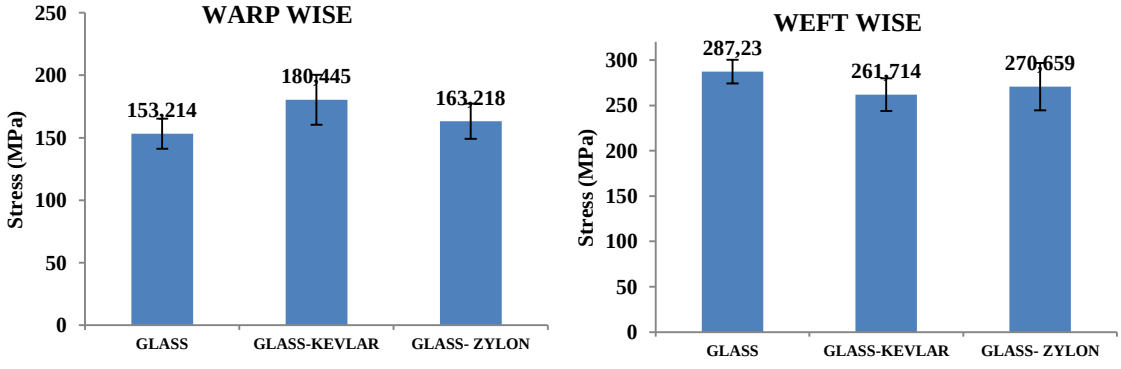

Source: Own

Fig. 13: *Bar diagram for 3 point bending stress and modulus of different structures in warp way and weft way*

The load deflection curve generated from 3 point bending test, the tested samples and the bar diagram depicting values of stress of different composites have been shown in Fig. 11, Fig. 12 and Fig. 13 respectively. The failure of a composite during 3 point bending test is dependent

on three main factors: (1) the constituent materials, (2) the sequence in which the fibers are aligned and (3) the type of loading experienced in a specific direction. Common flexural loading failures include: compressive failure, tensile failure, shear and/or delamination. Delamination is the fracture along the direction of the fibre and is indicated by a laminate layer being separated from the composite. The other forms of failures will generally occur in the transverse direction because unidirectional composites are obviously anisotropic. The crack often initiates on the tension side of the beam and slowly propagates in an upward direction. Normally, the modulus is very sensitive to the matrix properties and matrix/fibre interfacial bonding. Tensile failures are not uncommon in flexural tests due to the fact that the outer layers undergo stretching. Should a composite fail in tension, it can be due to brittle failure or fibre pullout. Kinking is the most predominant form of compressive failure. However, composites might have also failed due to microbuckling, shear or splitting. Microbuckling of near surface stuffers does involve deflections out of the surface. In bending in-plane deflections of stuffers would have to occur in the weft direction and would therefore be strongly resisted by adjacent fillers [25-27].

Study of 3 point bending test results revealed that hybridization does not show up any particular trend on bending properties. However, almost 17% improvement in strength was observed in warp wise direction and 10% reduction in weft wise direction for glass Kevlar composite.

4.4 Impact Test

The bar diagram depicting values of peak deformation, peak energy, peak force and total energy absorbed by different composites and the impact tested samples have been shown in Fig. 14 and Fig. 15 respectively. The 3D hybrid composites clearly show better impact resistance compared to neat composites of comparable FVF. The glass zylon hybrid composite is found to absorb the highest amount of total energy, peak energy and peak force, followed by glass-kevlar and neat neat glass composite. Energy at peak is 39% and 13%, and total energy absorbed is 49% and 23 % higher for glass-zylon and glass-kevlar composites than the neat glass composites, due to incorporation of 15% yarn in Z direction. This may be due to the interlaminar toughening mechanisms, namely debonding, fracture, pull-out and, in particular, crack bridging of the z-binders impede the spread of delaminations from the impact site [28].

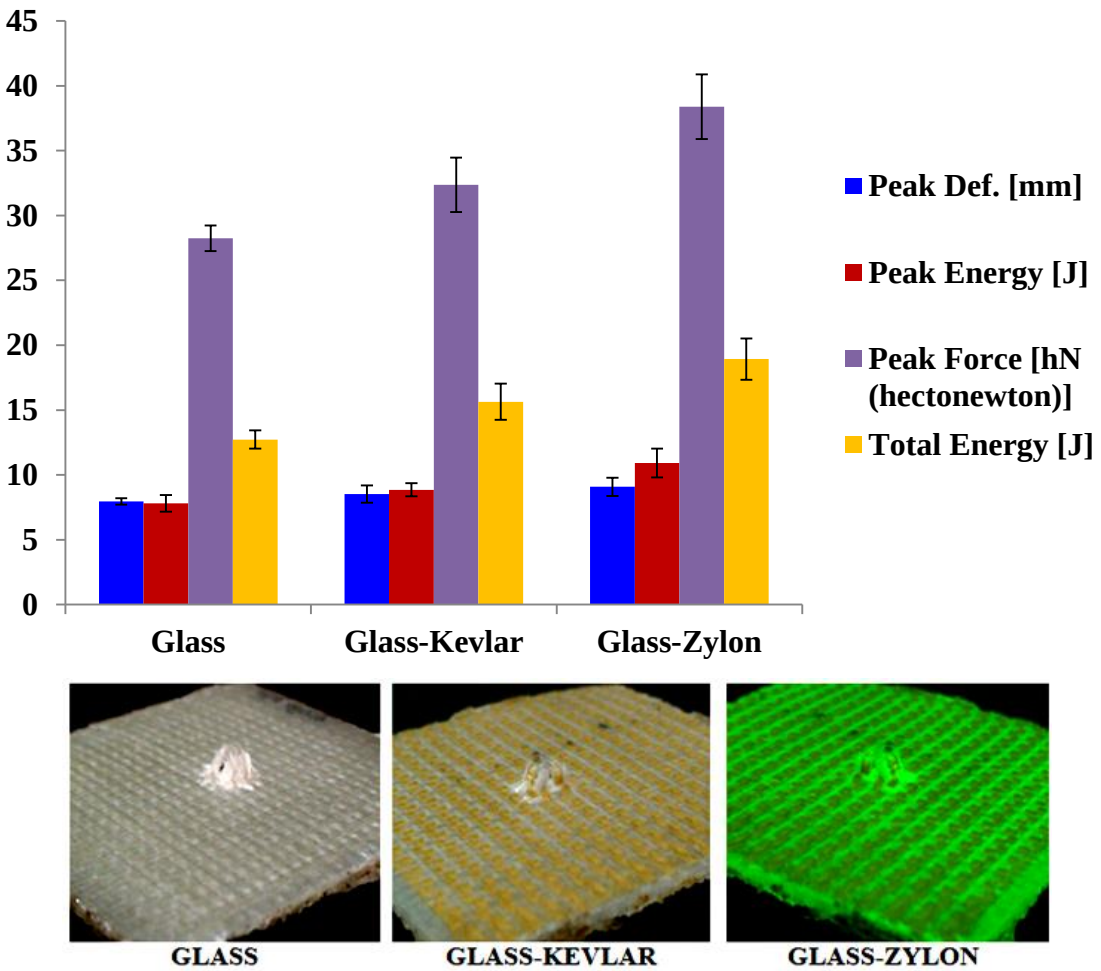

Source: Own

Fig. 14: *Bar diagram for low velocity impact properties of composites*

4.5 Knife Penetration Test

Different test results of knife penetration test have been depicted in Fig. 16. 3D woven hybrid fabric reinforced composite shows better stab resistance compared to the neat composite. The 3D glass-zylon reinforced composite was observed to generate best stab resistance of all the samples tested. Energy up to peak and Energy up to break was found to be 8%, and 10% higher for glass-Kevlar than that of neat glass composite. Similarly for glass-zylon composite Energy up to peak and Energy up to break was found to be 95 and 23% higher than pure glass composite.

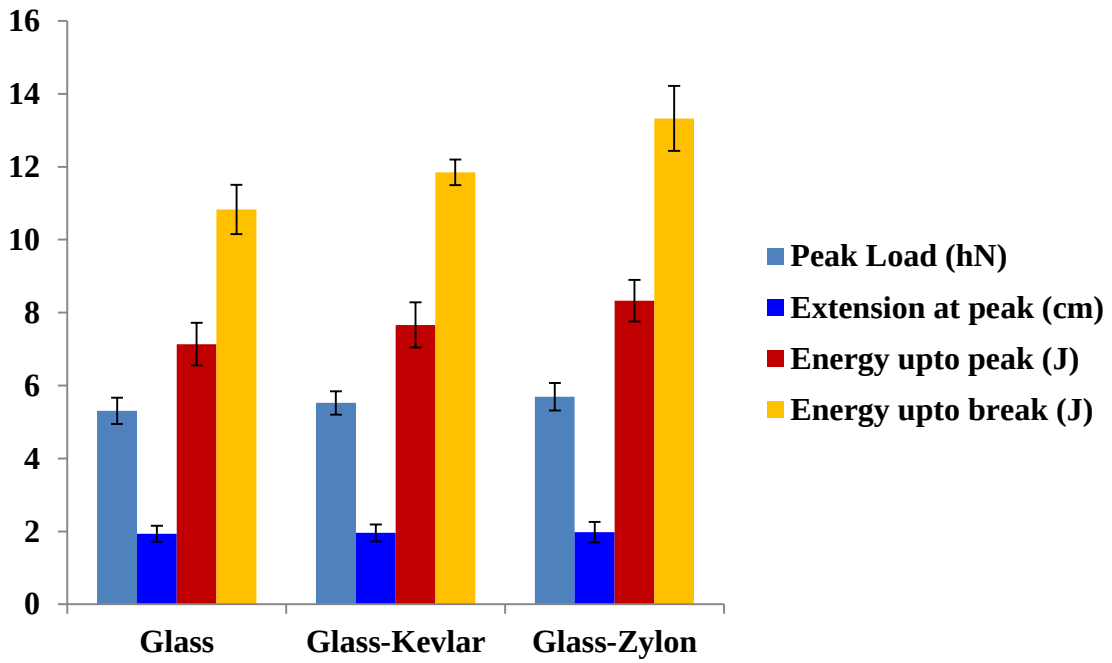

Source: Own

Fig. 15: *Bar diagram for Knife penetration properties of composites*

4.6 DMA Test

The Dynamic Mechanical Analysis is a high precision technique for measuring the viscoelastic properties of materials. Viscoelasticity is about elastic behaviors of materials. Most real-world materials exhibit mechanical responses that are a mixture of viscous and elastic behavior. Dynamic Mechanical Analyzer (DMA) deforms a sample mechanically and after that it measures the sample response. When a force is applied on a material, it suffers a change in shape, i.e. it deforms. DMA measures stiffness and damping, these are reported as modulus and tan delta. The ratio of the loss modulus to the storage modulus is the tan delta and is often called damping. It is a measure of the energy dissipation of a material. Damping is the dissipation of energy in a material under cyclic load. It is a measure of how well a material can get rid of energy and is reported as the tangent of the phase angle. It is a parameter to measure how good a material will be at absorbing energy. It varies with the state of the material, its temperature, and with the frequency. Modulus values change with temperature and transitions in materials can be seen as changes in the tan delta curves. This includes not only the glass transition and the melt, but also other transitions that occur in the glassy or rubbery plateau. The glass transition (Tg) is seen as a large drop in the storage modulus and a concurrent peak in the tan delta.

The study of storage modulus of composites reinforced with hybrid fabric, shown in Fig. 16 depict that the hybrid composites show higher values of storage modulus. When compared with the neat glass composite, 64% increase in storage modulus for glass-kevlar & 92% improvement for glass-zylon composites are observed, for almost similar FVF.

Observation of tan delta values in Fig. 17, with respect fiber hybridization reveal that the tan delta value is inversely proportional to the values of storage modulus i.e. it is highest for neat glass composite and lowest for glass-zylon composite. The Tg (Glass transition temperature), which is depicted by the picks of tan delta curve has occurred at 1060C for glass, 980 C for glass Kevlar and 950 C for glass zylon composites.

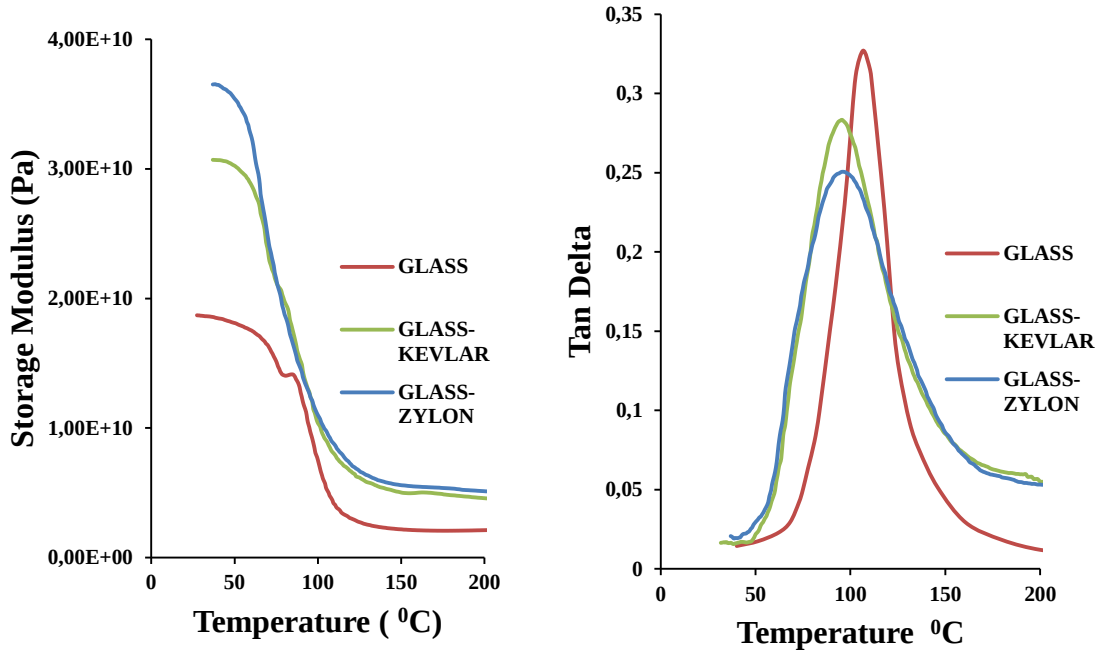

Source: Own

Fig. 16: *Effect of temperature on storage modulus and tan delta of different composites*

Conclusion

It has been observed that warp wise tensile stress increase by 23% and 31% for glass-kevlar and glass-zylon hybridization. In weftwise direction the hybrid composites are found to have less strength than the neat glass composite, but this deviatiation is not significant. Hybrid composites do exhibit poor compressive strength compared to neat one; in both warp way and weft way. But it has been found that the warp way reduction is not significant, whereas in weft way it is significant. Study of 3 point bending test results has revealed that hybridization does not show up any particular trend on bending properties. However, almost 17% improvement in strength has been observed in warp wise direction and 10% reduction in weft wise direction for glass Kevlar composite. The 3D hybrid composites clearly shows better impact resistance compared to neat composite of comparable FVF. 3D woven hybrid fabric reinforced composites show better stab resistance compared to the neat composite. The 3D glass-zylon reinforced composite has been observed to generate best stab resistance of all the samples tested, hybrid composites show higher values of storage modulus. The tan delta value is inversely proportional to the values of storage modulus i.e. it is highest for neat glass composite and lowest for glass-zylon composite.

Literature

[1] BRANDT, J. et al.: Manufacture and performance of carbon/epoxy 3D woven composites. In: *Proceedings of the 37th international SAMPE symposium*, Anaheim, CA, 1992.

[2] BRANDT, J; DRECHSLER, K.; ARENDTS, F. J.: Mechanical performance of composites based on various three-dimensional woven-fiber preforms. *Compos Sci Technol.* 1996; 56:381–6.

[3] TAN, P et al.: *Compos: Part A* 2000; 31:259–71.

[4] MOURITZ, A.P. et al.: Review of applications for advanced three dimensional fibre textile composites. *Compos: Part A* 1999; 30: 1445–61.

[5] CHOU, T. W.; KO, F. K.: *Textile structural composites. Distributors for the U.S. and Canada*. Amsterdam (NY, USA): Elsevier Science; 1989.

[6] MIRAVETE, A.: *3D textile reinforcements in composite materials*. Cambridge (UK): Woodhead Publishing Limited; 1999.

[7] BAHEI-EL-DIN, Y. A.; ZIKRY, M. A.: Impact-induced deformation fields in 2D and 3D woven composites. *Compos Sci Technol.* 2003; 63:923–42.

[8] CHOU, S; CHEN, H-C.; WU, C-C.: BMI resin composites reinforced with 3D carbon-fibre fabrics. *Compos Sci Technol.* 1992; 43:117–28.

[9] ABDULLAH, Al K. et al.: Study on the mechanical properties of jute/glass fiber-reinforced unsaturated polyester hybrid composites: effect of surface modification by ultraviolet radiation. *J Reinf Plast Compos*. 2006; 25(6):575–88.

[10] ANUAR H et al.: Tensile and impact properties of thermoplastic natural rubber reinforced short glass fiber and empty fruit bunch hybrid composites. *Polym Plast Tech. Eng*. 2006; 45:1059–63.

[11] XIE, H.Q.; ZHANG, S.; XIE, D.: An efficient way to improve the mechanical properties of polypropylene/short glass fiber composites. *J Appl Polym Sci.* 2005; 96:1414–20.

[12] PEGORETTI, A et al.: Intraply and interply hybrid composites based on E-glass and poly (vinyl alcohol) woven fabrics: tensile and impact properties. *Polym Int*. 2004; 53:1290–7.

[13] HARIHARAN, A. B. A.; KHALIL, H.: Lignocellulose-based hybrid bilayer laminate composite: Part I – studies on tensile and impact behavior of oil palm fiber-glass fiber-reinforced epoxy resin. *J Compos Mater*. 2005; 39:663–84.

[14] HARTIKAINEN, J et al.: Mechanical properties of polypropylene composites reinforced with glass fibres and mineral filters. *Plast Rubber Compos*. 2004; 33:77–84.

[15] IMIELINSKA, K.; GUILLAUMAT, L.: The effect of water immersion ageing on low-velocity impact behaviour of woven aramid-glass fibre/epoxy composites. *Compos Sci Technol*. 2004; 64:2271–8.

[16] MAROM, G.; FISCHER, S.; TULER, F. R.; WAGNER, H. D.: Hybrid effects in composites – conditions for positive or negative effects versus rule-ofmixtures behavior. *J Mater Sci.* 1978; 13:1419–26.

[17] KHALID, A. A.: The effect of testing temperature and volume fraction on impact energy of composites. *Mater Des*. 2006; 27:499–506.

[18] BAUCOM, J.; ZIKRY, M.: Low-velocity impact damage progression in woven E-glass composite systems. *Compos: Part A* 2005; 36:658–64.

[19] CHOU, S.; CHEN, H. C.; CHEN, H. E.: Effect of weave structure on mechanical fracture behavior of three-dimensional carbon fiber fabric reinforced epoxy resin composites. *Compos Sci Technol*. 1992; 45:23–35.

[20] NAIK, N. K.; SEKHER, Y. C. et al.: Damage in woven-fabric composites subjected to low-velocity impact. *Compos Sci Technol*. 2000; 60:731–44.

[21] MYERS, R. H.; MONTGOMERY, D. C. (1995), *Response Surface Methodology: Process and Product Optimization Using Designed Experiments*, Wiley, New York.

[22] MATUANA, L. M.; LI, Q. (2004), Statistical Modeling and Response Surface Optimization of Extruded HDPE/Wood-Flour Composite Foams, *J. Thermoplast. Compos. Mater*. 17(2), 185-199.

[23] MATUANA, L. M.; MENGELOGLU, F. (2002), Manufacture of rigid PVC/wood-flour composite foams using moisture contained in wood as foaming agent, *J. Vinyl & Addit. Technol*., 8(4), 264-270.

[24] MONTGOMERY, D. C. (2001), *Design and Analysis of Experiments*, 5th ed., Wiley, New York.

[25] PIGGOTT, M. R.; HARRIS, B.: Compression strength of hybrid fibre-reinforced plastics. *J Mater Sci.* 1981; 16:687–93.

[26] SUDARISMAN, D. I. J.: Flexural failure of unidirectional hybrid fibre-reinforced polymer (FRP) composites containing different grades of glass fibre. *Adv Mater Res.* 2008; 41–42:357–62.

[27] DONG, C.; RANAWEERA-JAYAWARDENA, H. A.; DAVIES, I. J.: Flexural properties of hybrid composites reinforced by S-2 glass and T700S carbon fibres. *Composites: Part B* 2012; 43 573–581.

[28] TONG, L; MOURITZ, A. P.; BANNISTER, M. K.: 3D Fibre Reinforced Polymer Composites, Elsevier Science Ltd 2002; ISBN 0-08-043938-1.

EXPERIMENTÁLNÍ VÝZKUM MECHANICKÉHO CHOVÁNÍ 3D HYBRIDNÍCH KOMPOZIT

Obecně platí, že cílem hybridizace je dosáhnout kompozitní struktury, která posílí vlastnosti obou materiálů a / nebo sníží náklady, protože jeden typ vlákna může být příliš drahý. V této studii je popsána 3D tkanina sklo/aramid/epoxid hybridního kompozitu vyrobená z Kevlaru a Zylonu ve směru Z, a skla v obou směrech X a Y. Byly zkoumány mechanické vlastnosti, jako je pevnost v tahu, tlaku, tříbodý ohyb, odolnost proti nárazu, odolnost proti propíchnutí a DMA. 3D hybridní kompozity ve srovnání s kompozitem FVF jasně ukazují lepší odolnost proti nárazu, odolnost proti probodnutí a vlastnosti DMA.

EINE EXPERIMENTELLE UNTERSUCHUNG DES MECHANISCHEN VERHALTENS VON 3D-GEWOBENEN HYBRIDGEMISCHEN

Allgemein gilt, dass das Ziel der Hybridisierung im Erreichen einer gemischten Struktur ist, welche die Eigenschaften beider Materialien stärkt und/ oder die Kosten senkt, weil eine einzige Fasersorte zu teuer werden kann. In dieser Studie wird ein 3D-Gewebe aus Glas, Aramid und einem Epoxid eines hybriden Gemischs beschrieben. Dieses wird aus Kevlar und Zylon in Richtung Z und aus Glas in beiden Richtung X und Y hergestellt. Es wurden dessen mechanischen Eigenschaften wie Zugfestigkeit, Druck, Dreipunktebeweglichkeit, Stoßfestigkeit, Stichfestigkeit und DMA-Eigenschaften untersucht. 3D-Hybridgemische weisen im Vergleich mit dem Gemisch FVF eindeutig eine bessere Stoßfestigkeit, Stichfestigkeit und DMA-Eigenschaften auf.

EKSPERYMENTALNE BADANIA MECHANICZNEGO ZACHOWANIA KOMPOZYTÓW HYBRYDOWYCH 3D

Ogólnie obowiązuje zasada, że celem hybrydyzacji jest osiągnięcie struktury kompozytowej, która poprawi właściwości obu materiałow i/lub zmniejszy koszty, ponieważ jeden typ włókna może być zbyt kosztowny. W niniejszym opracowaniu opisano tkaninę 3D szkło/aramid/epoksyd kompozytu hybrydowego wyprodukowanego z Kevlaru i Zylonu w kierunku Z oraz szkła w obu kierunkach X i Y. Badano właściwości mechaniczne takie tak wytrzymałość na rozciąganie, ciśnienie, trzypunktowe zginanie, odporność na uderzenie, odporność na przebicie i DMA. Kompozyty hybrydowe 3D w porównaniu z kompozytem FVF wykazują wyraźnie lepszą odporność na uderzenie, przebicie oraz właściwości DMA.

THE PREDICTION OF GRAIN SIZE OF THE HEAT AFFECTED ZONE OF WELDED S304H STEEL TUBES USING A MATHEMATICAL MODEL

Jaromír Moravec
*** Josef Bradáč**
**** Iva Nováková**
***** Heinz Neumann**

Technical University of Liberec
Faculty of Mechanical Engineering
Department of Engineering Technology
Studentská 2, 461 17, Liberec 1, Czech Republic
jaromir.moravec@tul.cz
** iva.novakova@tul.cz
*** heinz.neumann@tul.cz

* ŠkodaAuto University
Automobile Technology Department
Tř. V. Klementa 869, 293 60, Mladá Boleslav, Czech Republic
* josef.bradac@skoda-auto.cz

Abstract

Super 304H is an austenitic steel, which is mainly used for boilers in thermal power plants and the energy sector. Strength at high temperatures has become one of the most important attributes in the design of boiler tubes. The differences in material properties, especially in its creep resistance compared to other austenitic steels of similar composition, are mainly achieved by the addition of about 3 wt.-% of copper. The formation of fine Cu-rich precipitates during manufacture leads to an increased creep strength during the process of precipitation hardening. The impact of the welding cycle on the grain coarseness in the heat-affected zone (HAZ) for S304H steel will be demonstrated in this paper. The options and procedures for predicting grain size by mathematical modeling of welding and heat treatment will also be shown here. The method of acquiring the input data for the mathematical models, which predict the grain size, will also be described.

Introduction

The continuous trend of operational parameters to increase their energy and chemical conditions also requires the development of new materials, which are able to operate under such conditions. Heat-resistant steels can undoubtedly be classed as one of these materials. They have to fulfill many requirements, which are often contradictory. The main requirement lies in its enhanced resistance against long term loading under high temperatures. No less important is sufficient resistance against corrosion, which forms an oxide layer on the steel surface. [1]

Applications of such new materials and the inclusion of the technological processes for joining them together are often accompanied by the use of welding simulations and heat treatment computations. These computations can largely eliminate the risks, which are connected with the occurrence of unacceptable defects, or they can lead to the elimination of inner stresses caused by the process. The Sysweld program is one of the most commonly used programs for this type of computation.

When predicting the structure and resulting properties of the welded joints area, it is important to know not only the grain size in the initial state, but also during the welding process. For this reason, this paper describes the methodical procedures and the experimental results, which lead to the definition of a computational model. This model then enables the prediction of the austenitic grain size of the weldments made by S304H steel, especially in the heat-affected zone, but not in the weld area.

1 The Characteristics and Uses of S304H Steel

Generally speaking, austenitic steels have good mechanical properties and excellent corrosion resistance even at high temperatures, varying from 650-700°C. However, this advantage is countered by their unfavourable thermal-physical properties such as low thermal conductivity and high thermal expansivity. Another major drawback is the possible damage to the material through thermal fatigue, especially when these steels are used in power stations where they are working in cyclic thermal modes. The cost of these steels prohibits their use on a larger scale. [6] Currently austenitic heat resistant steels grade 304, are used in Europe, USA and Japan. Recently, S304H, which is a new type of austenitic stainless steel containing 3% copper, is being adopted for the production of super-heater /re-heater tubes of 600°C USC power plant boilers. [2]

The strength of this material at high temperatures is elevated and particularly its creep properties are improved by adding about 3 wt.-% of copper, increasing the carbon content and adding certain amounts of niobium and nitrogen. The addition of nitrogen leads to a solid solution heat strengthening of the material. This increases the tensile stress resistance. The stress resistance under creep conditions is mainly increased by the precipitation of a Cu-rich phase in the matrix. [4]The Cu-rich phase is mainly composed of Cu and also a part of Fe, Cr and Ni. The content of Cu in the Cu-rich phase is lower than 20 at pct at early stage of precipitation after 1 hour aging, and then it is increasing continually with aging time and reaches almost 90 at pct at centre when aging for 500 hours. These results represent that Cu atoms gradually concentrate to Cu-rich particles and the other elements (such as Fe, Cr, Ni etc.) diffuse away from Cu-rich particles to matrix with the increasing of aging time at ± 650°C. It is reasonable to suggest that Cu will be the only main composition in Cu-rich phase when aging for very long time. [11]

During manufacture, this Cu-rich phase and a niobium carbonitride phase precipitate simultaneously. S304H is characterized by an excellent precipitation hardening effect. It reaches peak hardness (246 HV) at 1000 h and maintains almost the same level till 8000 h at 650°C. [3]

The diffusion of chromium to the surface is accelerated and the formation of an adherent and dense chromium oxide (Cr2O3) layer is enhanced. This protective layer reduces further oxidation to a minimum.

Tubes of the material (ø 38 mm, wall thickness 6.3 mm) were used for grain size prediction. Its chemical composition analysis is shown in Table 1. Figure 1 shows the initial state microstructure of the tested material.

Tab. 1: *Chemical composition of tested material*

	C	Mn	Si	P	S	Cr	Ni	Nb	Cu	N
wt. %	0.090	0.873	0.243	0.005	0.015	18.8	8.449	0.508	3.515	0.091

Source: Own

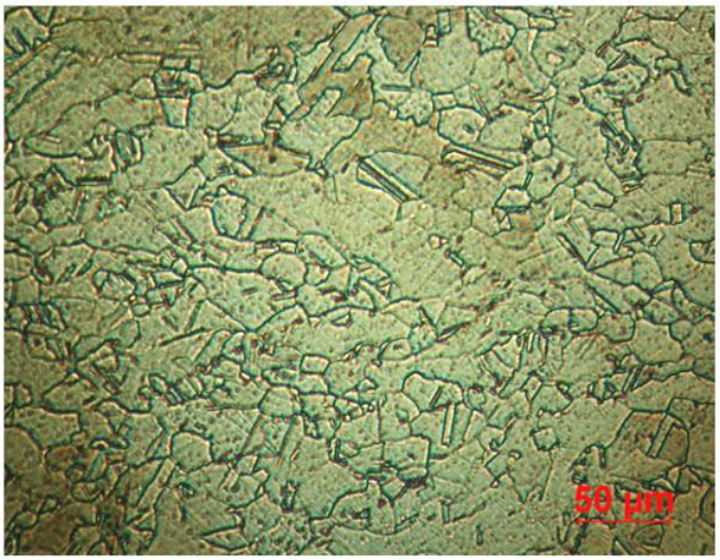

Source: Own

Fig. 1: *Initial state microstructure of S304H steel (80 ml HCl; 13 ml HF; 7 ml HNO3)*

2 The computation of grain size using the Sysweld program

The reduction of Gibbs surface free energy acts as the thermodynamic driving mechanism for grain growth. The grain growing process results in the reduction of the grain surface boundary and thus to a decrease in free energy. Grain size is important in two respects. It is important with regard to the mechanical properties of the material (e.g. brittleness), but also with respect to the influence on the transformation processes. The first models, which were built on the physical basis, were developed at the beginning of 1950s. In 1980, a new approach based on mathematical modelling was introduced. On the basis of computed simulations it was also possible to monitor the processes, which were previously difficult to observe, for example the volume change rate of the individual grains. Currently, the most commonly used simulation method is the "Monte Carlo Potts Model" method. A description of this method is given as an example in [5, 7]. An ideal rule for grain growth is given by equation (1). [8]

$$D^a - D_0^a = C \cdot e^{-\frac{Q}{R \cdot T}} \cdot t \tag{1}$$

D – grain diameter (mm), D_0 – initial grain size (mm),

C – material constant ($mm^a \cdot s^{-1}$), Q – activation energy ($J \cdot mol^{-1}$),

R – gas constant ($J \cdot K^{-1} \cdot mol^{-1}$), T – temperature (K),

t – time (s) a – coefficient (-).

It was established by experiments that coefficient values vary between 2 and 5. Value a=2 applies if the growing process is solely controlled by diffusion. Value a=4 is determined in the case where there is precipitation and diffusion along the grain boundary. Grain growing is, however, influenced by other factors, for example, heating rate and grain growth barriers. The computation of grain size proceeds in the Sysweld simulation program based on equation (2) which expresses the growing rate of the grain size.

$$\dot{D}^a = C \cdot \exp\left(-\frac{Q}{R \cdot T}\right) \tag{2}$$

Constant C is usually $0.4948 \cdot 10^{14}$ $mm^a.s^{-1}$. This computational equation is designed for cases when the amount of austenite is constant or is decreasing. If the amount of austenite increases, two developments are observed:

- Existing grains increase in size.
- New grains are generated with zero initial grain size.

By generalizing the conventional equation in order to determine the grain size, we arrive at the following equation (3).

$$\dot{D}^a = C \cdot \exp\left(-\frac{Q}{R \cdot T}\right) - \frac{\dot{\lambda}}{\lambda} \cdot D^a \tag{3}$$

In this equation, the λ value expresses the austenite proportion while the value $\dot{\lambda}$ shows the transformation rate of this phase. For $\dot{\lambda} > 0$ the austenite is created. If the austenite is not created, i.e. $\dot{\lambda} \leq 0$ then is the grain size expressed by the equation (2).

3 Experimental determination of grain size

For numerical analysis in Sysweld, it is important to know the input conditions defining the grain size changes, which depend on time and thermal exposure of the material. The test samples were 12 mm long rings cut from the given tube (ø 38 mm, wall thickness 6,3 mm). Since it concerned the moulding product, the specimens were measured longitudinally and transversely, because of the fact that the grains could by deformed during the moulding process. The specimens were thermally exposed in an oven at 1000°C, 1100°C for 4 and 8 hours and were subsequently cooled in water. While heating up to the test temperature the heating rate for all specimens was 420°C/hour.

Specimens for validating the structure were prepared according to a standard metallographic procedure. To accentuate the grain boundaries the specimens were cauterized in solution (80 ml HCl; 13 ml HF; 7 ml HNO_3). This solution had to be used because cauterization agents like Villela Bain or Vogel, which are commonly used for alloy materials, do not work with the used material. The grain size was evaluated according to CSN EN ISO 643 standard. The evaluation of the grain size was expressed by the intersection method and by the planimetric method. Based on these measurements, the average number of sections to one millimetre of measured line N_L was determined using the intersection method. Then, data such as the average length of linear sector l, the grain size number G1 and the number of grains in one mm^2 marked m were also determined. For the planimetric method it is important to determine the grain size number, G2 (based on this data it is possible to determine the average grain diameter $\bar{d}$ and the average grain surface area $\bar{a}$). From this, the real average grain surface area $\bar{a}_s$, the real average grain diameter $\bar{d}$ and the number of grains in one mm^2 can also be computed. [9] The determined values of the grain size for each set of experimental conditions for the intersection and planimetric method are shown in table 2.

Tab. 2: *Determined values of grain size*

Specimens S 304H		The data determined by help of intersectional method				The data determined by help of planimetric method			
		N_L	l	G1	Number of grains in 1mm^2	G2	Number of grains in 1mm^2	Middle grain surface [mm^2]	Middle grain diameter [mm]
Initial state	LD	52.326	0.01911	8	2048.0	8	2131.3	0.0004691	0.02166
	TD	47.007	0.02127	8	2048.0	8	2325.7	0.0004301	0.02074
1000 °C 4 hours	LD	40.716	0.02456	7-8	1536.0	8	2045.5	0.0004888	0.02211
	TD	53.353	0.01874	8	2048.0	8	1949.6	0.0005129	0.02265
1000 °C 8 hours	LD	45.857	0.02181	8	2048.0	8	1917.6	0.0005214	0.02284
	TD	67.634	0.01479	9	4096.0	8	2365.1	0.0004228	0.02056
1100 °C 4 hours	LD	41.222	0.02426	7-8	1536.0	7	847.8	0.0011794	0.03434
	LD	35.911	0.02785	7	1024.0	7	949.0	0.0010537	0.03246
	TD	45.880	0.02180	8	2048.0	7	1011.2	0.0009888	0.03145
	TD	51.672	0.01935	8	2048.0	7	1337.9	0.0097474	0.02734
1100 °C 8 hours	LD	21.842	0.04578	6	512.0	6	591.2	0.0016915	0.04113
	TD	36.882	0.02711	7	1024.0	6	544.5	0.0018365	0.04286

N_L – average number of grains gripped to the line unit length, **l** – average length of linear sector, **G1** – grain size number evaluated with intersectional method, **G2** – grain size number evaluated with planimetric method, **LD** – longitudinal direction, **TD** – transversal direction

Source: [9]

4 Mathematical computation of grain size using Sysweld

The experimentally determined values of grain size (see table 2) were used as input data for the grain size calculation in the Sysweld simulation program. The computations of this program are based on equations (2) and (3). The value of the activation energy, Q, can be set in the definition of the computation model by using a positive power constant, a, and the constant, C.

In the first phase, the input data leads to a computed grain size, which corresponds to the experimentally determined grain size. Based on experience, it can be said that the main parameter for predicting grain size by mathematical simulation is the activation energy, Q. Constant C remain unchanged, $C=0{,}4948 \cdot 10^{14}$ mm^4.s^{-1} and the power constant, a, usually matches a=4 (the case of precipitation and diffusion along the grain boundary). Based on these results, the activation energy Q or the ratio Q/R is then determined. In the case of S304H steel it is optimal to keep the ratio Q/R=73400 for a temperature of 1000°C and Q/R=74800 for a temperature of 1100°C. [10]

This validated model is consequently used for the calculation of the grain size based on non-stationary temperature fields appearing during welding. Figure 2 depicts a 3D simulation model of a weld made up of three weld beads as well as the weld´s basic geometry. All the weld beads on the simulation model are only created by using an additional material. However, the simulation model the of heat source correspond with melting boundaries to the real weld geometry of individual weld beads.

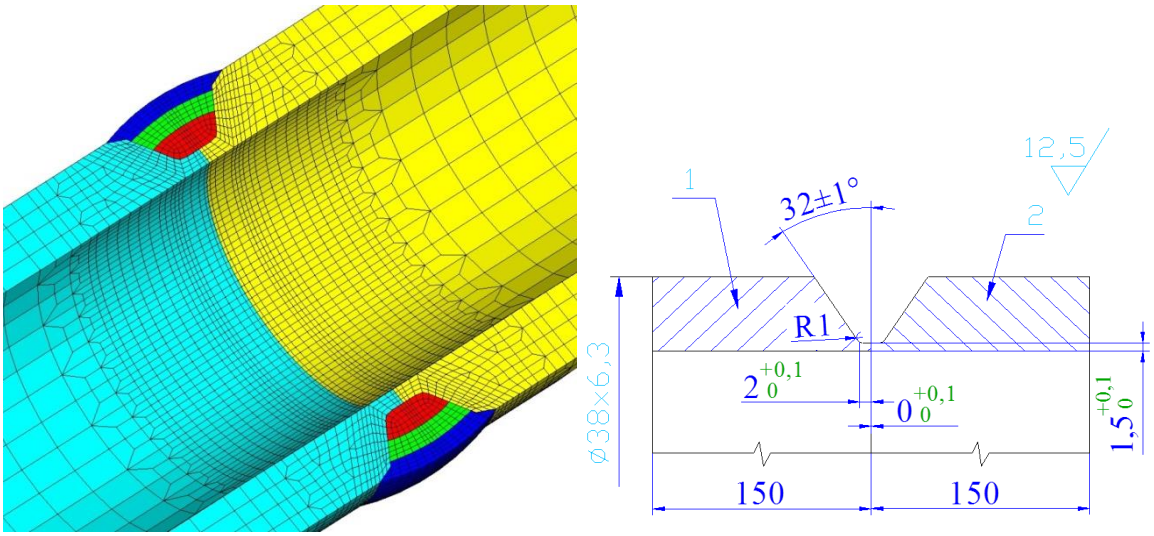

Source: [10]

Fig. 2: *3D simulation model of the weld with three weld beads and the weld geometry*

Figure 3 shows the results of computing the grain size in HAZ for the weld made on S304H steel tube ø 38, wall thickness 6.3 mm. The weld was made by an automated machine using GTAW method. Three weld beads were made with a preheating temperature of 180°C, an interpass temperature of 290 °C and using additional material Thermanit MTS 616. The edges of the individual weld beads were reciprocally shifted by 120° while the welding directions of the successive beads were reversed. None of the weld beads was finished immediately after 360°, they all overlapped their edges at least by 10 mm. Experimental welds were made in Vítkovice Steel company and the welding parameters are their know-how. The asymetricity of the austenite grain distribution in HAZ in rotary symmetrical model (fig.3) occurs in the areas where the ends of original beads were rewelded by about 10 mm.

Figure 4 displays the details of grain coarseness in HAZ on the boundary of the second and third weld bead.

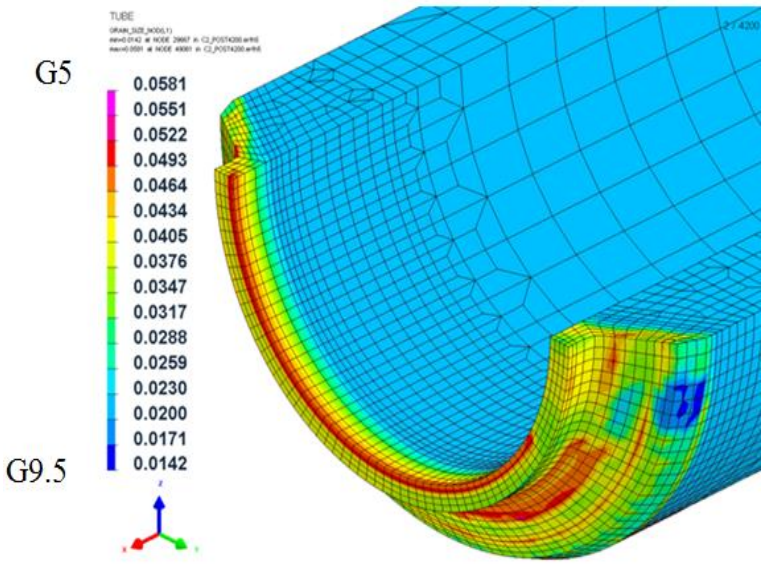

Source: [10]

Fig. 3: *The results of computing grain size in HAZ after welding (S304H)*

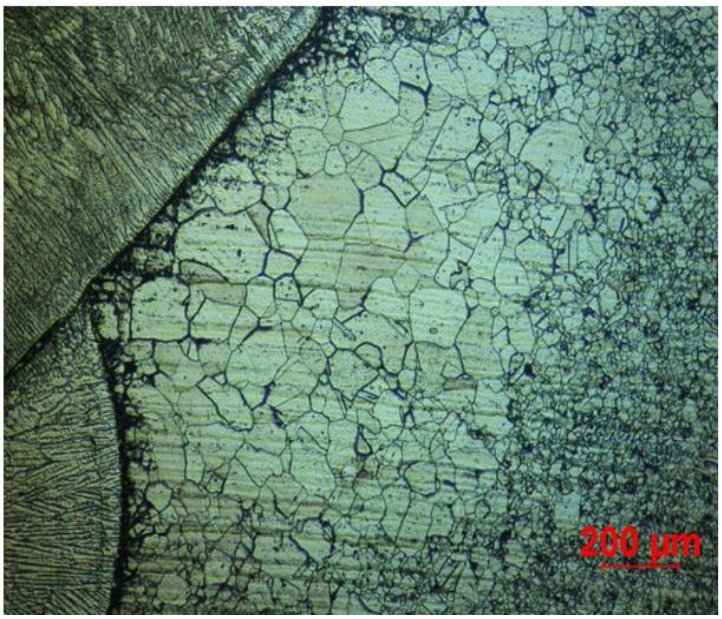

Source: Own

Fig. 4: *Detail Details of grain coarseness in HAZ after welding on the boundary of the second and third weld bead (S304H)*

Following the real-life welding experiment, the computed data of the grain size and the real-life grain size formed in HAZ were compared. Specifically points 0.5; 1; 1.5; 2; 2.,5; 3 and 5 mm from the melting boundary (MB) were compared. Table 3 shows the comparison of the grain size results computed numerically and formed experimentally.

Tab. 3: *Comparison of the grain size results computed numerically and formed experimentally*

Distance from the MB [mm]	**0.5**	**1.0**	**1.5**	**2.0**	**2.5**	**3.0**	**5.0**
Middle grain size [mm], **experiment**	0.0880	0.0845	0.0272	0.0239	0.0209	0.0190	0,0207
Number of grains in 1 mm^2, **exper.**	129	140	1348	1749	2289	2752	2325
Grain size number G, **exper.**	G4	G4	G7	G8	G8	G8	G8
Middle grain size [mm], **computation**	0.0539	0.0512	0.0296	0.0243	0.0204	0.0204	0.0204
Number of grains in 1 mm^2, **comp.**	344	381	1141	1693	2403	2403	2403
Grain size number G, **comp.**	G5	G5	G7	G8	G8	G8	G8

Source: Own

Conclusion

The computational program module for the determination of grain size using the Sysweld program was developed as a marginal module, mainly meant for public purposes. However, we can now see an increasing demand for this type of simulation computation. That is why one of the aims of the TA02010992 project is the validation and, if necessary, the modification of this program module, thus the predicted values of austenitic grain size after welding or heat treatment correspond to the real situation. The most important aspect is the optimization of the HAZ results, because the processes are very dynamic there and thus we can expect intensive grain growth in that area.

From Table 3 it is evident that the prediction of austenitic grain size using mathematical models reflects the reality very well. This close agreement is especially evident at 1.5 mm from the melting boundary. In the area with the highest thermal gradients to the area 1.5 mm from the melting boundary, the grains predicted by simulations (G5) are smaller than those determined experimentally (G4). This discrepancy is probably caused by the computational program module design, which, at present, makes it impossible to insert the input data in the form of temperature dependency. This particular inaccuracy could also be caused by the grain size determination method according to CSN EN ISO 643 standard.

According to this norm, the grain size is determined at the defined surface. There is irregular temperature distribution in the HAZ of the weld and the grain size decreases as the distance of the melting boundary increases. However, there are no standard instructions for predicting grain size in the HAZ and thus the selected method provides the most relevant results.

Acknowledgements

The article was prepared within the scope of the TA02010992 grant project.

Literature

[1] SHINGLEDECKER, J.P.; MAZIASZ, P.J.; EVANS, N.D.; POLLARD, M.J.: Alloy additions for improved creep-rupture properties of a cast austenitic alloy. *Proceedings of the Conference of Creep Deformation and Fracture, Design, and Life Extension, The Materials Society*, Warrendale, PA, 2005, pp. 129-138.

[2] PRABHA, B.; SUNDARAMOORTHY, P.; SURESH, S.; MANIMOZHI, S.; RAVISHANKAR, B.: Studies on Stress Corrosion Cracking of Super 304H Austenitic Stainless Steel. *Journal of Materials Engineering and Performance.* December 2009, Volume 18, Issue 9, pp 1294–1299.

[3] TOHYAMA, A.; HAYAKAWA, H.; MINAMI, Y.: Development of high strength steel boiler tube (TEMPALOY AA-1). *NKK Technical review*, No. 84, 2001, p. 30-35.

[4] SAWARAGI, Y.; OGAWA, K.; KATO, S.; NATORI, A.; HIRANO, S.: Development of the economical 18-8 stainless steel (SUPER 304H) having high elevated temperature strength for fossil fired boilers. *The Sumitomo search*, No. 48, 1992, pp. 50-58.

[5] ZÖLLNER, D.; STREITENBERGER, P.: Three-dimensional normal grain growth: Monte Carlo Potts model simulation and analytical mean field theory. *Scripta Materialica 54*. 2006, pp 1697–1702.

[6] CABRILLAT, M.T.; ALLEGRE, P.; PLUYETTE, E.; MICHEL, B.: Intergranular reheat cracking in S 304H components. *Experiments and damage evaluation. Transactions*, SMiRT 16, 2001.

[7] ZÖLLNER, D.; STREITENBERGER, P.: Monte Carlo Potts Model Simulation and Mean-Field Theory of Normal Grain Growth. *Shaker Verlag GmbH*, Germany, 2006, 170 p.

[8] KHZOUZ, E.: Grain Growth Kinetics in Steels. *A Major Qualifying Project Report*. Worcester polytechnic institute, April 2011, 144 p.

[9] MORAVEC, J.; NOVÁKOVÁ, I.: Measurement of austenitic grain size by S304H steel.*Technical report TUL-Z-12-VZ-03*. 2012, 8 p.

[10] SLOVÁČEK, M.; TEJC, J.; KOVAŘÍK, J.; BEJVL, J.; RICHTER, T.; VANĚK, M.: Development and validation of material models, current state characterization. *Technical report Mecas ESI M_Z_12_024_R01*. 2012. 44 p.

[11] CENGYU, CH.; HONGYAO, Y.; JIANXIN, D.; XISHAN, X.; ZHENGGIANG, C.; XIAOFANG, CH.; FUSHENG, L.: Strengthening effect of Cu-rich phase precipitation in 8Cr9Ni3CuNbN austenitic heat-resisting steel. *Acta Metallurgica Sinica (Engl. Lett.) Vol. 24*, April 2011, pp 141–147.

VLIV SVAŘOVÁNÍ NA TEPELNĚ OVLIVNĚNOU OBLAST U TRUBEK Z OCELI S304H SE ZAMĚŘENÍM NA PREDIKCI VELIKOSTI ZRNA POMOCÍ NUMERICKÝCH SIMULACÍ

Austenitické oceli S304H se využívají především pro parní kotle tepelných elektráren a jiných energetických zařízení. Jednou z nejdůležitějších vlastností u trubek v parních kotlích je jejich vysokoteplotní odolnost. Rozdíly materiálových vlastností ocelí S304H, především creepové odolnosti, v porovnání s austenitickými ocelemi obdobného složení jsou dosaženy hlavně přidáním cca 3 hm. % mědi. Tvorba na měď bohatých precipitátů během provozu vede ke zvýšení creepové odolnosti precipitačním zpevněním. Příspěvek popisuje vliv svařovacího cyklu u materiálu S304H na zhrubnutí zrna v tepelně ovlivněné oblasti. Budou také uvedeny možnosti a způsoby predikce velikosti zrna pomocí numerických simulací svařování a tepelného zpracování. Dále bude ukázán a popsán princip získávání vstupních dat potřebných pro numerické simulace predikující velikost zrna.

VORHERSAGE DER KORNGRÖßE IN DER WÄRMEEINFLUSSZONE AN GESCHWEIßTEN ROHREN AUS S304H STAHL MIT NUMERISCHEN SIMULATIONEN

Austenitische Stähle, bezeichnet als S304H, werden besonders für Dampfkessel von thermischen Kraftwerken und andere Energieanlagen verwendet. Für die verwendeten Rohre im Dampfkessel ist eine der wichtigsten Eigenschaften ihre Festigkeit bei hohen Temperaturen. Unterschiede der Werkstoffeigenschaften, besonders der Kriechbeständigkeit, werden im Vergleich zum austenitischen Stählen der gleicher Zusammensetzung bei diesen Werkstoffe durch die Zugabe von etwa 3% (Gew.) Kupfer erzielt. Die Bildung kupferreicher Ausscheidungen während des Betriebes führt zu einem Anstieg der Kriechfestigkeit durch die Härtung der Ausscheidung. Der Beitrag zeigt den Einfluss des Schweiß-Zyklus auf die Kornvergröberung in der Wärmeeinflusszone des S304H Stahl. Es wird die Art und Weise der Vorhersage der Korngröße mit numerischen Simulation von Schweißen und Wärme Behandlung gezeigt. Es wird auch das Prinzip der Einholung der erforderlichen Eingabedaten für die numerische Simulationen zur Vorhersage der Korngröße vorgestellt und beschrieben.

WPŁYW SPAWANIA NA STREFĘBĘDĄCĄ POD WPŁYWEM CIEPŁA W PRZYPADKU RUREK WYKONANYCH ZE STALI S304H Z UWZGLĘDNIENIEM PROGNOZOWANIAWIELKOŚCI ZIARNA PRZY POMOCYSYMULACJI NUMERYCZNYCH

Stale austenityczne o oznaczeniu S304H są wykorzystywane głównie do produkcji kotłów parowych pracujących w elektrociepłowniach oraz innych urządzeniach energetycznych. Jedną z najważniejszych właściwości rurek w kotłach parowych jest ich odporność na wysokie temperatury. Różne właściwości stali S304H, w szczególności żaroodporność, w porównaniu do stali austenitycznych o takim samym składzie są uzyskiwane przede wszystkim poprzez dodanie ok. 3 obj. % miedzi. Tworzenie się precypitatów bogatych w miedź podczas procesu prowadzi do zwiększenia żaroodporności materiału poprzez wzmocnienie precypitacyjne. W artykule opisano wpływ cyklu spawalniczego na rozrost ziarna w strefie wpływu ciepła stali S304H. Ponadto przedstawiono możliwości oraz sposoby prognozowania wielkości ziarna przy wykorzystaniu analiz numerycznych procesów spawania i obróbki cieplnej. Oprócz tego także opisano sposób pozyskiwania niezbędnych danych wejściowych do celów symulacji numerycznej prognozującej wielkość ziarna.

TESTING PHYSIOLOGIC COMFORT OF FUNCTIONAL CLOTHING

Ladislav Nagy
***Antonín Havelka**
****Zdenek Kůs**
*****Soňa Jandová**

Technical University of Liberec
Faculty of Textile Engineering
Department of Clothing Technology
Studentská 2, 461 17 Liberec, Czech Republic
ladislav.nagy@tul.cz

*Technical University of Liberec
Faculty of Textile Engineering
Department of Clothing Technology
Studentská 2, 461 17 Liberec, Czech Republic
antonin.havelka@tul.cz

**Technical University of Liberec
Faculty of Textile Engineering
Department of Clothing Technology
Studentská 2, 461 17 Liberec, Czech Republic
zdenek.kus@tul.cz

***Technical University of Liberec
Faculty of Science, Humanities and Education
Motor Activity Laboratory, Department of Physical Education
Studentská 2, 461 17 Liberec, Czech Republic
sona.jandova@tul.cz

Abstract

The subject of research work carried out at the Department of Clothing of the Faculty of Textile at the Technical University of Liberec was innovation and monitoring of physiologic properties of the first layer of functional clothing for sportsmen, army, firemen, police, etc.

Physiologic properties of clothing are ones of the properties requested from functional clothing and they are important because they significantly influence not only the wearer's feelings but also psyche and performance of sportsmen, soldiers, policemen, etc. No universal clothing, which would be suitable for all weather conditions and physical exercise of the wearer can be designed, however, more suitable textile materials and more elaborated designs of clothing for improvement of clothing comfort can be used. The focus of research work was laboratory testing with proband's simulated load with monitoring of temperatures and moisture in the limit layer of clothing. Based on the analysis of measured values and test results of set of T-shirts, a set of optimum structures of textile materials for functional clothing was designed.

Introduction

Clothing is an inseparable part of human life. The prime role of clothing is to protect body against unstable environs. Human body can be considered as an open system, which is always in the state of physical, chemical and biological interaction with the environs. Clothing is a protective system, in which heat and moisture penetrate. Penetration of heat and moisture

depends on the construction, cut, used textile material and parameters of the clothing layer. Clothing helps thermoregulation of the organism in the cases when the body itself is not capable of auto-regulation.

Comfort as such can then be defined as a state of organism when physical functions of organism are in optimum and when environs of the human, including clothing, do not produce any unpleasant perceptions.

1 Test methodology used for investigation

In view of the fact that comfort is directly related to physiologic process, it can be measured quantitatively. Comfort of clothing can be evaluated by measuring selected physical properties of textiles and clothing (water vapours and air permeability, thermal resistance, etc.) that influence physiologic comfort. A more objective way is to carry out testing with probands. These can be carried out under real conditions – using clothing in real conditions or under controlled climatic conditions and activities in a laboratory. Measurement under controlled conditions has significant advantages, testing conditions are reproducible and sensors can be connected to the person's body with the aim to gain objective data. Such data may include heart rate, temperature and skin moisture in various points of proband's body in the limit layer or in the clothing structure, including sensory assessment of clothing. Figure 1 shows how the test is carried out. The research activity consisted in testing the set of T-shirts proband's defined load and under defined conditions of the environment with the choice of monitoring selected quantities, which provide possibilities of clothing comfort evaluation.

Source: Own

Fig. 1: *Proband while testing the 1st layers of clothing in the laboratory of physiologic comfort.*

1.1 Theoretical analysis

Water vapours permeability is fundamental to functional clothing, during intense activities of a person, production of sweat can reach 1000g/hour and such quantity must be transported

through clothing. Increasing moisture on the skin, especially in liquid form, means immediate worsening of comfort and decreasing of person's performance and concentration and that is why transfer of moisture is important [1].

Water vapours permeability is closely connected with the material, from which the structure of clothing is created; it is also connected with the structure and porosity of the fabric. Porosity is a characteristic affecting the breathability of fabrics. It may be defined as the pore volume to the total volume of fabric. Porosity determines the amount of the volume of air contained in the fabric surface, but says nothing about the position, type and size of pores, or their mutual arrangement (1):

$$p = \frac{\rho_{fc} - \rho_V}{\rho_{fc}} * 10^2 [\%] \tag{1}$$

where: ρ_{fc} density of air conditioned fibers [kg·m^{-3}],

ρ_V material bulk density [kg·m^{-3}].

Basically, there are two factors – sorption capacity of fibres and desorption capacity and then surface tension on fibres, structure and wetting capacity of fibres. Sorption capacity of fibres can have positive effect in the first moments of dampening but on the other hand, fibre remains wet for a long time and so it does not contribute to good comfort of clothing [2]. The profile of fibres, which, in sophisticated construction, allows perfect wetting, and thereby intense transport of liquid moisture, is applied fundamentally.

The moisture transport generally proceeds also by other mechanisms (capillary, sorption), but we can presume that the diffusion way will be the more dominant.

It is possible to describe moisture transport by a relation (2) for mass transport [3][4]:

$$q_{dif_i} = -D_i \cdot \nabla \cdot \rho_i \tag{2}$$

where: D_i coefficient of diffusion transport of mass for the ith – component [m^2·s^{-1}],

$\nabla\rho_i$ gradient of partial mass density for the ith - component [kg·m^{-3}].

For a unit flow of moisture as a compound of gaseous environs with a partial pressure of p_i' (p_i' – partial pressure inside of porous clothing material, p_i'' – partial pressure outside the porous clothing material) it is possible to use a relation (3):

$$q_{dif_i} = D_i \frac{M_i}{RmT} \frac{p_i' - p_i''}{s} \tag{3}$$

where: Rm universal gas constant [kJ·kmol·K^{-1}],

M_i molar mass [mol],

T temperature [K],

S layer thickness [m].

Based on the results of theoretic analysis of physiologic comfort, the following experiments had been planned and consequently carried out:

a) testing the selected set of T-shirts, from natural materials to modern Smart textiles during simulated load on stationary bicycle when monitoring heat and moisture and measuring temperature fields using Thermocam.

b) measuring the properties determining clothing comfort in the laboratories of physiologic comfort at different temperatures and moisture in a set of knitting suitable

especially for the first layer of clothing allowing comparison of classical and modern synthetic fibres of these fabrics [5].

2 Simulating load of proband with T-shirt

The experimental measurement was carried out in the Laboratory of Physiologic Comfort at the Clothing Department, Faculty of Textile, Technical University of Liberec.

Proband performed physical activity on stationary bicycle in air-conditioned room. Temperature in the room was set to 21 ± 1°C, humidity to 60 ± 5%. Physical exercise was carried out at a defined heart rate for 45 minutes. Load was set to reach and maintain the value of heart beat ranging between 140-145 beats per minute. Proband maintained heart beat within this interval for all the time of testing. Heart beat was monitored using heart beat sensing band attached to proband's trunk.

13 T-shirts of different material composition and weight were tested. Material parameters of tested T-shirts are stated in Table 1.

Tab. 1: *Material parameters of tested T-shirts*

Marking	Material	Producer / Origin	Structure	Thickness [mm]	Weight [g/m^2]	Air permeability [l/min/m^2]	Resistance against water vapours R_{et} [m^2.Pa.W^{-1}]	Thermal resistance R_{ct} [m^2.K.W^{-1}]
T-shirt 1	100% CO	KAJA s.r.o / Armed forces of the Czech Republic	weft single plain	0.69	170.22	2089.00	2.56	0.019
T-shirt 2	100% WO	DEVOLD MSM / Norway	weft double	0.94	216.85	>12000.00	2.59	0.037
T-shirt 3	100% PP	SPOLSIN s.r.o. / Czech Republic	weft interlock	1.51	189.16	6060.00	5.12	0.046
T-shirt 4	100% PL	ADIDAS / Philippines	weft interlock	0.59	132.19	9750.00	2.00	0.011
T-shirt 5	95%CO/ 5% EL	SPOLSIN s.r.o. / Czech Republic	weft single plated jbutted	0.77	225.69	1620.00	4.15	0.025
T-shirt 6	100% CO	French Armed Forces	weft single plain	0.67	161.17	5057.00	3.06	0.020
T-shirt 7	100% CO	Romanian Armed Forces	weft single plain	0.91	220.02	1993.00	3.78	0.017
T-shirt 8	50%CO/50%PL	United Stated Army	weft single plain	0.72	153.86	5786.00	3.23	0.024
T-shirt 9	100% CO	Italian Armed Forces	weft single plain	0.69	151.61	5014.00	2.92	0.015
T-shirt 10	50%CO/50%PL	Macedonian Armed Forces	weft single plain	0.67	156.95	6600.00	2.82	0.020
T-shirt 11	100% CO	British Army	weft single plain	0.83	215.89	1294.00	3.38	0.018
T-shirt 12	100% PL	Polartec / USA	weft interlock	0.92	179.42	>12000.00	3.14	0.003
T-shirt 13	100% PL	Polartec / USA	weft single plated jbutted	0.57	124.17	4170.00	1.30	0.008

Source: Own

2.1 Procedure and conditions of testing T-shirts

Before the test, 5 sensors were attached, always in equal placement, to a T-shirt. The sensors were placed into vapour-permeable "pockets" made of "Neoshell-Polartec" material. Before the measurement, the tested T-shirt was placed into an air-conditioned room with the temperature of 21 ± 1°C and moisture of 60 ± 5% for 30 minutes. See [6] for detailed data.

At the beginning and during the test, sensory perception of clothing comfort by proband was monitored. The aim of the monitoring was to evaluate the first layer of clothing on the base of the monitored individual's feelings during a long-term physical exercise, and the following parameters were found out:

- proband's thermal sensations (criterion: thermal receptiveness), rating scale 1-10 – 1- thermal balance, 10 – too warm or too cold
- proband's sensations of moisture (criterion: dampness), rating scale 1-10 – 1- no sensation of dampness, 10 – extreme dampness
- proband's sensory sensations (criterion: prickliness, rustling), rating scale 1-10 – 1- very pleasant, 10 - unpleasant
- proband's physical activity (criterion: physical fatigue), rating scale 1-10 – 1- not tired, fresh, 10 – tired out

2.2 Evaluation of the experiment

Within the phases, the experiment continuously focuses on three parts important for overall evaluation of T-shirts:

1. Material evaluation of T-shirts
2. Objective evaluation of T-shirts
3. Subjective evaluation of T-shirts

This paper primarily focuses on subjective evaluation of T-shirts, which is an important part of overall evaluation of functional clothing by the wearer. Phases 1 and 2 will be subjects of the following papers.

For each T-shirt, a questionnaire for subjective evaluation of T-shirt by the proband was designed and subsequently assessed.

Visual display of subjective evaluation of the T-shirt by proband and their mutual comparison before, during and at the end of the test is shown in the following radial diagrams. From the diagrams, see Fig. 2-4, it is evident that subjective sensing of the T-shirt by proband is getting worse during long-term physical exercise.

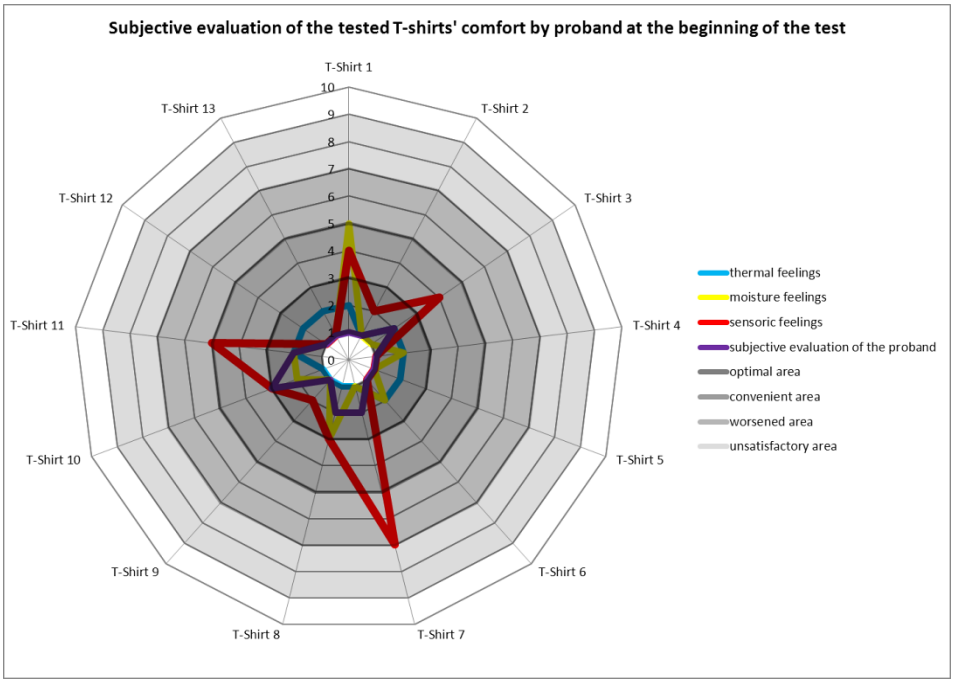

Source: Own

Fig. 2: *Subjective evaluation of the tested T-shirts' comfort by proband at the beginning of the test.*

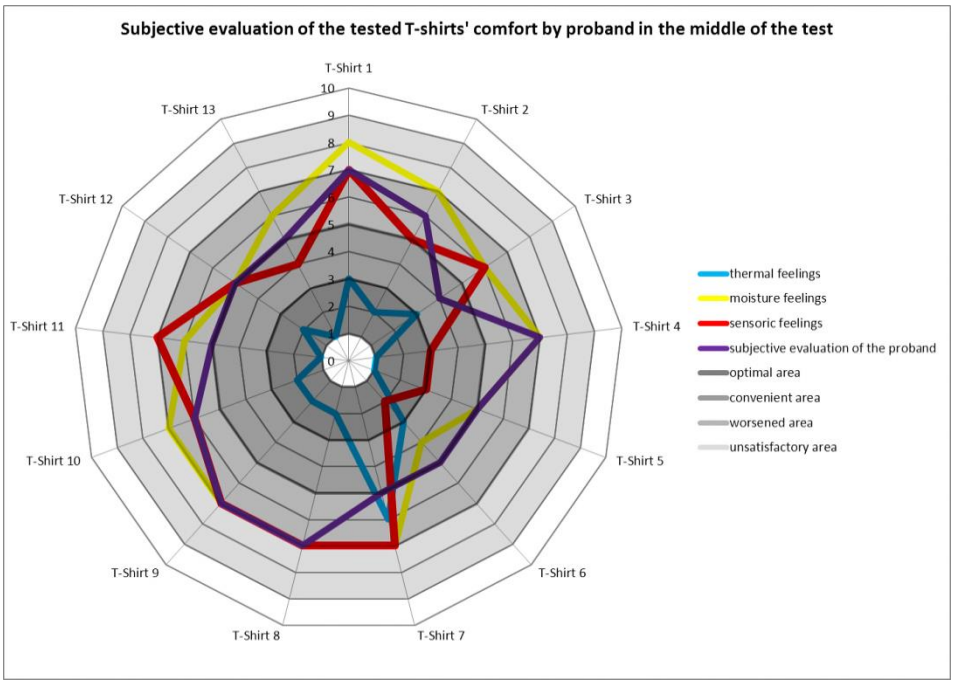

Source: Own

Fig. 3: *Subjective evaluation of the tested T-shirts' comfort by proband during the test.*

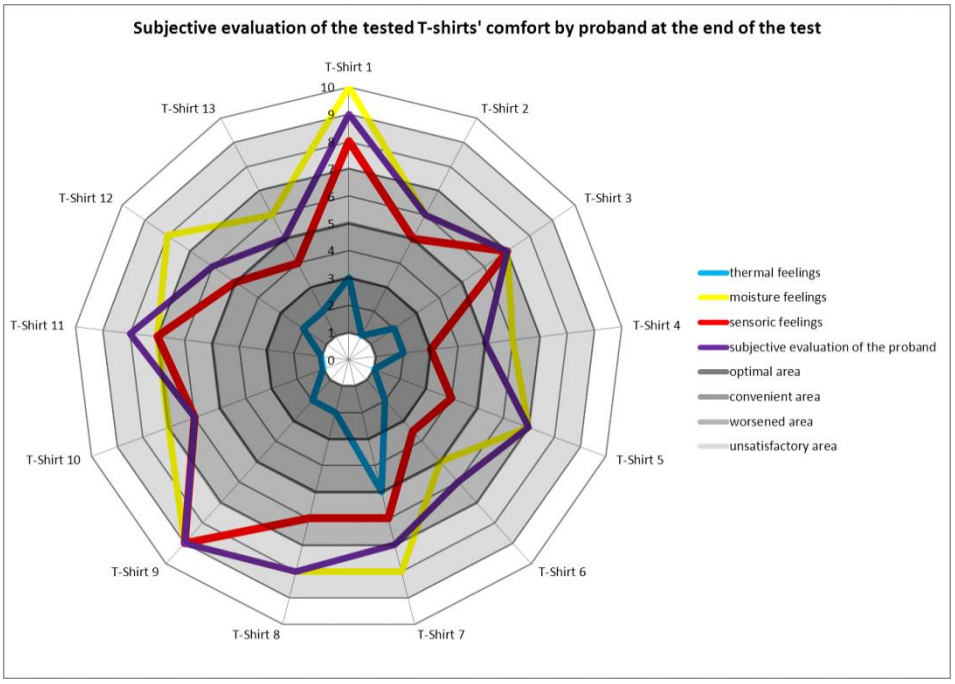

Source: Own

Fig. 4: *Subjective evaluation of tested T-shirts' comfort by proband at the end of the test.*

The T-shirt, individual curves of which deviate from optimum limits, or correspond with the diagram area displayed in dark grey colour in the middle of the diagram, is assessed as the best. It applies that an ideal T-shirt would take up the area in the middle of the diagram with the radius of 1.

Overall subjective evaluation of clothing by proband is shown in the following Table 2. At the end of the test, each T-shirt was awarded an overall grade in accordance with commonly used school classification 1 – the best, 5 – the worst (extending the final mark by a plus or minus sign was allowed). The ranking of individual T-shirt is divided into 5 colour zones for better

comprehensibility. The final marks are used for assessment in multi-criteria assessment of clothing [6].

Tab. 2: *Overall subjective evaluation of T-shirts by proband.*

Proband		
Overall ranking of T-shirt	Marking of T-Shirt	Awarded grade
1	T-shirt 2	1
2	T-shirt 13	1-
3	T-shirt 12	2+
4	T-shirt 6	2
5	T-shirt 5	2-
6	T-shirt 10	2-
7	T-shirt 4	3
8	T-shirt 3	3
9	T-shirt 8	3-
10	T-shirt 11	4+
11	T-shirt 7	4-
12	T-shirt 9	5
13	T-shirt 1	5

Source: Own

Conclusion

The first layer of clothing, which is in contact with the skin and, in addition, must transfer moisture and heat in order to reach the area of temperature and moisture with good comfort is crucial for thermo-physiologic and sensory comfort of functional clothing.

Primarily the experiment focused mainly on the first layer of clothing, which influences the wearer's physiologic comfort most. Common materials of T-shirts such as for example cotton or the mixture of cotton/PL, or cotton/elastane as well as new sophisticated fibres and structures (Polartec, Adidas, and Moira) were selected for the set of tested materials.

The overall complex evaluation of T-shirts results from three independent aspects:

- Subjective evaluation of clothing by proband
- Monitoring temperature and moisture at proband's defined load under laboratory conditions
- Measured results of the properties in physiologic comfort laboratories FT-KOD, which influence clothing comfort

From the above mentioned diagrams, Fig. 2-4, it is evident that there are minimum differences in subjective perception of clothing comfort by the proband at the beginning of the test. With increasing long lasting exercise the different structures and material compositions of individual T-shirts start presenting themselves and the proband starts to feel worsening comfort of clothing. The greatest differences in perceiving the clothing comfort by proband,

compared to the beginning of the test, are found out at the end of the test. The T-shirt, in which the least deterioration of subjective sensory comfort is reached, can then be considered as the most appropriate first layer for a long time physical activity.

Based on the measured results of proband's subjective evaluation and based on the overall subjective evaluation of material stated in Table 1, T-shirt No. 12 (Polartec® Power Dry® FR) was selected for the next phase of testing as the first layer of functional clothing. T-shirt 12 and T-shirt 2 gained the best subjective evaluation of comfort by proband, and that is why these T-shirts have the best preconditions for achieving as good proband's physiologic comfort as possible during long-term exercise.

Literature

[1] MOTAWE, H., M.: *Factor affecting garment's thermophysiological properties in tropical weather countries.* Liberec: Technická univerzita v Liberci, Fakulta textilní, Katedra oděvnictví, 2012. PhD. Thesis, sv.180

[2] MOTAWE, M.; HAVELKA, A.; KŮS, Z. Thermophysiological investigation of cottonfabrics and viscose fabrics made from bamboo plants. *ACC JOURNAL XVIII*. 2012, 1, s. 49-57. Technická univerzita v Liberci, 2012, ISSN 1803-9782

[3] ŠESTÁK, J., RIEGER, F.: *Přenos hybnosti, tepla a hmoty*. Praha: Vydavatelství ČVUT, 2005. 299 s.

[4] HAVELKA, A.; KŮS, Z. Innovations in Textile materials & Protective clothing. Monograph, Warsaw, 2012: Technical university of Lodz press. The importance of moisture transport in the insulating properties of sandwich structures, smart clothes, s. 137-144. ISBN 978-83-7283-493-5.

[5] HAVELKA, A.; KŮS, Z. The transport phenomena of semi-permeable membrane for sport cloth. *International Journal of Clothing Science and Technology*, Volume 23, Number 2/3, 2011, s. 119-130. ISSN 0955-6222.

[6] HAVELKA, A.: *„Fyziolog"– Inovace a monitorování fyziologických vlastností speciálních oděvů pro ozbrojené síly a oděvy pro zraněné a nemocné.,* Liberec 2012. 226 s. Závěrečná zpráva o realizaci projektu č. 907980. Technická univerzita v Liberci, Fakulta textilní, Katedra oděvnictví.

TESTOVANÍ FYZIOLOGICKÉHO KOMFORTU FUNKČNÍCH ODĚVŮ

Předmětem výzkumných prací, prováděných na Katedře oděvnictví Fakulty textilní Technické univerzity v Liberci, byla inovace a monitorování fyziologických vlastností první vrstvy funkčních oděvů pro sportovce, vojsko, hasiče, policii atd. Fyziologické vlastnosti oděvů jsou jednou z požadovaných vlastností na funkční oděv a jsou důležité, protože významně ovlivňují nejen pocity nositele, ale i psychiku a výkon sportovců, vojáků, policie atd. Nelze navrhnout univerzální oděv, který bude vyhovovat při všech povětrnostních podmínkách a fyzické zátěži nositele, ale lze použít vhodnější textilní materiály a propracovanější design oděvů pro zlepšení oděvního komfortu. Těžištěm výzkumných prací byly laboratorní testy při simulované zátěži probanda s monitorováním teplot a vlhkosti v mezní vrstvě oděvů. Na základě analýzy naměřených hodnot a výsledků testů souboru T-Shirt byl navržen soubor optimálních struktur textilních materiálů pro funkční oděv.

PRÜFUNG DES PHYSIOLOGISCHEN KOMFORTS DER FUNKTIONSKLEIDUNG

Gegenstand der Forschungsarbeiten, die an dem Lehrschul für Bekleidungsindustrie an der Textilfakultät der Technischen Universität in Liberec durchgeführt wurden, waren Innovationen und die Überwachung der physiologischen Eigenschaften der ersten Schicht der Funktionskleidung für Sportler, die Armee, die Feuerwehr, die Polizei etc. Die physiologischen Eigenschaften der Kleidung sind eine der erforderlichen Eigenschaften der Funktionskleidung und sie sind wichtig, da sie nicht nur die Gefühle des Trägers, sondern auch die Psyche sowie die Leistung der Sportler, der Soldaten, der Polizei etc. bedeutend beeinflussen. Es kann keine Universalkleidung entworfen werden, die allen Witterungseinflüssen und der physischen Belastung des Trägers entsprechen wird, aber es können geeignetere Textilmaterialien und ein durchgearbeitetes Kleidungsdesign für die Verbesserung des Kleidungskomforts verwendet werden. Der Schwerpunkt der Forschungsarbeiten waren Labortests bei einer simulierten Belastung einer Testperson mit der Überwachung von Temperaturen und der Feuchtigkeit in der Grenzschicht der Kleidung. Auf Grund der Analyse der gemessenen Werte und der Testergebnisse des T-Shirt-Komplexes wurde ein Komplex von optimalen Strukturen der Textilmaterialien für eine Funktionskleidung entworfen.

TESTOWANIE KOMFORTU FIZJOLOGICZNEGO ODZIEŻY FUNKCYJNEJ

Przedmiotem prac badawczych, prowadzonych w Katedrze Odzieżownictwa Wydziału Tekstylnego Uniwersytetu Technicznego w Libercu, była innowacja i monitorowanie właściwości fizjologicznych pierwszej warstwy odzieży funkcyjnej dla sportowców, wojska, straży pożarnej, policji, itd. Właściwości fizjologiczne odzieży należą do wymaganych właściwości odzieży funkcyjnej i są ważne, ponieważ w znacznym stopniu wpływają nie tylko na odczucia osoby noszącej, ale również na psychikę i wyniki sportowców, żołnierzy, policjantów, itd. Nie można opracować uniwersalnej odzieży, która będzie odpowiednia w każdych warunkach atmosferycznych i przy różnym obciążeniu fizycznym osoby noszącej, ale w celu poprawy komfortu można zastosować lepsze materiały tekstylne i lepiej opracowane wzornictwo odzieży. Głównym przedmiotem prac badawczych były testy laboratoryjne z symulowanym obciążeniem probanta i z monitorowaniem temperatury i wilgotności w warstwie granicznej odzieży. Na podstawie analizy pozyskanych wartości i wyników testów zespołu T-Shirt opracowano zbiór optymalnych struktur materiałów tekstylnych dla odzieży funkcyjnej.

ABOUT THE THERMAL CONDUCTIVITY OF MULTI-LAYER CLOTHING

*** Priscilla Reiners**
Yordan Kyosev

Hochschule Niederrhein – University of Applied Sciences
Faculty of Textile and Clothing Technology
Mönchengladbach, Germany
* priscilla.reiners@hs-niederrhein.de

Abstract

Measurement of thermal conductivity of textile structures for clothing is still a big challenge. This is because the values are below or at the limits of the bottom range of existing equipment of current testing devices. On the other hand, the optimisation of the thermal comfort of clothing values is required, because there are several single layers in men´s suits or women´s costumes and only with complete information about each layer more complex computations and calculations are possible.

This work presents a part of larger experimental investigations, related to the R_{ct} values of woven and knitted structures combined into several layers. Compressibility and thickness of single and multiple layers were measured; both using standard testing equipment and analysing cross sections of the layers embedded into resin. In order to investigate the influence of the air between multiple layers, the R_{ct} values of five layers of the same structure were estimated using the PERMETEST device of the company Sensora. Some correlations were found and statistically proven between the R_{ct}, the number of layers and the volume of the air layer between the layers.

Finally, different configurations with the same layers in everyday clothing from underwear to suit were experimentally analysed and compared with the theoretically calculated values, based on a layered model of heat transfer through this clothing.

Introduction

The importance of clothing functionality has increased over the years with the development of textile technologies. Clothing should be a barrier to the outside environment and should also transport heat and moisture from the body to the surrounding environment.

The thermal exchange between the body and the environment is done through heat convection, conduction and radiation, the moisture transport occurs through perspiration [1]. Within these mechanisms, the conduction and convection are the most important ways of the heat transfer in textiles. The thermal comfort is reached when a balance between heat production and heat loss is achieved. Therefore, the human-clothing-environment system must work. These phenomena were investigated in detail in the past, but garments normally consist not just of one layer, but of several layers. An addition of the thermal resistance values of the individual layers deviates to the measurement of the multilayer garment. One reason is that the transfer of heat and moisture between the layers and between the layers to the environment is neglected. But in fact, the heat transfer was not just investigated on the textile layers, but also on the included air and the air layer on the outer surface.

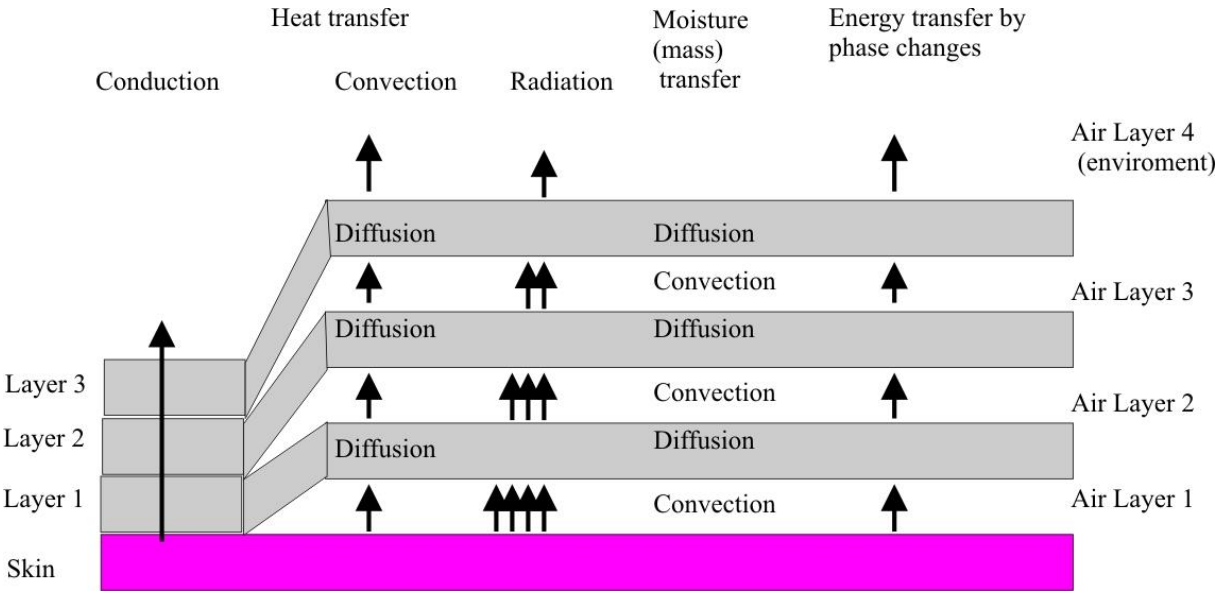

Source: Own

Fig. 1: *Schematic view of the mechanisms of heat, moisture and energy transfer on a multilayer system*

The thermal conductivity is the exchange of kinetic energy of particles through a stationary boundary between two systems. The heat conduction is measured by using the Fourier's law of heat conduction [2].

$$q = kA\frac{\Delta T}{d}\,(\mathrm{W}) \tag{1}$$

where q = rate of conduction heat transfer in Watt, k= the specific thermal conductivity of the fiber material in W/mK, A= Area perpendicular to heat flow in m², $\Delta T = (T_1\text{-}T_2)$ temperature difference between the areas in °K, d = the thickness of the fabric in m.

The total thermal resistance Rct is given by

$$R_{ct} = \frac{T_S - T_E}{q_{dry}} \tag{2}$$

where q_{dry} is the total heat flux through the layers. The fabric thermal resistance R_{cf} is given by

$$Rcf = Rct - Rct0 \tag{3}$$

where R_{ct0} is the thermal resistance without the fabric layer.

To calculate the effective thermal resistance, the clothing system should have reached a steady state and there should be no mass transfer, so it can be referred as the dry condition, and the fabric system is modulated in a multilayer structure.

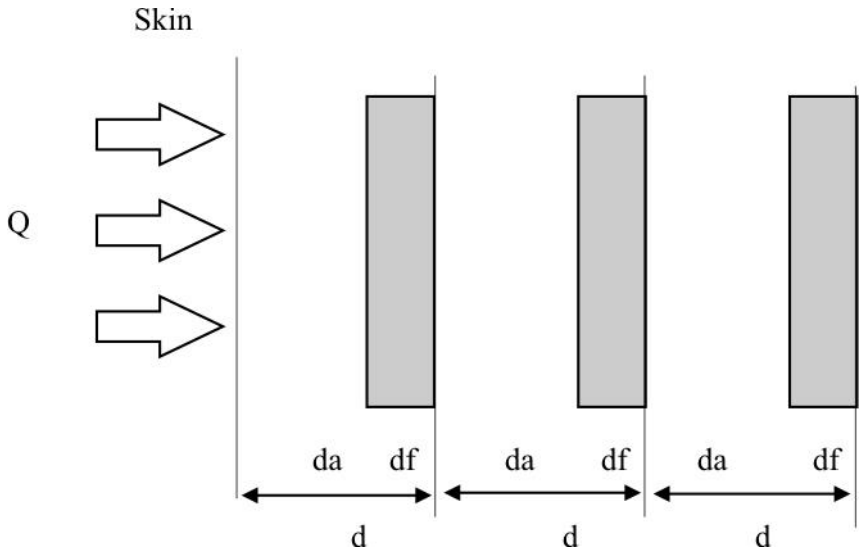

Source: Own

Fig. 2: *Modulated simple fabric structure*

Where df and da are the thickness values of the fabrics and the air gaps in the fabric structure, whereas kf and ka are the thermal conductivity values for the fibers and still air.

Accordingly the thermal resistance can be simplified and calculated as follows [3]:

$$Rct = \frac{df}{kf} + \frac{da}{ka} \text{ (m²K/W)} \quad (4)$$

where $df = df_1 + df_2 + \cdots + df_n$ and $da = da_1 + da_2 + \cdots + da_n$.

for the simple layers 1 to n. This equation only actually considers the conductivity.

A difference between the calculated and measured results is expected. The reason is that it is not possible to determine the microclimate between skin and garment, which is important for the heat transfer.

1 Experimental

The aim of this work is to investigate these transitions from heat between the textile layers and intermediate air layers and also the transitions between the textile layer and the ambient air. The main focus is on the question of whether it is possible to predict the behaviour of the multilayer structure, based on the measurement of the single layers and the information about the air between them.

The key points of this study are to analyze dependencies and interrelationships between test parameters. Therefore, two different cotton samples were measured from one to five layers; the values were analyzed to find out correlations between expected and calculated values with the measured multilayer samples. In addition, typical combinations of menswear clothing items were compiled and physical properties measured. The relationships between individual layers and multi-layered fabrics were checked.

1.1 Thickness of woven and knitted structures

Two methods for testing the thickness were applied – the standard one, using the pressure, and the other using analysis of the layer. The standard testing method eliminates the air between the layers, which is very important for thermal comfort. Because of this, the fabrics were embedded in resin in a relaxed state. So, more realistic information about the air gap between them can be obtained. The results between both methods are presented.

The first part of the measurement involves a comparison of two different textile samples tested for their properties on one to five layers. For a visual representation of the multi-layered textiles being tested, the layers were embedded in resin, polished and photographed at a 200-fold microscopic magnification. Except for the visual representation of the number of layers it also serves the measured differences in porosity to be visually presented.

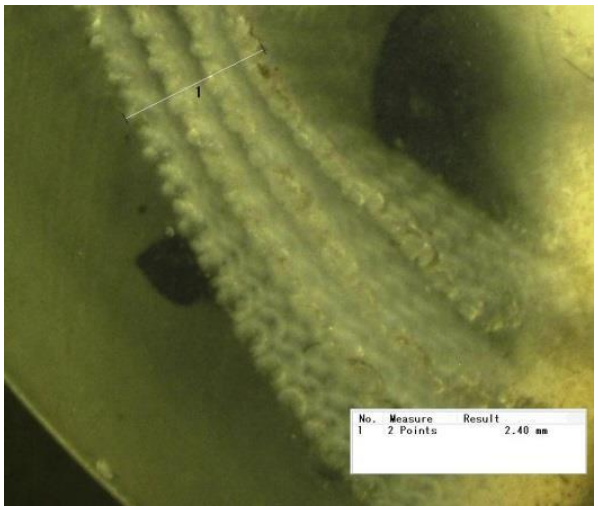

Source: Own

Fig. 3: *Example of cross section of multilayered structures*

These are clearly visible in direct comparison of when using knitted and woven fabrics. In addition, the dimensions of the textile layer thicknesses were recorded, in order to show that such measurements give a good indication of the dimensions.

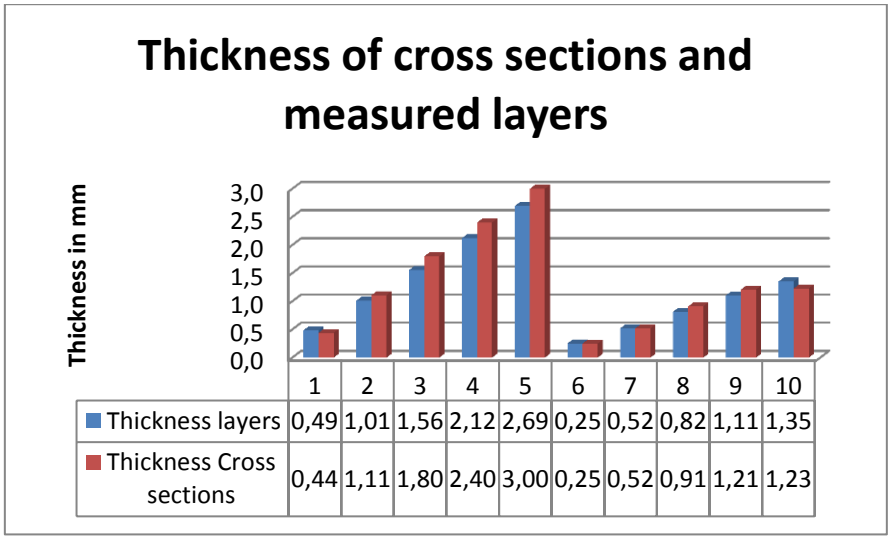

	1	2	3	4	5	6	7	8	9	10
Thickness layers	0,49	1,01	1,56	2,12	2,69	0,25	0,52	0,82	1,11	1,35
Thickness Cross sections	0,44	1,11	1,80	2,40	3,00	0,25	0,52	0,91	1,21	1,23

Source: Own

Fig. 4: *Cross-sections vs. measured thickness*

Figure 4 shows the connection between the cross-sectional thickness and measured thicknesses of the textiles. By pouring the resin over the samples there may be differences, since the samples were previously fixed and thus partially squeezed. Nevertheless, such samples are a good indication of the dimensions of textile samples, even if they have not been tested according to standards. But it is also quite clear that the air gap is higher and the "standard" testing method for thickness is underestimated.

1.2 Analysis of the interdependence of separately measured and calculated textile layers

The fabrics were contrasted, the layers were measured and the sum of the individual layers was calculated. It is noteworthy that in both series of measurements, a linear increase is observed, but the added values are lower than with the tested layers. Figure 5 shows the respective increases in thermal resistances of the multilayer samples measured and the added values of the individual measurements. Since the single measurement is a pure addition of the textile layers, without the intervening air-layers being taken into account, it can be assumed that this is the reason for the lower values. Nor should it be forgotten that almost all measurements are below the measurement accuracy of the PERMETEST device. That is why inaccuracies are expected.

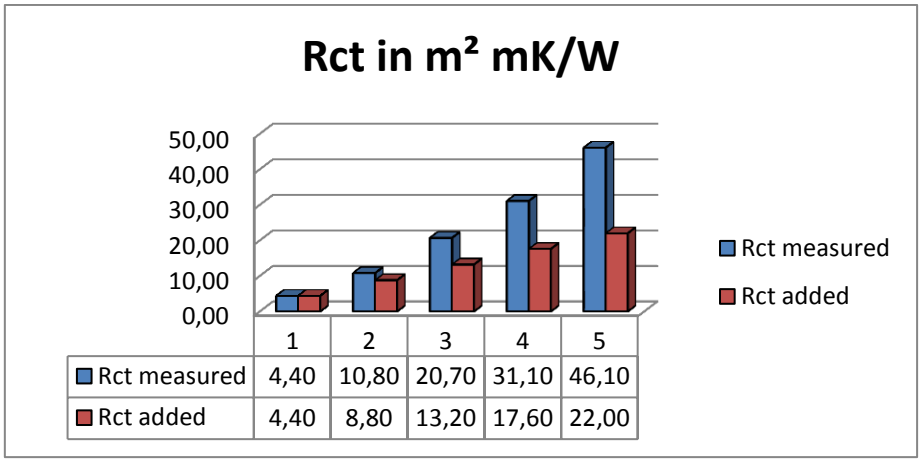

	1	2	3	4	5
Rct measured	4,40	10,80	20,70	31,10	46,10
Rct added	4,40	8,80	13,20	17,60	22,00

Source: Own

Fig. 5: *Thermal resistance of measured and calculated multilayer knitting*

Based on the regression line of the heat transfer measurements in Figure 6 a linear relationship between individual measurements and multilayer measurement is shown. This is very strong, which is why we can say that the insulation values of the air layers conclusions of the single measurement are to be considered in the case of a multilayer textile.

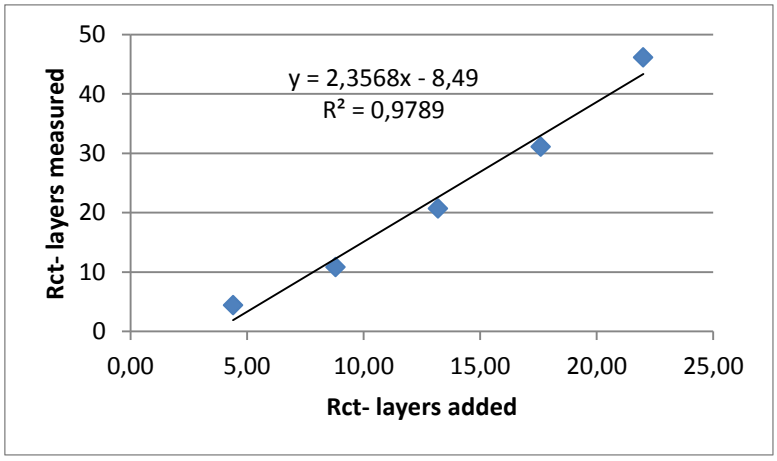

Source: Own

Fig. 6: *Comparison between measured and calculated knitted structures*

The heat transfer resistance increases linearly with more layers. As was already stated, the multilayered textiles tested always show higher values in the thermal resistance than the added values. This is because the values of the air layers are completely ignored or not

correctly measured when calculating the value of the multilayered structure based on the single layer values.

1.3 Measurement of garment combinations for men

Usual combinations of menswear clothing items were chosen and tested as a single layer, as well as multilayered combinations. By using one to three-layer coatings it should have been proved that further layers effect the thermal insulation. A comparison between the measured single layers and the combinations of garments shows that there are no statistical proven interdependences between them. To check the accuracy of the measurements the results were compared to the results found in the ISO 9920. The clothing combinations that are included in the standard are between 0.15 to 0.30 m² K / W. Measured combinations are between 0.011 m² K / W, which consists of a T-shirt, a long sleeved T-shirt and a jacket, and 0,043 m² K / W for the combination of a T-shirt, a long sleeved T-shirt and a fleece pullover. These are the values, which define the standard and have an approximately ten times higher insulation than the examined items of clothing. A comparison of the individual layers, such as the T-shirt according to standard should have had a value of 0.012 m² K / W, but the measurement yielded a result of 0.0044 m² K / W, it means just over a third of the given data. The shirt could not be measured and showed a value of zero, while a value of 0.045 m² K / W is given in the standard. Since the samples were tested with the PERMETEST device, and most measurements were outside the measurement range of the instrument, an exact comparison is not possible at this point.

Conclusion

The collection of physiological data is very complex. The measurement with the skin model or the PERMETEST device according to DIN EN 31092 [2013] can only make very limited statements about the overall comfort of clothing. Although it provides information about the stationary heat and water vapor transmission of materials, and therefore brings some evidence to select specific textiles, the comparison with the insulation values of the standard DIN EN ISO 9920 [2009] shows that the results do not match. In addition, the two measures of heat and water vapor resistance are determined in separate experiments and therefore do not allow assessment of the interaction between these two parameters.

The measuring range of PERMETEST device starts at 0.02 m² K / W, most clothing textiles were substantially lower than this value, so the results are inaccurate. In addition, these steady-state measurements provide meaningful results only if the clothing does not store heat or moisture and it does not lead to condensation in the textile. Since this is different but usual in practice, these measurements are well comparable.

In order to evaluate the comfort, the clothing combination must always be measured, as it is worn. Measurements on single-layer fabrics can be very inaccurate compared to the heat transfer of a multilayer combination. With several layers of the same fabric we see a linear relationship in the measurement of the thermal resistance, even if the results increase with the number of layers. The water vapor resistance coincides very well. For clothing combinations of different materials, these correlations, however, confirmed to be less significant. It could also be shown that the statements on the addition of the results of the thermal resistance of multilayer fabrics are incorrect.

The measurements according to DIN EN 31092 [2013] give the overall thermal resistance, but not the kind of heat transfer and not the heat passes through each layer. The knowledge of these phenomena in the textile must be deepened to make a modeling of the various processes possible. For this, the processes of heat and moisture transport should be identified and

analyzed separately. For example, moisture can evaporate and condense from one layer into or onto another. These processes release energy, which in turn affects the temperature of the body. A quantification of these processes is not possible; this is why these processes should be given more attention to in the future.

Literature

[1] HES, L.: Laboratory measurement of thermophysiological comfort, in N. Pan, P. Gibson, *Thermal and moisture transport in fibrous materials*, Woodhead Publishing Limited, 2011.

[2] DING, D; TANG, T.; SONG, G.; MCDONALD, A.: Characterizing the performance of a single layer fabric system through a heat and mass transfer model- Part I: Heat and mass transfer model, *Textile Research Journal*, 2011 81: 398.

[3] OGLAKCIOGLU, N.; KYOSEV, Y.: About the computation of the effective thermal resistance of weft knitted structures, *Aachen Dresden International Textile Conference*, Aachen, 24.-25.11.2011.

[4] *DIN EN ISO 9920, 2009, Ergonomics of the thermal environment – Estimation of thermal insulation and water vapor resistance of a clothing ensemble*.

[5] *DIN EN 31092, 2013: Physiological effects; Measurement of thermal and water-vapor resistance under steady-state conditions*.

TEPELNÁ VODIVOST TEXTILNÍCH STRUKTUR NĚKOLIKAVRSTEVNATÉHO OBLEČENÍ

Měření tepelné vodivosti textilních struktur pro oblečení je stále velkou výzvou. Důvodem je, že tyto hodnoty jsou na hranici spodního rozsahu stávajícího vybavení současných zkušebních zařízení, nebo i nižší. Na druhé straně je ale vyžadována optimalizace tepelného komfortu oděvů. Pánské i dámské oděvy jsou vytvářeny z několika vrstev, a pouze s kompletními informacemi o každé vrstvě jsou možné složitější výpočty a kalkulace.

Tato práce prezentuje část rozsáhlejších experimentálních studií, týkajících se R_{ct} hodnot tkaných a pletených struktur sestávajících z několika vrstev. Byla změřena stlačitelnost a tloušťka jednotlivých vrstev i vícevrstvých struktur. V obou případech byla použita standardní testovací zařízení a provedena analýza příčného řezu vrstev zalitých do pryskyřice. Za účelem zkoumání vlivu vzduchu mezi několika vrstvami byly R_{ct} hodnoty pěti vrstev se stejnou strukturou odhadnuty pomocí zařízení PERMETEST společnosti Sensora. Byly zjištěny a statisticky prokázány jisté korelace mezi hodnotami R_{ct}, počtem vrstev a objemem vzduchové vrstvy mezi jednotlivými vrstvami.

Různé kombinace vrstev materiálů používaných na běžné ošacení, od spodního prádla po vrchní vrstvy oděvů, byly experimentálně analyzovány a porovnány s teoreticky vypočtenými hodnotami.

LEITFÄHIGKEIT VON WÄRMER TEXTILER STRUKTUREN VON MEHRSCHICTIGER KLEIDUNG

Die Messung der Wärmeleitfähigkeit textiler Strukturen für Kleidung stellt unverändert eine große Herausforderung dar. Der Grund dafür besteht darin, dass diese Werte sich an der unteren Grenze der bestehenden Ausstattung der gegenwärtigen Versuchseinrichtungen oder sogar noch darunter bewegen. Auf der anderen Seite wird eine Optimierung des Wärmekomforts der Bekleidung angestrebt. Damen- und Herrenkleidung besteht aus mehreren Schichten, und nur mit vollständigen Informationen über jede Schicht sind kompliziertere Berechnungen und Kalkulationen möglich. Diese Arbeit präsentiert einen Teil umfangreicher experimenteller Studien, welche die R_{ct}-Werte gewobener und gestrickter Strukturen betreffen, die sich aus mehreren Schichten zusammensetzen. Es wurden die Kompressibilität und die Dicke der einzelnen Schichten und auch der mehrschichtigen Strukturen gemessen. In beiden Fällen wurde von einer Standardtesteinrichtung Gebrauch gemacht und eine Analyse des Querschnitts von in Harz eingegossenen Schichten durchgeführt. Zur Untersuchung der Wirkung der Luft zwischen mehreren Schichten wurden die R_{ct}-Werte von fünf Schichten mit der gleichen Struktur mit Hilfe der Eirichtung PERMETEST der Gesellschaft Sensora geschätzt. Es wurden dabei bestimmte Korrelationen zwischen den R_{ct}-Werten, der Anzahl der Schichten und dem Umfang der Luftschichten zwischen den einzelnen Schichten festgestellt und auch statistisch bewiesen. Verschiedene Kombinationen von Schichten aus Materialien, die für gewöhnliche Kleidung – von Unterwäsche bis zu Oberbekleidung – verwendet werden, wurden experimentell analysiert und mit den theoretisch berechneten Werten verglichen.

PRZEWODNOŚĆ CIEPLNA STRUKTUR TEKSTYLNYCH UBRAŃ KILKUWARSTWOWYCH

Pomiar przewodności cieplnej struktur tekstylnych stosowanych do ubrań pozostaje wciąż dużym wyzwaniem. Wynika to z tego, że wartości te są na granicy dolnego zakresu istniejącego wyposażenia obecnych urządzeń testujących, a nawet niższe. Z drugiej strony

wymagana jest jednak optymalizacja komfortu cieplnego ubrań. Ubrania męskie i damskie są produkowane z kilku warstw a bardziej zaawansowane obliczenia i kalkulacje są możliwe tylko wówczas, gdy posiadamy kompleksowe informacje na temat każdej warstwy.

Niniejsze opracowanie przedstawia część bardziej obszernych badań eksperymentalnych, dotyczących wartości R_{ct}- struktur tkanych i plecionych składających się z kilku warstw. Dokonano pomiaru ściśliwości i grubości poszczególnych warstw i struktur kilkuwarstwowych. W obu przypadkach wykorzystano standardowe urządzenia testujące i wykonano analizę przekroju poprzecznego warstw zalanych żywicą. W celu zbadania wpływu powietrza pomiędzy kilkoma warstwami, wartości R_{ct} pięciu warstw o takiej samej strukturze oszacowano przy pomocy urządzenia PERMETEST firmy Sensora. Stwierdzono i statystycznie udowodniono pewne korelacje między wartościami R_{ct}, liczbą warstw a pojemnością warstwy powietrza pomiędzy poszczególnymi warstwami.

W sposób eksperymentalny przeanalizowano różne połączenia warstw materiałów stosowanych do zwykłych ubrań, od bielizny po wierzchnie okrycia, i porównano je z teoretycznie obliczonymi wartościami.

PRODUCTION OF BICOMPONENT GELATIN/OLIVE OIL NANOFIBERS FOR BIOMEDICAL APPLICATIONS USING COAXIAL SPINNERET

*** Çağlar Sivri**
**** Kasım Aksoy**
***** Sena Demirbağ**

* Süleyman Demirel University
Faculty of Engineering
Textile Engineering Department
Isparta, Turkey
caglarsivri@sdu.edu.tr

** Süleyman Demirel University
Technical Sciences Vocational School
Biomedical Device Technology Program
Isparta, Turkey

*** Süleyman Demirel University
Faculty of Engineering
Textile Engineering Department
Isparta, Turkey

Abstract

In this study, production of electrospun nanofibers containing olive oil was carried out using gelatin polymer. Olive oil is a natural green vegetable oil, which is abundant in vitamin, carotene and many trace elements. Olive oil has many functions in nutrition and health care and it is rich in essential fatty acids, including Vitamin A, D, E, K and other antioxidant substances, which can be rapidly absorbed by the body and can maintain skin elasticity and moisture. For this reason, in this study we focused on fabrication of nanofibrous mat containing olive oil that can be used in medical field. Nanofibers spun by bicomponent electrospinnig method using coaxial spinneret.

Gelatin polymer was dissolved in distilled water/acetic acid at concentration 10%. Then olive oil was added to solution at a rate of 9:1 wt. Electrospinning from solution was carried out at varying process parameters such as feeding rate and applied voltage and also different mixture of polymer and olive oil. Bicomponent electrospun fibers were characterized by FT-IR spectroscopy and SEM instrument. FT-IR spectroscopy was used to prove the presence of olive oil in fiber structure.

Introduction

Nanofibers can be produced using a solution via electrospinning setup that could be assembled at a reasonable cost. Electrospinning setup is comprised of a power source that is able to work at high voltages, electronic syringe pump, syringe and a collector plate. The principle of the system based on transferring the polymer solution into the electrostatic drawing area through a needle at a feeding rate and latter to be collected in the form of nanofibers onto the collector plate after exposure to a high drawing force in this area [1, 2].

Electrospinning is a versatile technique to produce nanofibers for medical, filtration, transport and energy applications. It can be utilized using co-axial and/or different spinneret designs to produce bicomponent nanofibers [3].

McCann et al. conducted a research on availability of co-axial electrospinning to produce core-sheath, hollow, or porous nanofibers from mineral oil as a core component and PVP $(TiOiPr)_4$ as a sheath component using co-axial spinneret. They have concluded that electrospinning will become an essential and useful top-down technique for the fabrication of one-dimensional nanostructures with hollow interiors [4].

Wang et al. investigated the morphological and structural properties of multifunctional scaffolds for bone tissue engineering that were constructed via dual-source dual-power electrospinning (DSDPES). Emulsion electropinning used to produce rhBMP-2 (recombinant human bone morphogenetic protein)/PDLLA fibers and a composite suspension containing Ca–P/PLGA nanocomposite fibers were prepared and then bicomponent scaffolds were constructed by DSDPES. Further investigations showed that bicomponent scaffolds developed using this method could provide balanced osteoinductivity and osteoconductivity [5].

Apart from specific spinneret designs, bicomponent nanofibers can be produced by preparing a bicomponent solution. Mincheva et al. prepared a bicomponent solution including N carboxyethylchitosan and poly(vinyl alcohol) polymers and developed a tissue engineering scaffold for biomedical applications via electrospinning. They found that their bicomponent nanofibers can be used as biomedical scaffolds due to their bicompatibility, water-resistance of cross-linked mats and aligned nanofibrous structure [6].

As it could be seen from present literature, bicomponent nanofibers developed for medical applications intensified on tissue engineering and scaffolds. In this study, instead, we have designed a bicomponent nanofibrous material that could be used in therapeutics and wound care within medical field.

1 Materials and Methods

1.1 Materials

Type A gelatin was purchased from Sigma company. Olive oil used as purchased. Acetic acid as a solvent from Sigma company used as received. Collector plate was covered by an aluminum foil.

1.2 Electrospinning of Gelatin/Olive Oil

Gelatin of 10 g (10 wt%) was dissolved in acetic acid (80 wt%) and 20 ml pure water mixture and the solution was stirred for 6 hours using a magnetic stirrer (WiseStir) and then stayed overnight in laboratory. To the comparison aim, bicomponent nanofibers were produced both preparing a bicomponent solution and using coaxial spinneret in different feeding ratios of Gelatin polymer and olive oil.

1.2.1 Electrospinning of Bicomponent Solution of Gelatin/Olive Oil

Three different concentrations of Gelatin (G)/Olive Oil (OO) bicomponent solution were prepared and electrospun using standard electrospinning apparatus in different conditions given in Table 1:

Tab. 1: *Electrospinning of 1:9 OO/G solution at 12 kV and 8 cm distance and varying feeding rates*

Feeding Rate	Status of Electrospinning
1.5 ml/hr	Regular nanofiber production
2 ml/hr	Regular nanofiber production
2.5 ml/hr	Dripping over collector plate plus nanofiber production due to higher feeding rate

Source: Own

1:9 OO/G was the first concentration prepared by adding 2 ml olive oil into the 18 ml Gelatin solution (10wt%) and total solution volume defined as 20 ml. Finally, 0.2 g spun 20 surfactant (0.1 ml spun 20 for 10 ml) added to the solution and the whole solution was stirred and materials within solution were well dispersed. The other concentrations of 2:8 OO/G and 3:7 OO/G were prepared in the same manner. The only electrospinning process could be achieved by concentration of 1:9 OO/G while it could not be achieved for other solutions due to phase separation. The best voltage applied defined as 12 kV and distance between grounded collector and needle tip fixed at 8 cm.

1.2.2 Co-axial Electrospinning of Gelatin/Olive Oil

In this part, Gelatin of 10 wt%, whose preparation had been previously explained, and pure olive oil were co-axially electrospun (Gelatin polymer was fed from outer side of spinneret and olive oil was fed from inner/core side of the spinneret) in varying feeding and voltage rates using a co-axial spinneret apparatus. The distance between grounded collector and needle tip fixed at 8 cm. Firstly, bicomponent nanofibers co-axially electrospun in five different solution feeding rates given table 2.

Tab. 2: *Co-axial Electrospinning of Gelatin (G) /Olive Oil (OO) at 18 kV and 8 cm distance*

G Feeding Rate (ml/hr)	OO Feeding Rate (ml/hr)	Status of Electrospinning
0.7	0.2	Nanofiber production at 30 seconds intervals with a dripping a few drops of olive oil
1	0.2	Nanofiber production couldn't be achieved
1.3	0.2	Almost regular nanofiber production
1.6	0.2	Almost regular nanofiber production plus dripping a few drops of olive oil
1.9	0.2	Poor nanofiber production

Source: Own

Secondly, after defining the best feeding rate of Gelatin polymer as 1.3 ml/hr bicomponent nanofibers co-axially electrospun in four different voltages is given in table 3.

Tab. 3: *Table 3. Co-axial Electrospinning at a feeding rate of 1,3 ml/hr Gelatin (G) / 0,2 ml Olive Oil (OO) and 8 cm distance*

Voltage Applied (KV)	**Status of Electrospinning**
14	Poor nanofiber production plus dripping a few drops of olive oil
16	Almost regular nanofiber production plus dripping a few drops of olive oil
18	Almost regular nanofiber production
19	Regular nanofiber production

Source: Own

1.3 SEM Analysis

Bicomponent nanofibers produced using bicomponent solution and co-axial spinneret were characterized using a Scanning Electron Microscopy (SEM) to define morphological properties.

1.4 FT-IR Analysis

Olive oil and gelatin content of bicomponent nanofibers and chemical bonds within structure were analyzed using FT-IR.

2 Results and Discussion

2.1 SEM Investigation

Fig. 1 and Fig. 2 have revealed the morphological information for bicomponent nanofibers from bicomponent solution and coaxial spinneret, respectively.

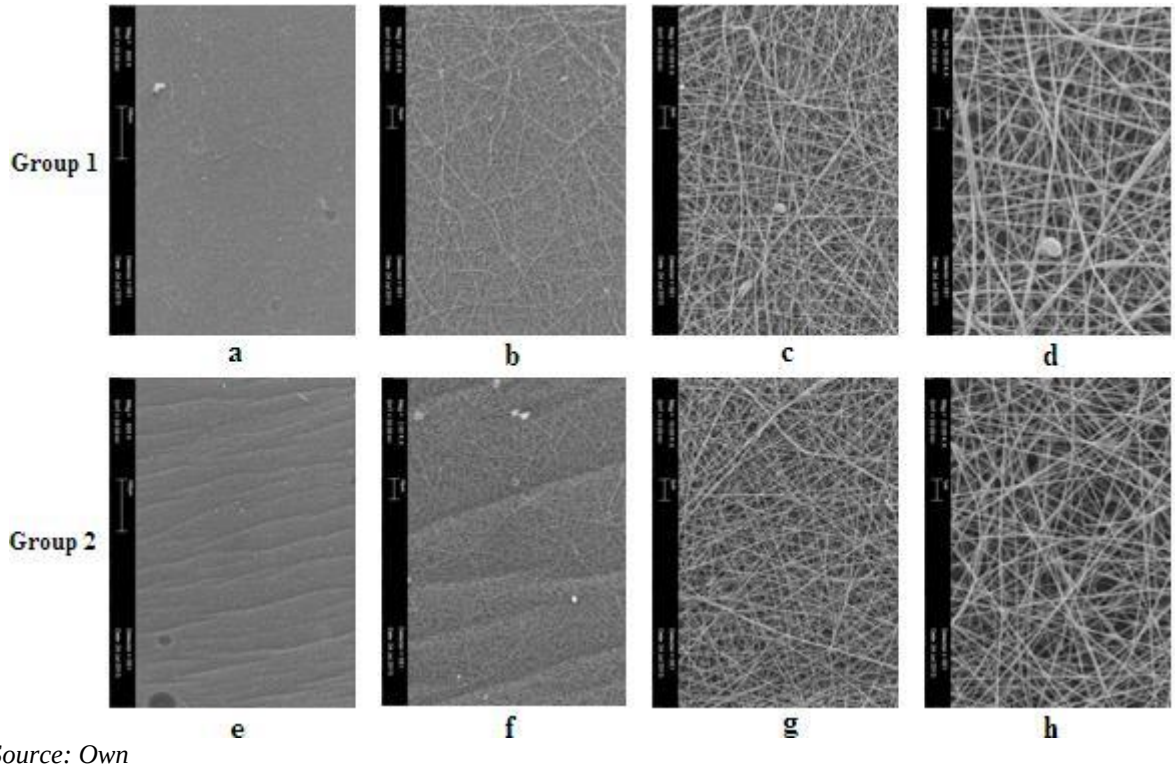

Source: Own

Fig. 1: *SEM images of bicomponent nanofibers electrospun from bicomponent solution of Gelatin/Olive Oil in 1:9 ratio divided in 2 groups by different process parameters; Group1: Electrospun at 11.2 kV, 1.5 ml/hr solution feeding rate, 8 cm collector distance, SEM magnification rates: (a) 500x, (b) 2kx, (c) 10kx, (d). Group 2: Electrospun at 11.2 kV, 2 ml/hr solution feeding rate, 8 cm collector distance, SEM magnification rates: (a) 500x, (b) 2kx, (c) 10kx, (d) 20 kx*

Fig. 1 shows bicomponent solution yielded nanofibers in a defined orientation and changing feeding rate has leaded a little change on morphology of the nanofibers such as small lines seen in image within Group 2, e and f.

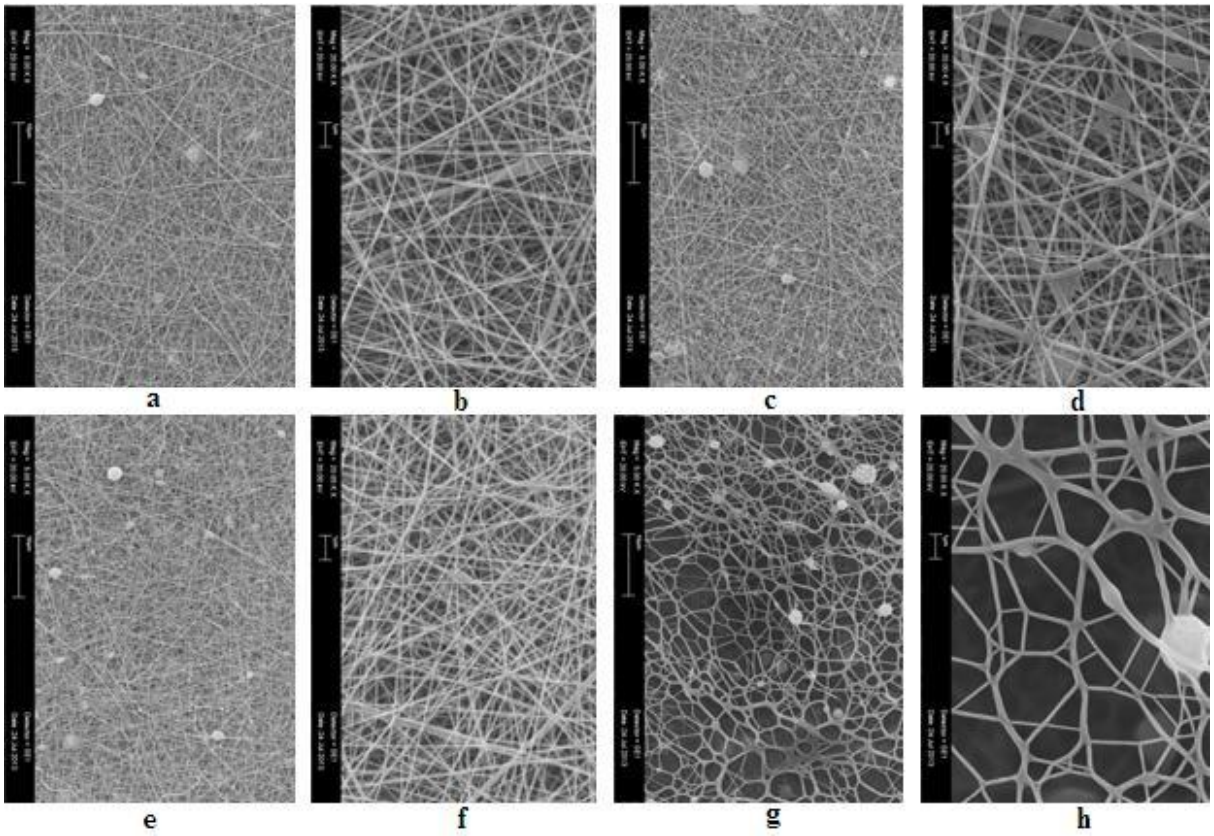

Source: Own

Fig. 2: *SEM images of bicomponent nanofibers electrospun using co-axial spinneret in different process parameters and feeding rates of Gelatin and Olive Oil; nanofibers electrospun at 18 kV with a gelatin feeding rate of 1.6 ml/hr and olive oil feeding rate of 0.2 ml/hr a:5 kx and b:20 kx; nanofibers electrospun at 18 kV with a gelatin feeding rate of 1.3 ml/hr and olive oil feeding rate of 0.2 ml/hr c:5 kx and d:20 kx; nanofibers electrospun at 19 kV with a gelatin feeding rate of 1.3 ml/hr and olive oil feeding rate of 0.2 ml/hr e:5 kx and f:20 kx; nanofibers electrospun at 18 kV with a gelatin feeding rate of 1.9 ml/hr and olive oil feeding rate of 0.2 ml/hr g:5 kx and h:20 kx,8 cm distance from collector for all samples.*

Fig. 2 demonstrated that voltage change has not changed the morphology much, but when feeding rate of gelatin increased to 1,9 ml/hr, rapid phase separation occurred and soap bubble-like or spider web-like structures have been generated. In addition, diameters of the nanofibers have remarkably decreased. Related literature assumes that formation of such structures may result from rapid phase separation and minimal energy principle [7].

2.2 FT-IR Analysis

FT-IR spectrum seen at Fig. 3 shows olive oil content trapped into the bicomponent nanofibrous structures produced using bicomponent solution and coaxial spinneret. The steep peak seen at 2924 and 2852 cm^{-1} belong to the symmetrical and asymmetrical -C-H stretching within olive oil structure. These peaks are respectively seen at 2925-2854 cm^{-1} in the spectra of sample 1 and sample 2, which are bicomponent nanofibers produced using coaxial spinneret respectively at 18 kV and 19 kV with a Gelatin feeding rate of 1.3 ml/hr and olive oil feeding rate of 0.2 ml/hr. these peaks also seen at 2928-2857 cm^{-1} in the spectra of sample 3, which is bicomponent nanofibers produced using bicomponent solution at 11.2 kV and 1.5 ml/h feeding rate, within FT-IR spectrum belongs to all three samples that produced 8 cm collector distance. It proves that all three bicomponent nanofiber samples contain olive oil.

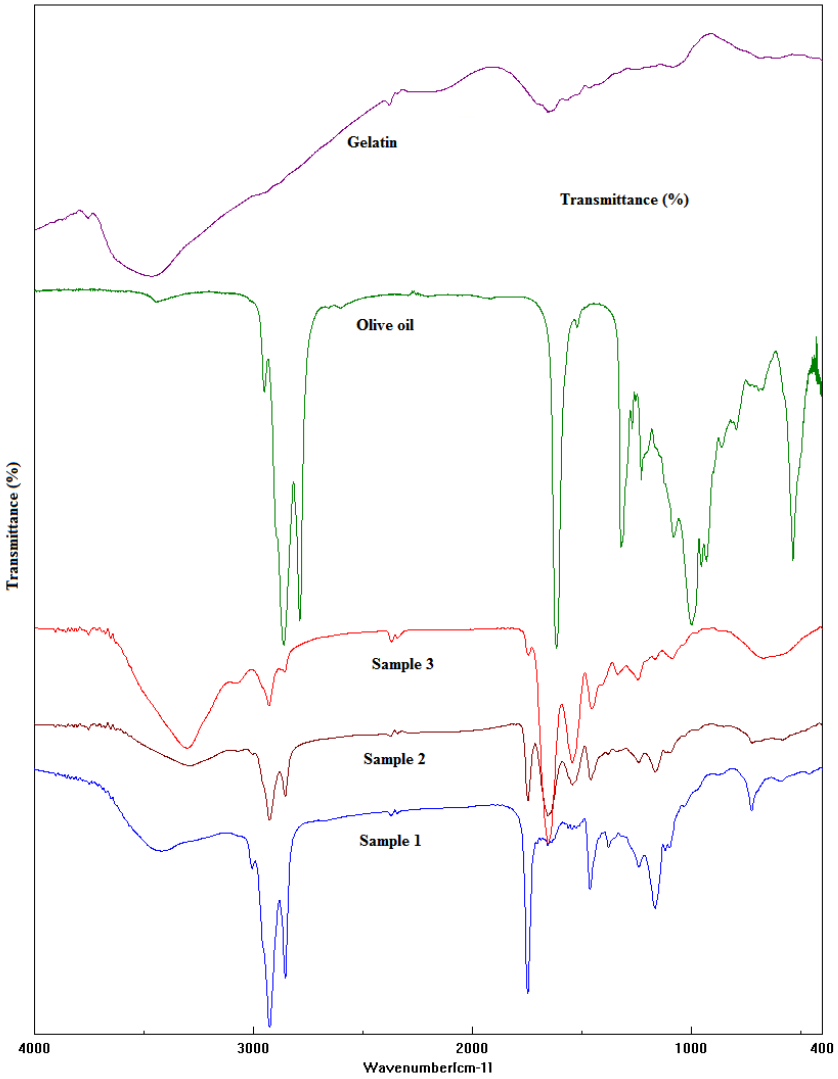

Source: Own

Fig. 3: *FT-IR Analysis of Gelatin/Olive Oil Bicomponent Nanofibers*

Conclusion

To answer the question whether olive oil added to bicomponent nanofibers can be produced using either a bicomponent solution or a coaxial spinneret for medical field and therapeutic applications, the production trials were carried out at changing applied voltages, solution feeding rates while distance between needle tip and grounded collector plate was fixed at 8 cm. Changing applied voltage did not have a crucial effect over morphology of the bicomponent nanofibers produced using a bicomponent solution, while little changes have occured within the structure such as small lines occurrence due to an increase in feeding rate of solution from 1.5 ml/hr to 2 ml/hr. Again, voltage change did not have a crucial effect on morphology of the bicomponent nanofibers produced using a coaxial spinneret while increasing the feeding rate of Gelatin polymer caused rapid phase separation, which concluded with development of soap bubble-like structures or spider web-like structures and fibers with lower diameter. FT-IR analyzes proved that olive oil content in both bicomponent nanofibers which means these nanofibers could be used in medical field such as wound closure materials due to their therapeutic activity. Finally, use of coaxial spinneret has provided different morphological possibilities such as the development of biomimetic nanofibers and nanofibers with lower diameters and containing active agents.

Literature

[1] MALAKHOV, S. N.; KHOMENKO, A. Yu.; BELOUSOV, S. I.; PRAZDNICHNYI, A. M.; CHVALUN, S. N.; SHEPELEV, A. D.; BUDYKA, A. K.: Method of Manufacturing Nonwovens by Electrospinning from Polymer Melts. *Fibre Chemistry*. (2009) 41 (6):355-359.

[2] SIVRI, Ç.; DAYIK, M.: Development of Superior Sound Absorbing Nonwoven Media via Mechanical Nanofiber Spinning Method, *EDANA Nonwovens Research Academy*, 19-20 April 2012, Gothenburg, Sweden.

[3] RAMAKRISHNA, S.; FUJIHARA, K.; TEO, W. E.; LIM, T. C.; Ma, Z.: An Introduction to Electrospinning and Nanofibers. *World Scientific*, Singapore, 2005.

[4] MCCANN, J. T.; LI, D.; XIA, Y. Electrospinning of nanofibers with core-sheath, hollow, or porous structures. *J. Mater. Chem.* 2005, 15, 735–738.

[5] WANG, C.; Wang, M.: Dual-source dual-power electrospinning and characteristics of multifunctional scaffolds for bone tissue engineering. *J Mater Sci: Mater Med.* (2012) 23:2381–2397.

[6] MINCHEVA, R.; MANOLOVA, N.; RASHKOV, I.: Bicomponent aligned nanofibers of N-carboxyethylchitosan and poly(vinyl alcohol). *European Polymer Journal* 43 (2007) 2809–2818.

[7] LIN, J.; WANG, X.; DING, B.; YU, J.; SUN, G.; WANG, M.: Biomimicry via Electrospinning. *Critical Reviews in Solid State and Materials Sciences*. (2012) 37:94–114.

VÝROBA NANOVLÁKEN ELEKTROSPUNINGEM ZA POUŽITÍ KOAXIÁLNÍ SNOVACÍ TRYSKY, VYUŽITÍ OLIVOVÉHO OLEJE A ŽELATINOVÉHO POLYMERU

Tato studie pojednává o výrobě nanovláken elektrospuningem (elektrostatickým zvlákňováním) obsahujícím olivový olej s pomocí želatinového polymeru. Olivový olej je přírodní zelený rostlinný olej, který je bohatý na vitaminy, karoten a mnoho stopových prvků. Olivový olej má mnoho funkcí ve výživě a zdravotní péči a je bohatý na esenciální mastné kyseliny, včetně vitamínu A, D, E, K a dalších antioxidačních látek, které mohou být rychle vstřebávány v těle a pomáhají udržovat pokožku pružnou a vlhkou. Z tohoto důvodu jsme se v této studii zaměřili na výrobu nanovlákenné vrstvy obsahující olivový olej, která může být využita v oblasti medicíny. Nanovlákna jsou tažena metodou dvousložkového elektrostatického zvlákňování za použití koaxiální snovací trysky.

PRODUKTION VON NANOFASERN DURCH ELEKTROSTATISCHE VERSPINNUNG UNTER VERWENDUNG VON KOAXIALEN SCHÄRDÜSEN, NUTZUNG VON OLIVENÖL UND GELATINEPOLYMEREN

Diese Studie befasst sich mit der Produktion von Nanofasern durch elektrostatische Verspinnung unter Einsatz von Olivenöl mit Hilfe von Gelatinepolymeren. Beim Olivenöl handelt es sich um ein natürliches grünes Pflanzenöl, das reich an Vitaminen, Karotin und vielen Spurenelementen ist. Olivenöl hat viele Funktionen innerhalb der Ernährung und der Gesundheitspflege und ist auch reich an essenziellen Fettsäuren. Darunter befinden sich die Vitamine A, D, E, K und andere Antioxidantien, die vom Körper schnell absorbiert werden können und dazu beitragen, die Haut elastisch und feucht zu halten. Aus diesem Grunde konzentrieren wir uns in dieser Studie auf die Erzeugung einer Nanofaserschicht, die Olivenöl enthält und auch auf medizinischem Gebiet Verwendung finden kann. Nanofasern werden mit der Methode der zweikomponentigen elektriostatischen Verspinnung unter dem Einsatz von koaxialen Schärdrüsen gezogen.

PRODUKCJA NANOWŁÓKIEN METODĄ ELEKTROPRZĘDZENIA PRZY WYKORZYSTANIU IGŁY KOAKSJALNEJ, Z ZASTOSOWANIEM OLIWY Z OLIWEK ORAZ POLIMERU ŻELATYNOWEGO

Niniejsze opracowanie poświęcone jest produkcji nanowłókien metodą elektroprzędzenia przy wykorzystaniu oliwy z oliwek i polimeru żelatynowego. Oliwa z oliwek jest naturalnym zielonym olejem roślinnym, bogatym w witaminy, karoten oraz wiele pierwiastków śladowych. Oliwa z oliwek ma wiele funkcji w żywieniu i opiece zdrowotnej oraz zawiera wiele esencjalnych kwasów tłuszczowych, w tym witaminy A, D, E, K oraz inne przeciwutleniacze, które mogą się szybko wchłaniać, pomagając w utrzymaniu elastycznej i nawilżonej skóry. Z tego powodu w prowadzonych badaniach skupiliśmy się na produkcji warstwy nanowłóknowej zawierającej oliwę z oliwek, która może być wykorzystana w dziedzinie medycyny. Nanowłókna wytwarzane są metodą dwuskładnikowego elektroprzędzenia przy wykorzystaniu dyszy (igły) koaksjalnej.

LIST OF AUTHORS

LIST OF REVIEWERS OF ACC JOURNAL

Name	Work Location
Aneja Ritu, Prof.	Geogia State University
Andrášová Hana, PaedDr., Ph.D.	Jihočeská univerzita v Českých Budějovicích
Anchor John R., Dr.	University of Huddersfield
Antlová Klára, doc., Ing., Ph.D.	Technická univerzita v Liberci
Antoch Jaromír, Prof., RNDr., CSc.	Matematicko-fyzikální fakulta UK v Praze
Bachmann Pavel, Ing., Ph.D.	Univerzita Hradec Králové
Baraniecka Anna, Dr.	Uniwersytet Ekonomiczny we Wroclawiu
Barči Tomáš, PhDr., Ing., Ph.D.	EGAP, a.s., Praha
Barták Miroslav, PhDr., Ph.D.	Univerzita J. E. Purkyně v Ústí nad Labem
Behera B. K., Prof., M.Tech, Ph.D.	Indian Institute of Technology in Delhi
Bejrová Martina, Ing., Ph.D.	ŠKODA AUTO, a.s.
Berki Jan, Mgr.	Technická univerzita v Liberci
Betáková Lucie, doc., PhDr., MA, Ph.D.	Jihočeská univerzita v Českých Budějovicích
Biniek Kamila (Jeleńska), Mgr	Karkonoska państwowa szkoła wyższa w Jeleniej Górze
Blechová Beáta, Ing., Ph.D.	Slezská univerzita v Opavě
Blin Jutta, Prof. Dr. phil.	Hochschule Zittau/Görlitz
Borozdina, Olga, Dr.	Univerzita St. Petersburg
Brauweiler Jana, Dr. rer. pol.	Internationales Hochschulinstitut Zittau
Budaj Pavol, Ing., Ph.D.	Katolícka univerzita v Ružomberku
Bureš Vladimír, doc., Ing., Ph.D.	Univerzita Hradec Králové
Busch-Lauer Ines Andrea, Prof., Dr.	Fachhochschule Zwickau
Čech Jaroslav, Prof., Ing., CSc.	Vysoké učení technické v Brně
Čiháková Silvia Aguilar, Ing., Ph.D.	Technická univerzita v Liberci
Daněk Ladislav, doc., Ing., CSc.	Vysoké učení technické v Brně
Delakowitz Bernd, Prof., Dr. rer. nat	Hochschule Zittau/Görlitz
Dipayan Das, Prof., Ph.D.	IIT Delhi
Domosławski Zbigniew, Prof., Dr. hab. N. Med.	Karkonoska państwowa szkoła wyższa w Jeleniej Górze
Doucek Petr, Prof., Ing., CSc.	Vysoká škola ekonomická v Praze
Dynybyl Vojtěch, Prof., Ing., CSc.	ČVUT Praha
Eck Vladimír, doc., Ing, CSc.	ČVUT Praha

Name	Work Location
Felixová Kateřina, Ing., Ph.D.	Univerzita J. E. Purkyně v Ústí nad Labem
Ficek Jaromír, Ing., Ph.D.	VÚTS, a.s., Liberec
Fielko Eva, Ing., Ph.D.	Metropolitní univerzita v Praze
Fliegel Vítězslav, doc., Ing., CSc.	Technická univerzita v Liberci
Gerstlberger Wolfgang, Univ.-Prof., Dr. rer. pol. habil.	University of Southern Denmark
Griebel Bernd, Prof., Dr. phil.	Hochschule Zittau/Görlitz
Hájek Ladislav, Prof., Ing., CSc.	Univerzita Hradec Králové
Harland Peter E., Prof., Dr.	Internationales Hochschulinstitut Zittau
Herzig Ingo, M.A., PhDr.	Technická univerzita v Liberci
Hes Aleš, doc., Ing., CSc.	Česká zemědělská univerzita v Praze
Heßberg Silke, Prof., Dr.-Ing.	Westsächsische Hochschule Zwickau
Hinke Jana, Ing., Ph.D.	Západočeská univerzita v Plzni
Hlavatý Ivo, doc., Ing., Ph.D.	Technická univerzita Ostrava
Hokr Milan, doc., Ing., Ph.D.	Technická univerzita v Liberci
Homišin Jaroslav, Prof., Ing., CSc.	Technická univerzita v Košiciach
Holá Jana, Ing., Ph.D.	Univerzita Pardubice
Honců Jan, Prof., Ing., CSc.	Technická univerzita v Liberci
Hortel Milan, Ing., DrSc.	Akademie věd ČR, Praha
Hruš Miroslav, Ing., CSc.	Odborný poradce, Liberec
Hyžík Jaroslav, Prof., Ing., CSc.	Technická univerzita v Liberci
Chocholoušková Hana, Mgr.	Státní archiv Liberec
Ircingová Jarmila, Ing., Ph.D.	Západočeská univerzita v Plzni
Jáčová Helena, PhDr., Ing., Ph.D.	Technická univerzita v Liberci
Jakubíková Dagmar, doc., Ing., Ph.D.	Vysoká škola hotelová v Praze
Jihlavec Jan, Mgr., DiS.	Technická univerzita v Liberci
Jílková Jiřina, Prof. Ing., CSc.	Univerzita J. E. Purkyně v Ústí nad Labem
Jirčíková Eva, Ing., Ph.D.	Univerzita Tomáše Bati ve Zlíně
Jirman Pavel, Ing.	Technická univerzita v Liberci
Kala Tomáš, Ing., DrSc., DBA.	Univerzita Hradec Králové
Kasper Tomáš, Doc., PhDr., Ph.D.	Technická univerzita v Liberci
Kellner Jan, Ing., Ph.D.	KPMG Česká republika, s.r.o.
Klápšťová Květoslava, Mgr., Ph.D.	Technická univerzita v Liberci

Name	Work Location
Klíma Radek, Ing.	Cadence Innovation s.r.o., Liberec
Knápková Adriana, Ing., Ph.D.	Univerzita Tomáše Bati ve Zlíně
Kocourek Aleš, Ing., Ph.D.	Technická univerzita v Liberci
Koláčková Ludmila, Mgr.	Univerzita obrany Brno
Kovárník Jaroslav, Ing., Ph.D.	Univerzita Hradec Králové
Kretschmar Gerlinde, Prof., Dr.-Ing.	Hochschule Zittau/Görlitz
Krzywinski Sybille, Prof. Dr.-Ing. habil.	Technische Universität Dresden
Kurek Robert, Dr.	Uniwersytet Ekonomiczny we Wroclawiu
Ładysz Jerzy, Dr.	Uniwersytet Ekonomiczny we Wroclawiu
Lachout Martin, PhDr., Ph.D.	Metropolitní univerzita Praha
Landorová Anděla, Prof., Ing., CSc.	Vysoká škola obchodní v Praze
Lässig, Jörg, Prof., Dr.	Hochschule Zittau/Görlitz
Lizák Pavol, doc., Ing., Ph.D.	Trenčianska univerzita Alexandra Dubčeka
Lori Willfried, Prof., Dr.-Ing.	Westsächsische Hochschule Zwickau
Lungová Miroslava, Ing., Ph.D.	Technická univerzita v Liberci
Marouśková Marie, Prof., PhDr., CSc.	Univerzita J. E. Purkyně v Ústí nad Labem
Maršíková Kateřina, Ing., Ph.D.	Technická univerzita v Liberci
Mejzlík Petr, Ing.	Honeywell International, s r.o.
Militký Jiří, Prof., Ing., CSc.	Technická univerzita v Liberci
Modrlák Osvald, doc., Ing., CSc.	Technická univerzita v Liberci
Mohelská Hana, doc., Ing., Ph.D.	Univerzita Hradec Králové
Mráz Jan, Ing., Ph.D.	EGAP, a.s., Praha
Müller Hardy, Prof., Dr.	Westsächsische Hochschule Zwickau
Müller Miloš, Ing., Ph.D.	LENAM s.r.o., Liberec
Mužáková Karina, Ing., Ph.D.	Technická univerzita v Liberci
Nehls Uwe, Prof., Dr.- Ing.	FH Oldenburg
Neuhoff Antje, M.A.	Technische Universität Dresden
Norková, Alena, Mgr.	Univerzita J. E. Purkyně v Ústí nad Labem
Nouza Jan, Prof. Ing. CSc.	Technická univerzita v Liberci
Nováková Kateřina, Ing.	Česká školní inspekce Liberec
Opa Miroslav, Ing., Ph.D.	Demoautoplast, s.r.o., Čelákovice
Ortová Martina, Ing., Ph.D.	Technická univerzita v Liberci
Paseková Marie, doc., Ing., Ph.D.	Univerzita Tomáše Bati ve Zlíně

Name	Work Location
Pavelka Tomáš, Ing., Ph.D.	Vysoká škola ekonomická v Praze
Pawłowski Maciej, Dr., Inż.	Politechnika Wrocławska
Pełczyńska Marzena, M.D., Ph.D.	Karkonoska państwowa szkoła wyższa w Jeleniej Górze
Pełka Marcin, Mgr.	Uniwersytet Ekonomiczny we Wrocławiu
Pešková Radka, Ing., Ph.D.	VŠEM Praha
Pfeifer Václav, Ing.	Honeywell International, s r.o.
Picek Jan, Doc. RNDr., CSc.	Technická univerzita v Liberci
Piotrowski Przemyslaw, Mgr.	Karkonoska państwowa szkoła wyższa w Jeleniej Górze
Pištěk Luděk, Ing.	TOS Varnsdorf
Procházka Martin, Ing.	Okresní hospodářská komora Liberec
Radzik Tadeusz, Prof., Dr.	Karkonoska państwowa szkoła wyższa w Jeleniej Górze
Rahmanová Šárka, Ing., MBA, Ph.D.	Aareal Capital Corporation
Richter Ernst, Dr.-Ing.	Hochschule Zittau/Görlitz
Rozkovec Jiří, Mgr.	Technická univerzita v Liberci
Seidler Christine, Dr.	Internationales Hochschulinstitut Zittau
Schmidt Fritz Jochen, Prof., Dr.-Ing. habil.	Hochschule Zittau/Görlitz
Schöne Karin, M.A.	Technische Universität Dresden
Schönherr Jürgen, Prof., Dr.-Ing.	Hochschule Zittau/Görlitz
Skála Marek, Mgr. Ing., Ph.D.	Technická univerzita v Liberci
Skrbek Jan, doc. Dr., Ing.	Technická univerzita v Liberci
Sovová Ilona, Mgr.	Technická univerzita v Liberci
Stößel Bernd, Prof., Dr.-Ing.	Hochschule Zittau/Görlitz
Strahl Danuta, Prof., Dr. hab.	Uniwersytet Ekonomiczny we Wroclawiu
Svoboda Milan, PhDr., Ph.D.	Technická univerzita v Liberci
Svobodová Marie, Ing., Ph.D.	UJP Praha, a.s.
Szargot Maciej, Prof., Dr. hab.	Uniwersytet Humanistyczno przyrodniczny, Piotrków Trybunalski
Šámalová Terezie, Mgr., Ph.D.	Ústav informatiky AV ČR
Ševčík Ladislav, Prof., Ing., CSc.	Technická univerzita v Liberci
Štěpánek Libor, PhDr., Mgr., Ph.D.	Masarykova univerzita v Brně
Štrach Pavel, doc., Ing., Ph.D. et Ph.D.	ŠKODA AUTO Vysoká škola o.p.s.

Name	Work Location
Tesárková Klára Kouřil	Bodycote HT s.r.o., Liberec
Tettenborn Oliver, M.A.	Internationales Hochschulinstitut Zittau
Theilig Holger, Prof., Dr.-Ing. habil.	Hochschule Zittau/Görlitz
Trešl Jiří, Doc., Ing., CSc.	Vysoká škola ekonomická v Praze
Turnerová Lenka, doc., Ing., CSc.	Vysoká škola ekonomická v Praze
Tvrdoň Michal, Mgr., Ing., Ph.D.	Slezská univerzita v Opavě
Ungerman Otakar, Ing., Ph.D.	Technická univerzita v Liberci
Urbánek Václav, doc., Ing., CSc.	Vysoká škola ekonomická v Praze
Vacek Jiří, doc., Ing., CSc.	Technická univerzita v Liberci
Vašutová Jaroslava, doc., PaedDr., Ph.D.	Univerzita Karlova v Praze
Veselý Jiří, RNDr.	Matematicko-fyzikální fakulta UK v Praze
Vítek Leoš, Doc., Ing., Ph.D.	Vysoká škola ekonomická v Praze
Vlčková Kateřina, Mgr. et Mgr., Ph.D.	Masarykova univerzita Brno
Vogt Matthias-Theodor, Prof., Dr.	Hochschule Zittau/Görlitz
Vomáčková Helena, doc., Ing., CSc.	Univerzita J. E. Purkyně v Ústí nad Labem
Walter Johann Heinrich, Prof., Dr.-Ing., Dipl.-Math.	HS für Technik und Wirtschaft Dresden
Wierick Dieter, Prof. (em.), Dr.-Ing.	Hochschule Zittau/Görlitz
Will Markus, Dipl.-Ing. (FH)	Hochschule Zittau/Görlitz
Winnicki Tomasz, Prof. zw. Dr. hab. Inż.	Karkonoska państwowa szkoła wyższa w Jeleniej Górze
Winzeler Marius, Dr. Des., lic. phil.	Städtische Museen Zittau
Woldt Claudia, Dr.	Technische Universität Dresden
Worlitz Frank, Prof., Dr.-Ing.	Hochschule Zittau/Görlitz
Zaremba – Warnke Sabina, Dr.	Uniwersytet Ekonomiczny we Wroclawiu
Zelenka Jaroslav, Mgr.	Technická univerzita v Liberci
Žambochová Marta, RNDr., Ph.D.	Univerzita J. E. Purkyně v Ústí nad Labem
Žďánská Vladimíra, MUDr.	Privátní lékař, Liberec
Žižka Miroslav, doc., Ing., Ph.D.	Technická univerzita v Liberci

GUIDELINES FOR CONTRIBUTORS

Guidelines for contributors are written in the form of a template, which is available as a Word document at http://acc-ern.tul.cz/images/journal/ACC_Journal_Template.docx.

EDITORIAL BOARD

Název časopisu (*Journal Title*)	ACC JOURNAL
Ročník (*vol./year/issue*)	XIX (1/2013/Issue A)
Autor (*Author*)	kolektiv autorů (*composite author*)
Vydavatel (*Published by*)	Technická univerzita v Liberci Studentská 2, Liberec 1, 461 17 IČO 46747885, DIČ CZ 46 747 885
Schváleno rektorátem TU v Liberci dne	6. 5. 2013, č. j. RE 20/13
Vyšlo (*Published*)	30. 6. 2013
Počet stran (*Number of pages*)	119
Vydání (*Edition*)	první (*first*)
Číslo publikace (*Number of publication*)	55-020-13
Evidenční číslo periodického tisku (*Registry reference number of periodical print*)	MK ČR E 18815
Tištěná verze ISSN (*ISSN printed version*)	1803-9782
Počet výtisků (*Number of copies*)	80 ks (*pieces*)
Adresa redakce (*Address of the editorial office*)	Technická univerzita v Liberci Akademické koordinační středisko v Euroregionu Nisa (ACC) Studentská 2, Liberec 1 461 17, Česká republika Tel. +420 485 352 318, Fax +420 485 352 229 e-mail: acc-journal@tul.cz http://acc-ern.tul.cz
Tiskne (*Print*)	Vysokoškolský podnik, s.r.o. Hálkova 6, Liberec 1 460 01, Česká republika

Upozornění pro čtenáře

Příspěvky v časopise jsou recenzovány a prošly jazykovou redakcí.

Readers' notice

Contributions in the journal have been reviewed and edited.

Předplatné

Objednávky předplatného přijímá redakce. Cena předplatného za rok je 900,- Kč mimo balné a poštovné. Starší čísla lze objednat do vyčerpání zásob (cena 200,- Kč za kus).

Subscription

Subscription orders must be sent to the editorial office. The price is 40 € a year excluding postage and packaging. It is possible to order older issues only until present supplies are exhausted (8 € an issue).

Časopis ACC JOURNAL vychází třikrát ročně (červen, září, prosinec).
Three issues of ACC JOURNAL are published every year (June, September, December).

ISSN 1803-9782

Euroregion Neisse-Nisa-Nysa k 31. 12. 2009

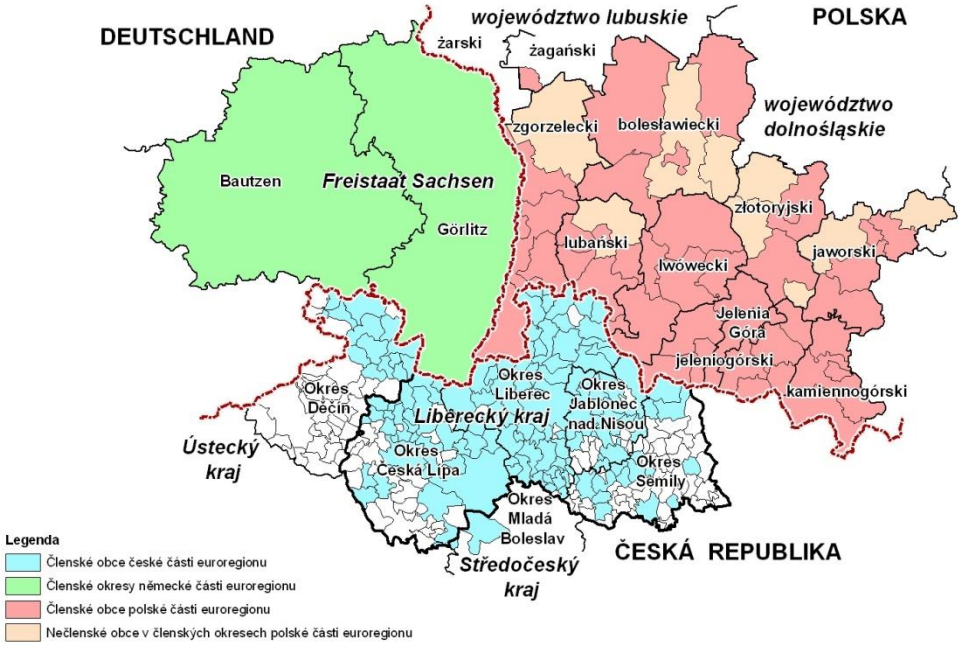

ISSN 1803978-2